Theoretical Analysis and Numerical Algorithm for Frictionless Multiple Impacts in Multibody Systems

Caishan Liu, Zhen Zhao, Bernard Brogliato

INRIA

INSTITUT NATIONAL DE RECHERCHE EN INFORMATIQUE ET EN AUTOMATIQUE

Theoretical analysis and numerical algorithm for frictionless multiple impacts in multibody systems

Caishan Liu — Zhen Zhao —
Bernard Brogliato

N° ????

January 2007

Thème NUM

ISSN 0249-6399 ISRN INRIA/RR--????--FR+ENG

INSTITUT NATIONAL
DE RECHERCHE
EN INFORMATIQUE
ET EN AUTOMATIQUE

INRIA

centre de recherche
GRENOBLE – RHÔNE-ALPES

Theoretical analysis and numerical algorithm for frictionless multiple impacts in multibody systems

Caishan Liu *, Zhen Zhao †,
Bernard Brogliato ‡

Thème NUM — Systèmes numériques
Équipe-Projet Bipop

Rapport de recherche n° ???? — January 2007 — 76 pages

Abstract: Using rigid body dynamics to solve multi-impact problems poses many difficulties and unanswered questions. Experiments and numerical simulation by using all kinds of compliant contact models clearly show that the outcomes of the post-velocities are not only influenced by the local dissipated energy, but also significantly effected by the coupling between various contacts. Based on the idea that the local dissipated energy depends on the constitutive relationship of the compliances, while the couplings among contacts exhibit the wave behaviors, this paper presents a new method that can well deal with multi-impact problems and produce energetically consistent and unique solutions to the post-impact velocities. Stronge's energetic coefficient is used as the energetic constraint to reflect the local dissipated energy at each impact, and the wave effects are coupled into rigid body models by using a distributing law that is associated with the *relative contact stiffness and the relative potential energy* stored at contact points. The evolution of energy is mapped into the impulsive-velocity level by stretching the time scale into the impulsive scale such that multi-impact processes can be described as a set of differential equations with respect to a normal impulse. Combining the distributing law with the Darboux-Keller's method of taking the normal impulse as an independent "time-like" variable can make multi-impact problems calculable and respect the energy constraints. The guidelines related to the selection for the independent normal impulse are presented and a numerical algorithm is developed in this paper. Comparisons between the theoretical predictions and the experimental results found in the literature as well as the numerical results obtained with

* State Key Laboratory for Turbulence and Complex Systems, College of Engineering, Peking University, Beijing, China, 100871; liucs@pku.edu.cn

† State Key Laboratory for Turbulence and Complex Systems, College of Engineering, Peking University, Beijing, China, 100871

‡ INRIA, Bipop Team-Project, ZIRST Montbonnot, 655 Avenue de l'Europe, F-38334 Saint-Ismier, France; bernard.brogliato@inrialpes.fr

Centre de recherche INRIA Grenoble – Rhône-Alpes
655, avenue de l'Europe, 38334 Montbonnot Saint Ismier
Téléphone : +33 4 76 61 52 00 — Télécopie +33 4 76 61 52 52

compliant contact models are presented. Robustness analysis through numerical simulations is carried out and shows that the method proposed in this paper can well keep the essential mechanical features of the real system as it respects the evolution of motion in the energy sense. We use this method to investigate some interesting phenomena found in granular systems, and hope to extend it to the modeling of multiple impacts with friction, an issue that will be tackled in the future.

Key-words: Multiple Impacts, Darboux-Keller's Dynamics, Wave Effects, Energy Restitution Coefficient.

Impacts multiples dans les systèmes multicorps: Analyse théorique et algorithme numérique

Résumé : Ce papier propose une extension du modèle de choc de Darboux-Keller, dans le cas d'impacts simultanés dans un système mécanique multicorps. Dans une premier temps la dynamique du choc est développée. Puis un schéma numérique d'intégration est proposé. De nombreux résultats numériques sont présentés et comparés avec soin avec des résultats expérimentaux obtenus dans d'autres publications.

Mots-clés : Impacts multiples, Dynamique de Darboux-Keller, Ondes, Coefficient de restitution energétique

Nomenclature

- M Mass matrix
- $\mathbf{q}$ Generalized coordinates
- h_i the unilateral constraint i
- Σ_i i-th hypersurface of constraint
- $\mathcal{C}$ Configuration space
- $P_j(t)$ the normal impulse at j-th contact
- α, γ the mass and stiffness ratios
- $\alpha_1, \alpha_2, \Delta$ parameters related to α and γ
- k, ω the spring stiffness and the frequency
- δ_i and λ_i the contact deformation and the normal contact force at contact point i
- dP_i the increment of the normal impulse at contact point i
- K_i the contact stiffness
- η the exponent for the contact modes (linear or Hertz stiffness)
- $f(P_i)$ a function with respect to the normal impulse P_i
- E_i the residual potential energy at contact point i
- γ_{ij}, E_{ij} the ratios of the contact stiffness and the residual potential energy between contact points i and j
- $W_{r,j}$, $W_{c,j}$ the work done by the contact force during expansion and compression phases, respectively
- $\delta_{e,j}$, $\delta_{c,j}$ the variable of the contact deformation at contact point j in expansion and compression phases, respectively.
- $\delta_{e,j}^{(\cdot)}$, $\delta_{c,j}^{(\cdot)}$ the contact deformation of contact point j at the location $(\cdot)$ in expansion and compression phases, respectively
- $\delta_{m,j}$ the maximum value of contact deformation of contact point j at the end of the compression phase
- $\delta_{r,j}$ the plastic deformation of contact point j at the end of the expansion phase
- $e_{s,j}$ the energetic coefficient at contact point j
- $\lambda_{e,j}$, $\lambda_{c,j}$ the variables of the contact forces in expansion and compression phases, respectively

- t_0, t_f the time of the beginning and the end of a impact
- t_c, $P_j(t_c)$ the time and the normal impulse at the end of the compression phase
- s the number of the unilateral constraints

1 Introduction

Systems with multiple impacts have a time-varying structure due to the unilateral features of constraints. Moreover the configurations and the possible flexibilities at the contact points significantly influence the outcomes [1-13]. Consequently these phenomena require a special treatment for analytical and numerical solution methods. There are basically four ways of modelling a contact/impact phenomenon in multibody systems: **(i)** the finite element method to directly discretize the contact bodies [14-17], **(ii)** a compliant model (spring–dashpot, with linear or nonlinear stiffness) and the second order dynamics [18-29], **(iii)** a purely algebraic impact law (or mapping) of the form $\dot{q}^+ = \mathcal{F}(\dot{q}^-, q, p)$ where p is a set of parameters [4,7,10-12,30-37] [57], **(iv)** the first order Darboux-Keller impact dynamics [6] [38-42] [44].

It is well-known that the interaction between bodies usually experiences a multi-scale process depending on the materials of contact bodies, the geometric shape, as well as the loading conditions [13, 14, 15]. Model **(i)** permits to analyze the complex process in a stress-strain level and to obtain precise informations associated with the force/displacement. However the requirement of large computation resources and overrich information often hampers its application in complex multibody systems.

Model (**ii**) seems to be an efficient method by using some centralized parameters representing the complex behaviors of colliding bodies. However, other problems will arise, such as the numerical difficulties due to stiff differential equations [23], problems to identify properly the contact parameters (the damping and stiffness coefficients used in a compliant contact model) [26, 45], and the inability to correctly represent some physical effects like waves and dispersion [66].

Model **(iii)** is an algebraic way to deal with impact problems. Directly applying the classical impact laws, such as the Newton's and Poisson's coefficients, cannot provide an appropriate behavior (i.e. outcomes that agree with the experiments and which satisfy some physical constraints like energy loss) when more than one contact point participates in a shock process [5, 29, 36] (or when there is one contact but with Coulomb friction [49, 50]). Kane [50] stated that the Newton's coefficient may yield some dynamical singularities when friction is added at the contacts. The proper energetical behaviour of impact mappings when tangential and normal restitutions are introduced, is treated in [4, 57]. For multi-impact problems, d'Alembert [1] concluded that dividing the multiple impacts into the sum of percussions computed for each pair of solids seems to be impossible, and the elastic deformation at contact points should be involved. The fundamental importance of good restitution mappings and coefficients has been shown in [60] for chains of beads. The dynamics of some other granular media seems to be less sensitive to the restitution model [4, 62].

When the colliding bodies can be well approximated by rigid bodies between the impacts, usually the detailed information associated with the force/displacement models has little significance on understanding the collision process. In addition, the anticipation in many applications is how to grasp the overall characteristics of systems at a more macroscopic level such as the impulse or the energy sense. This motivates researchers to look for a feasible solution for multi-impact problems in the framework of rigid body dynamics that respect the basic physical laws [1, 9, 11, 14, 5, 8, 12, 25, 26]. Model **(iv)** is a significant method that not only allows one to model the local dissipated energy in a simple way, but also can cope with the coupling between the normal and tangential motions. In the simplest case, the Darboux-Keller dynamics merely says that an impact is represented by a first order differential equation of the form $M\frac{dv}{dP} = 1$, where M is the mass, v is the velocity, and P is the impulse of the contact force. It has been extended to more complex cases [6, 30, 37, 38, 39, 40, 41] of two bodies colliding with friction. The energy local dissipation phenomena are so complex (plastic deformation, viscoelastic behaviour, light, noise, etc [53]) that it happens to be more reliable to shrink all these effects into a single coefficient: the energetical restitution coefficient has proved to be a good candidate in many previous works dealing with single impacts [6, 30] and relying on Darboux-Keller's dynamics. At present, this method is only available to solve the collisions with a single contact point. How to extend it to multiple impacts is central in this paper.

Two factors should be carefully considered when impact/contact processes are understood in the energetical sense: the local dissipated energy at contact/impact points, and the global transfer of energy between various motions. The common difficulties arising when using rigid body models are how to separate the local dissipated energy from the total energy of the systems and how to analyze the coupling of various motions. The first difficulty is associated with the definition of a good restitution coefficient, and the second one is related to the mechanism of energy transfer and waves. In the following the modeling framework of multiple impacts is briefly introduced, as well as the contribution of this work and a short review of the literature.

1.1 General features of multiple-impacts laws

Let us consider a mechanical lagrangian system with an n-dimensional generalized coordinate q and configuration space $\mathcal{C}$. This system is supposed to have a mass matrix $M(q) = M^T(q) > 0$, and is subject to several unilateral constraints $h_i(q) \geq 0$, $1 \leq i \leq s$, where the functions $h_i(\cdot)$ are supposed differentiable and the set $\Phi = \{q \in \mathcal{C} \mid \ h_1(q) \geq 0, h_2(q) \geq 0, ..., h_s(q) \geq 0\}$ has an interior with positive volume. We define the s hypersurfaces $\Sigma_i = \{q \in \mathcal{C} \mid \ h_i(q) = 0\}$. A multiple impact is an impact that occurs at the intersection of two (or more than two) surfaces Σ_i. Physically, this corresponds to have several points at which contact is established simultaneously. There may be several types of multiple impacts, as depicted in Figure 1 that gives a schematic representation of the system in the plane. We may name an impact that occurs at a codimension $m_k \leq s$ surface, an m_k-impact.

There are many properties and characteristics which are associated with a multiple impact, independently of the chosen class of models **(i)**–**(iv)**. Let us provide a rapid summary:

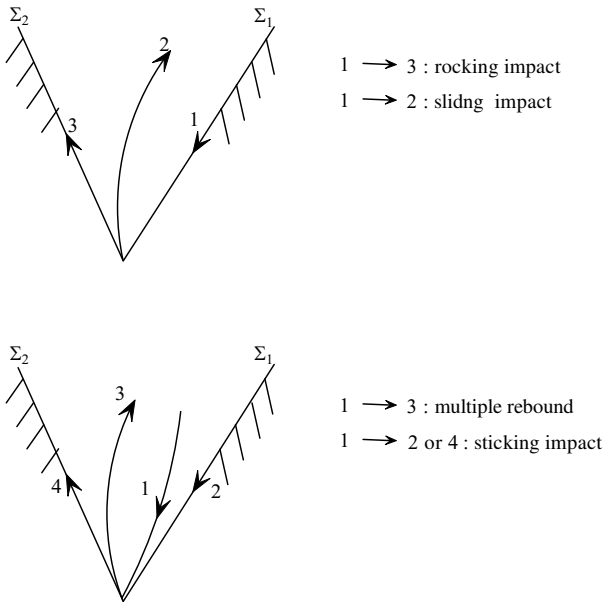

Figure 1: Several types of multiple impacts.

- (1) the kinetic angle between the surfaces Σ_i involved in the impact,
- (2) the continuity of the solutions with respect to the initial data,
- (3) the kinetic energy behavior at the impact,
- (4) the wave effects due to the coupling between various contacts,
- (5) the local energy loss during impacts,
- (6) the ability of the impact rule to span the whole admissible post-impact velocities domain,
- (7) the ability of the parameters defining the impact rule to be identified from experiments,
- (8) the (in)dependence of these parameters on the initial data,
- (9) the physical meaning of the parameters of the impact rule,
- (10) the ability of the impact rule to provide post-impact velocities in agreement with experimental results,
- (11) the well-posedness of the nonsmooth dynamics when the impact rule is incorporated in it,
- (12) the law should be applicable (or easily extendable) to general mechanical systems,
- (13) the determination of the impact termination,
- (14) the impact law has to be numerically tractable.

Finding a collision law that respects and fulfills all the items (3) through (14) is quite a hard task. Item (6) means that the various impacts in Figure 1 should be covered. Items (1) (3) (6) enter into the geometrical considerations in [31] to develop a framework for multiple impacts, extending Moreau's sweeping process rule [5, 57]. Property (2) is important, as it implies that sequences of single impacts may completely fail to deduce the multiple impact law (moreover in general impacts are not propagated in a sequential way through the contacts [25, 26, 28]). It is also related to (11) and to (1). Indeed under some conditions on the kinetic angles, continuity of the solutions (2) may hold. These cases may be considered as isolated cases, however. Item (4) implies that the coupling between various contacts will generate possible "distance" effects, i.e. a collision may be propagated through the system and induce a detachment at another contact point. This implies that other relationships than the usual restitution coefficients at each contact, have to be discovered. For instance Ceanga and Hurmuzlu [12] were the first ones to quantitatively study the coupling effects by introducing an impulse correlation ratio (ICR), even though their theory has a limited application due to some basic assumptions on the ICR to be valid for triplets of balls, which is not satisfied in general [25, 26, 28]. Another approach using the ICR and a global energetic coefficient is proposed in [25, 26]. It somewhat mixes **(iii)** and **(iv)** in the sense that the ICRs are computed from a simplified second order compliant dynamics, and then injected into the algebraic impact equations. Other examples with different "coupling" coefficients may be found in [7, 4], however they may fail to satisfy item (9), rendering (7) tricky. Item (5) is related to the meaning of the restitution of coefficient. Newton's coefficient reflects the local energy loss on the velocity level, while the Poisson's coefficient puts the energy loss on the impulse level. Obviously these variables must change due to item (4) and may violate the basic law of energy conservation [50, 57]. Items (7) (8) (9) (10) are related to the choice of the parameters that enter the impact law. They are fundamental from the point of view of the practical usefulness of the law. For instance one may want that some parameters be identified through simple experiments before being injected in a rule for a more complex collision (e.g. identify restitution coefficients between pair of balls and then use them in a chain of balls, or identify the ICR of [12] between triplets of balls, then use the obtained values in a complete chain with n balls). It is noteworthy that the main drawback of models **(ii)** is the necessity to identify stiffness and damping parameters, which is usually not easy when there are many contacts with various materials. Item (12) is closely linked to (4), since the wave effects may differ a lot depending on the bodies shapes, materials, etc. Item (4) also indicates that a guideline should be established for item (13) since the separations of contacts do not occur simultaneously. The last item is not the least one. It has led several researchers to look for multiple-impacts laws that lend themselves to a Linear Complementarity Problem formulation [31, 4, 7], and are extensions of the Newton or Poisson restitution models.

In the book [5] many constructive remarks on historical works related to impact dynamics are made, and this may be the first time one points out that the relative quantity of flexibility is a significant factor for multiple impacts. It is also pointed out that contrary to the single impact frictionless case, the energetical behavior is not sufficient to determine in a unique way the restitution coefficients. This looks like the situation of hyperstatic problems in rigid body statics: one cannot determine the solutions of constraint forces even though all

energy is assumed to be stored in constraints, and some consistent conditions depending on the constraint properties should be provided. Glocker and Pfeiffer [9] proposed a general method based on the Darboux-Keller's equations to solve the multi-impact problems. However, the integrating process for the impulsive process is ignored due to the assumptions adopted in their theory, which may much influence the outcomes of multiple impacts. Pioneering works related to the multi-impact problems can also be found in [29, 8, 3, 2], etc, in which some special situations related to multiple impacts were solved by introducing various assumptions.

1.2 The necessity of a multiple-impact law

Let us clarify the role played by items (1) and (2) above. For this we consider a chain of two balls which collide a wall, as in Figure 23. The dynamics is given by

$$\left\{\begin{array}{l} m_1\ddot{q}_1(t) = -m_1 g + \lambda_1 \\ \\ m_2\ddot{q}_2(t) = -m_2 g - \lambda_1 + \lambda_2 \\ \\ 0 \leq \lambda_1 \perp h_1(q) = q_1 - q_2 - R_1 - R_2 \geq 0 \\ \\ 0 \leq \lambda_2 \perp h_2(q) = q_2 - R_2 \geq 0 \end{array}\right. \tag{1}$$

with obvious notations. The kinetic angle between the two surfaces Σ_1 and Σ_2 is given by

$$\cos\theta_{12} = -\frac{\sqrt{m_1}}{\sqrt{m_1+m_2}} < 0 \tag{2}$$

so that $\pi > \theta_{12} > \frac{\pi}{2}$. In such a case we may expect from the results in [65] that solutions are discontinuous with respect to the initial data. This implies that different sequences of impacts will produce different post-impact velocities, and the limit of the process when all impacts occur simultaneously does not exist. We associate a Newton's impact law to each contact, with restitution coefficients e_1 and e_2, respectively. The upperscript $-$ means pre-impact velocity, whereas $+$ means post-imapct velocity. When there are several impacts we indicate it as $++$ or $+++$. The sequence of impacts B_2/wall (Σ_2) and B_1/B_2 (Σ_1) produces the outcomes

$$\left\{\begin{array}{l} \dot{q}_1^{+} = \frac{m-e_1}{1+m}\dot{q}_1^{-} - e_2\frac{1+e_1}{1+m}\dot{q}_2^{-} \\ \\ \dot{q}_2^{++} = \frac{m(1+e_1)}{1+m}\dot{q}_1^{-} - e_2\frac{1-e_1 m}{1+m}\dot{q}_2^{-} \end{array}\right. \tag{3}$$

with $m = \frac{m_1}{m_2}$. The sequence of impacts B_1/B_2 (Σ_1) and B_2/wall (Σ_2) and then B_1/B_2 (Σ_1) again, produces the outcomes

$$\left\{\begin{array}{l} \dot{q}_1^{++} = \frac{m-e_1}{1+m}\left\{\frac{m-e_1}{1+m}\dot{q}_1^{-} + \frac{1+e_1}{1+m}\dot{q}_2^{-}\right\} - e_2\frac{1+e_1}{1+m}\left\{\frac{m(1+e_1)}{1+m}\dot{q}_1^{-} + \frac{1-e_1 m}{1+m}\dot{q}_2^{-}\right\} \\ \\ \dot{q}_2^{+++} = \frac{m(1+e_1)}{1+m}\left\{\frac{m-e_1}{1+m}\dot{q}_1^{-} + \frac{1+e_1}{1+m}\dot{q}_2^{-}\right\} - e_2\frac{1-e_1 m}{1+m}\left\{\frac{m(1+e_1)}{1+m}\dot{q}_1^{-} + \frac{1-e_1 m}{1+m}\dot{q}_2^{-}\right\} \end{array}\right. \tag{4}$$

Clearly the final values in (3) and (4) are not the same. For such a simple system it is not possible to deduce a restitution mapping when the collision occurs at $\Sigma_1 \cap \Sigma_2$ by studying sequences of impacts. One therefore has to follow another path to obtain a multiple-impact law for this system. Most of the mechanical systems that will be examined in the next sections have solutions which are discontinuous with respect to the initial data. For such systems it is hopeless to expect accurate numerical results with approaches **(iii)** or **(iv)** without a good multiple impact law. Notice that using Poisson's coefficient will not change the conclusion since Newton and Poisson's approaches are equivalent for such impacts.

1.3 The importance of a good multiple-impact law

The energy of a mechanical system during a multiple impact is transferred and re-distributed among the various contact points, except for the local dissipations. Therefore, it is crucial to consider the wave effects when getting a good impact law for multi-impact problems. This can be explained by using the classical example of a Newton's cradle with N balls, when the balls are attached to a horizontal rod with strings, and are subjected to gravity.

Without going into further details, one may say that the usual outcome of such a chain of N balls when the first ball strikes the others, and all the other $N-1$ balls are at rest with closed contacts (that is an $N-1$-impact), is that the first $N-1$ balls are at rest (ball B_1 stops and balls B_2 to B_{N-1} do not move), while the last ball B_N takes all the kinetic energy. Then the process is repeated in the other direction when the ball B_N comes to collide with the chain of balls B_1 to B_{N-1} at rest. One easily concludes that this continues indefinitely. However, the observation of most Newton's cradle shows that after a while, all the balls are stuck and the whole chain rocks (hence the name of a cradle) [52]. The initial energy of the first ball has been transferred to the chain with a certain length at first, then travels forward through the chain. A close observation of what happens after the first collision (that is a multiple impact) shows that balls B_1 to B_{N-1} have a very small but non zero post-impact velocity. This is a scattering phenomenon due to the rebounding motion of the balls after the wave passes through the ball, also known as the dispersive, or bead detachment effect [42]. Despite almost all the kinetic energy has been finally transferred through a wave to the ball B_N (typically 98% of the energy), the remaining energy in balls B_1 to B_{N-1} plays a crucial role in the subsequent motion of the whole chain.

The moral of the tale is that the first model provides an outcome that is close in absolute value to the real outcome: the law may be considered good from the *quantitative* point of view. However, this outcome is available only for the Newton's cradle with identical balls. If a different ball collides against the chain, or the chain consists of beads with different size or materials, the situation will be very far from the observed motion described in the tale. Thus the impact rule is very bad from the *physical* point of view as it doesn't discover the essential mechanism driving the multiple impacts. In other words, the observed motion in Newton's cradle is only a special phenomenon that appears in a uniform chain impacted by an identical particle. So the impact rule coming from Newton's cradle is subjective and brings nothing to the solution of the multi-impact problem. In fact, multiple impacts are very closely related to the

energy redistribution within the system during the collision, and often generate an impulsive wave that travels through the contact bodies. This phenomenon has been discovered in physics by using numerical simulation and experiments [43, 28, 46, 47, 48, 42, 59, 60, 61]. For a uniform cradle with N balls impacted by an identical ball, the energy will be distributed in the chain within five balls and travel with an approximately constant velocity, which depends on the initial impacting conditions.

Once the wave effects can be captured by a good impact law, the next question is how to define the local energy loss at each contact since this energy cannot be transformed into the kinetic form. If the colliding bodies are not viscosity materials, the dissipated energy will mainly be due to the plastic deformation generated at the local contact region. Since the plastic deformation usually depends on the static constitutive relationship at contact points, this may provide a convenient way of applying an energetic constraint to confine the local dissipated energy, such that the parameters added into the impact rule can satisfy the requirement of items (7), (8) and (9) mentioned in above.

1.4 Contribution of the paper

For multi-impact problems, it is obvious that the transfer of energy is implemented through the contact points. The exchange and distribution of energy must depend on the collocation of contact constraints and the elastic properties at the contact regions. Apparently, the information associated with the compliance at contacts should be added into rigid body models in order to discover the law of energy transfer and distribution during multiple impacts.

The properties of unilateral constraints can be represented by using some centralized parameters, and are expressed by the constitutive relationship between contact force and indentation. Under the assumption that the elastic vibration of colliding bodies can be ignored, the energy loss and transformation will only depend on the properties of the contact constraints.

The mechanism of energy dissipation is complex for contact/impact problems as illustrated in [53], and an index to reflect the energy loss should be defined for rigid body models (similar to the damping coefficient used in structural dynamics). Basically speaking, all kinds of restitution coefficients are just an index that defines the energy loss on different mechanical variables. For instance the Newton's coefficient presents a kinematic constraint to define the energy loss, while the ratio of impulses is used in Poisson's one. In fact, the values of these coefficients must be influenced by the transfer of energy between various contacts and have to be modified according to concrete problems [33, 54, 32]. Stronge defined a constant coefficient to establish a linear relationship between the input and output of the energy for an impact with a single compression/expansion cycle. Even though the relationship is nonlinear in nature according to FEM simulations [34, 13] and theoretical analysis [49, 14], the value of Stronge's coefficient can be identified independently from experiments as it is related to energy. Therefore, the energetical coefficient can be used as a constraint to confine the local energy loss.

Except for the dissipated energy, another part of the energy will be transferred from one form to another (kinetic to potential, or potential to kinetic), and be re-distributed among various contacts. The evolution of energy obviously depends on the collocation of contact points and the constitutive relationship

related to the contact properties. In order to discover the evolution law of energy, we stretch the time scale into an impulsive level, $t \mapsto \int_0^t \lambda(\tau)d\tau$, such that the energy of bodies can be mapped into the impulse-velocity level. Considering the variation of the normal impulses in space scale, we can establish the relationships between the increments of normal impulses at the same time interval. These relationships provide a distributing law of reflecting the changes of normal impulses with the relative contact stiffness and the relative potential energy stored at various contacts. If the normal impulse at the $i-th$ contact point changes, the normal impulses at other contacts will accompany the variation by obeying the distributing law.

The experimental observation of multiple impact processes show that the impact duration can be considered infinitesimal and the displacements of the system constant "during" the impact process [56]. Also the forces other than contact forces (like gravity) can often be neglected [42]. This allows one to conduct the following assumptions of rigid body dynamics into the multi-impact process:

- (a) the position q remains constant during the shock process,
- (b) the collision is made of compression/expansion phases during which the impulse of the contact force is strictly increasing,
- (c) all other forces but the contact/impact ones are neglected,

In order to analyze the coupling between normal and tangential motions for a single impact with friction, Darboux and then Keller developed a method by making the normal impulse replace the time scale as a new integration variable for the first order velocity/impulse dynamics obtained based on the above assumptions [37, 38]. The advantage of this method is in the following:

The unimportant information for the impulsive process, such as the displacements at contact points and the forces except for the contact ones is completely filtered out from the model, while the evolution of the motion at the contact points can be well described as in a compliant model.

It is also worthy to note that the evolution in Darboux-Keller's approach is reflected in the impulsive-velocity level, while the one in compliant contact model needs the extra information associated with the displacements and all the forces, such that some numerical difficulties will be generated. This method paves the way towards modelling the impact problems by using rigid body dynamics to consider the coupling between various motions, and have found successful application in dealing with single impacts (without and with friction) and the problems of tangential impacts [6, 44, 41, 42] and [5] for more references.

Combining the distributing law between various increments of normal impulses with the velocity/impulse dynamical equations results in a set of first order differential equations with respect to the normal impulses among which only one can change as a "time-like" independent variable, such that the multi-impact problem can be solved by using the Darboux-Keller's approach. However, contrary to the collision between a pair of bodies where the exclusive normal impulse can be selected, multi-impact processes will contain multiple normal impulses (one at each contact), and the selection for the independent

variable seems to be arbitrary. In order to avoid the numerical singularity generated by selecting the normal impulse at the contact point with relative small potential energy, and to respect the fact that the multi-impact process should be dominated by the contact point with the maximum value of accumulated energy, we present a guideline for the selection of the independent variable: *The normal impulse at the contact point with maximum potential energy is always selected as the independent time-scale variable*. This contact point is denoted as the primary contact point, and obviously changes with the evolution of the energy. Therefore, the Darboux-Keller ODE is a set of differential equations with the integral variable that is changed during the course of the integration. The integral interval is constrained by the energetical conditions in which the potential energy at contacts should be completely transformed into the kinetic form except for the local energy losses.

In summary, the main purpose of this paper is to solve the multi-impact problems in the energy sense, and some new developments are made:

- (1) clarifying the physical meaning of restitution coefficient, and taking the Stronge's coefficient as the energetical constraint to define the local energy loss during impacts.
- (2) stretching the time scale into the impulsive level to discover the properties of the energy evolution.
- (3) extending the Darboux-Keller's method into the multi-impact problems to obtain a set of first order differential equations with respect to the primary normal impulse, and solving the multi-impact problem at the velocity-impulse level.

Compared to the approach in [25, 26], the algorithm proposed in this work has the advantage of relying only on the stiffnesses ratios and on the local energetical coefficients to describe the multiple impacts. From a general point of view, the problem of integrating stiff compliant equations can be avoided, and the calculated outcomes are robust with respect to the uncertainties in the physical parameters. Moreover, this method can also present the information related to the contact forces and the durations of impacts if the force/displacement relationships at contacts could be provided based on the properties of the unilateral constraints. The contact forces are obtained from the absolute values of the potential energy, and the duration at each impact is calculated by dividing the impulses with contact forces.

1.5 Organisation of the paper

Section 2 is dedicated to study a simple chain of balls in order to highlight the main features of such a 2-impact, following and extending similar developments in [5, 28] and [12, 43]. In section 3, a general method to solve multi-impact problems by using impulsive dynamics is developed, in which the ratios for the distribution of the increments of normal impulses at all contact points are established based on a nonlinear spring contact model for contacts. The post-impact velocities can be obtained at the velocity-impulse level by integrating the differential equations and directly applying the energetical constraint to consider the

local energy loss, which are energetically and kinematically consistent. Section 4 presents a similar relationship for the distributing law, which is deduced from a bi-stiffness model that satisfies the energetical constraint. Section 5 provides a procedure for the numerical algorithm related to the differential equations with a changed integral variable and an integral interval depending on the integrating process. Several typical examples like the N-ball systems and the Bernoulli's problem are presented in sections 6 and 7 to test the method by comparing its outcomes with the solutions obtained from compliant methods and the experimental results found in [12]. The investigation of the robustness of the method related to an example of a chain against a wall is carried out in section 8. The application of the method in granular systems is presented in section 9, in which the contact force at the wall impacted by a 1-D column of beads is obtained according to the accurate contact model and is compared with the experimental results presented in [42]. Conclusions are given in the final section.

2 The effects of the compliance

In this section, a 3-ball system will serve as the example to illustrate the effects of the compliance. Han and Gilmore [29] have shown that this particular system would yield two possible solutions for the post-impact velocities when the assumption of either internal or sequential impacts was introduced. This indeterminate situation of rigid body model can be avoided by adding some compliance to the contact bodies [5, 12, 43, 26].

2.1 The theoretical results for the 3-ball system with linear springs

Let us assume that the three balls are located in a straight line to ensure only axial impact happens. Ball B_1 with initial velocity v_0 and mass m comes to strike other two stationary balls B_2 and B_3 that take the same mass αm. The variables x_1, x_2, x_3 and v_1, v_2, v_3 represent their center of mass positions and velocities, respectively. The interaction between two balls is realized through a linear spring in order to perform some analytical developments. The stiffness coefficient between B_1 and B_2 is k, while the one for the contact between B_2 and B_3 is γk. The governing equations at the instant of impact are

$$\begin{aligned} \frac{dP_1}{dt}(t) &= -k(x_1(t) - x_2(t)) \\ \frac{dP_2}{dt}(t) &= k(x_1(t) - x_2(t)) - \gamma k(x_2(t) - x_3(t)) \\ \frac{dP_3}{dt}(t) &= \gamma k(x_2(t) - x_3(t)) \end{aligned} \tag{5}$$

where $P_1 = mv_1$, $P_2 = \alpha m v_2$ and $P_3 = \alpha m v_3$. More generally this can be written as a piecewise linear system similarly to (5.37) in [5]. Let $\omega^2 = k/m$ and define the dimensionless displacements and velocities

$$\mathbf{q} = \left[\frac{x_1}{v_0 \cdot 1s}, \frac{x_2}{v_0 \cdot 1s}, \frac{x_3}{v_0 \cdot 1s}\right]^T, \dot{\mathbf{q}} = \left[\frac{P_1}{mv_0}, \frac{P_2}{mv_0}, \frac{P_3}{mv_0}\right]^T \tag{6}$$

In matrix notation, equation (5) becomes

$$\frac{d}{dt}\begin{bmatrix}\mathbf{q}\\ \dot{\mathbf{q}}\end{bmatrix} = \mathbf{H}\begin{bmatrix}\mathbf{q}\\ \dot{\mathbf{q}}\end{bmatrix} \tag{7}$$

with the initial condition $\mathbf{q}_0 = [\,0,0,0\,]^T$, $\dot{\mathbf{q}}_0 = [\,1,0,0\,]^T$. The analytical solution of equation (5) can be expressed as

$$\begin{bmatrix}\mathbf{q}(t)\\ \dot{\mathbf{q}}(t)\end{bmatrix} = \exp(\mathbf{H}\,t)\cdot\begin{bmatrix}\mathbf{q}_0\\ \dot{\mathbf{q}}_0\end{bmatrix} \tag{8}$$

Let us adopt the following notations:

$$\Delta = \sqrt{4\gamma^2 - 4\gamma\alpha + \alpha^2 + 2\alpha + 1}$$
$$\alpha_1 = \sqrt{(-\Delta + 2\gamma + \alpha + 1)/2\alpha},\ \ \alpha_2 = \sqrt{(\Delta + 2\gamma + \alpha + 1)/2\alpha}$$

Then the dimensionless displacements for each ball can be expressed as

$$\begin{aligned}
q_1(t) &= \frac{t}{2\alpha+1} + \frac{1}{\alpha_1\,\omega}\left[\frac{\alpha}{2\alpha+1} - \frac{\alpha^2-2\alpha\gamma}{(2\alpha+1)\Delta}\right]\sin(\alpha_1\,\omega\,t)\\
&\quad + \frac{1}{\alpha_2\,\omega}\left[\frac{\alpha}{2\alpha+1} + \frac{\alpha^2-2\alpha\gamma}{(2\alpha+1)\Delta}\right]\sin(\alpha_2\,\omega\,t)\\
q_2(t) &= \frac{t}{2\alpha+1} - \frac{1}{\alpha_1\,\omega}\left[\frac{1}{2(2\alpha+1)} - \frac{3\alpha+1-2\gamma}{2(2\alpha+1)\Delta}\right]\sin(\alpha_1\,\omega\,t)\\
&\quad - \frac{1}{\alpha_2\,\omega}\left[\frac{1}{2(2\alpha+1)} + \frac{3\alpha+1-2\gamma}{2(2\alpha+1)\Delta}\right]\sin(\alpha_2\,\omega\,t)\\
q_3(t) &= \frac{t}{2\alpha+1} - \frac{1}{\alpha_1\,\omega}\left[\frac{1}{2(2\alpha+1)} + \frac{\alpha+1+2\gamma}{2(2\alpha+1)\Delta}\right]\sin(\alpha_1\,\omega\,t)\\
&\quad - \frac{1}{\alpha_2\,\omega}\left[\frac{1}{2(2\alpha+1)} - \frac{\alpha+1+2\gamma}{2(2\alpha+1)\Delta}\right]\sin(\alpha_2\,\omega\,t)
\end{aligned} \tag{9}$$

These expressions have been obtained with MAPLE. The dimensionless velocities can be easily obtained from the time derivatives of the positions in expression (9). If one ball leaves the chain, the structure of the system will be changed into a 2-ball system with only one contact. Which contact is lost depends on the times t_1 and t_2 when the first and second balls separate, and when the second and third balls separate, respectively. Time t_1 is the solution of the following equation obtained by setting $q_1(t_1) = q_2(t_1)$:

$$\left[\frac{\Delta - (\alpha - 2\gamma + 1)}{2}\alpha_2 \sin(\alpha_1\,\omega\,t) + \frac{\Delta + (\alpha - 2\gamma + 1)}{2}\alpha_1 \sin(\alpha_2\,\omega\,t)\right] = 0 \tag{10}$$

Time t_2 is related to the solution of the equation $q_2(t_2) = q_3(t_2)$:

$$[\alpha_2 \sin(\alpha_1\,\omega\,t) - \alpha_1 \sin(\alpha_2\,\omega\,t)] = 0 \tag{11}$$

Clearly the mass ratio α and the stiffness ratio γ will significantly influence the separating time. If $t_1 < t_2$, then B_1 and B_2 separate first and the post-impact velocity $\dot{q}_1^+ = \dot{q}_1(t_1)$ can be determined at the instant t_1. After that the system experiences a time-variable process, and we should reconstruct the matrix $\mathbf{H}$ to form the governing equation for the two balls system with the initial conditions $q_2(t_1)$, $q_3(t_1)$, $\dot{q}_2(t_1)$ and $\dot{q}_3(t_1)$. Finally, the multiple impacts finishes at the instant when B_2 and B_3 have the same displacements. An analogous treatment can be used for the case $t_1 > t_2$.

2.2 Discussion on the theoretical results

Let us consider the special case of $\alpha = 1$ and $\gamma = 1$, widely studied by many authors [5, 12, 9, 29, 8, 28, 6]. Based on the above theory, the velocities of the identical balls can be expressed as the form with the following piecewise functions.

$$\dot{q}_1(t) = \begin{cases} \frac{1}{3} + \frac{1}{2}\cos(\omega t) + \frac{1}{6}\cos\left(\sqrt{3}\,\omega t\right) & t \in [0, t^*] \\ -0.1303 & t \in (t^*, \infty) \end{cases}$$

$$\dot{q}_2(t) = \begin{cases} \frac{1}{3} - \frac{1}{3}\cos\left(\sqrt{3}\,\omega t\right) & t \in [0, t^*] \\ 0.5651 - 0.3916\sin(\sqrt{2}(\omega t - t^*)) \\ \qquad -0.1373\cos(\sqrt{2}(\omega t - t^*)) & t \in (t^*, t^{**}] \\ 0.1502 & t \in (t^{**}, \infty) \end{cases} \tag{12}$$

$$\dot{q}_3(t) = \begin{cases} \frac{1}{3} - \frac{1}{2}\cos(\omega t) + \frac{1}{6}\cos\left(\sqrt{3}\,\omega t\right) & t \in [0, t^*] \\ 0.5651 + 0.3916\sin(\sqrt{2}(\omega t - t^*)) \\ \qquad +0.1373\cos(\sqrt{2}(\omega t - t^*)) & t \in (t^*, t^{**}] \\ 0.9801 & t \in (t^{**}, \infty) \end{cases}$$

In this situation, balls B_1 and B_2 will firstly separate at $t^* = 2.5548/\omega$, and then balls B_2 and B_3 lose contact at $t^{**} = 3.427/\omega$ as shown in [28]. It is easy to obtain the final dimensionless velocities of the balls: $\dot{q}_1(t^{**}) = -0.1303$, $\dot{q}_2(t^{**}) = 0.152$, $\dot{q}_3(t^{**}) = 0.9801$. This result shows that the post-impact velocities will not be affected by the absolute values of the mass and stiffness, but only by the ratios α and γ. Usually ω has a large value in mechanical systems, such that the impact duration is very short and the displacement of each ball changes very little on this period.

It may be interesting to study the limit cases for the 3-ball systems that should exhibit the phenomena of internal and sequential impacts defined by Han and Gilmore [29]. Let us set the mass ratio $\alpha = 1$, but change the value of the stiffness γ. In terms of the expression (5), the displacements before separation are

$$\begin{aligned} q_1(t) &= \frac{1}{3}t + \frac{1}{\alpha_1\,\omega}\left[\frac{1}{3} - \frac{1-2\gamma}{3\Delta}\right]\sin(\alpha_1\,\omega\,t) + \frac{1}{\alpha_2\,\omega}\left[\frac{1}{3} + \frac{1-2\gamma}{3\Delta}\right]\sin(\alpha_2\,\omega\,t) \\ q_2(t) &= \frac{1}{3}t - \frac{1}{\alpha_1\,\omega}\left[\frac{1}{6} - \frac{2-\gamma}{3\Delta}\right]\sin(\alpha_1\,\omega\,t) - \frac{1}{\alpha_2\,\omega}\left[\frac{1}{6} + \frac{2-\gamma}{3\Delta}\right]\sin(\alpha_2\,\omega\,t) \\ q_3(t) &= \frac{1}{3}t - \frac{1}{\alpha_1\,\omega}\left[\frac{1}{6} + \frac{1+\gamma}{3\Delta}\right]\sin(\alpha_1\,\omega\,t) - \frac{1}{\alpha_2\,\omega}\left[\frac{1}{6} - \frac{1+\gamma}{3\Delta}\right]\sin(\alpha_2\,\omega\,t) \end{aligned} \tag{13}$$

where Δ, α_1 and α_2 become $\Delta = 2\sqrt{\gamma^2 - \gamma + 1}$, $\alpha_1 = \sqrt{-\sqrt{\gamma^2 - \gamma + 1} + \gamma + 1}$, $\alpha_2 = \sqrt{\sqrt{\gamma^2 - \gamma + 1} + \gamma + 1}$. Let us consider the first case when $\gamma \to \infty$, from which we deduce that

$$\lim_{\gamma\to\infty} \Delta = 2\gamma,\ \lim_{\gamma\to\infty} \alpha_1 = 1,\ \lim_{\gamma\to\infty} \alpha_2 = \sqrt{2\gamma}$$

Obviously the last terms in expression (13) can be ignored due to $\alpha_2 \to \infty$. By setting $q_1(t_1) = q_2(t_1)$ and $q_2(t_2) = q_3(t_2)$, respectively, one can find

$$\sin(\alpha_1 \omega t_1) = \sin(\alpha_1 \omega t_2) = 0$$

This means t_1 and t_2 must converge to the same value π/ω, and the contacts among the three balls will break simultaneously. The final velocities (denoted with a superscript + to indicate the post-impact values) are therefore given by

$$\dot{q}_1^+ = -\tfrac{1}{3} \text{ m/s} \qquad \dot{q}_2^+ = \dot{q}_3^+ = \tfrac{2}{3} \text{ m/s} \tag{14}$$

So the phenomenon of internal impacts [29] can occur only when the stiffness between B_2 and B_3 is much greater than the one between B_1 and B_2. Now let us consider the case when $\gamma \to 0$ that will result in

$$\lim_{\gamma \to 0} \Delta = 2, \lim_{\gamma \to 0} \alpha_1 = 0, \lim_{\gamma \to 0} \alpha_2 = \sqrt{2}$$

The balls B_1 and B_2 will first separate at the instant $t_{\gamma \to 0} = \pi/(\sqrt{2}\,\omega)$ with the following velocities

$$\lim_{\gamma \to 0} \dot{q}_1(t_{\gamma \to 0}) = 0, \lim_{\gamma \to 0} \dot{q}_2(t_{\gamma \to 0}) = 1, \lim_{\gamma \to 0} \dot{q}_3(t_{\gamma \to 0}) = 0$$

After that, the balls B_2 and B_3 will continue to collide. Since the following collision is fully elastic, the balls will take the following final velocities when the multiple impact finishes:

$$\lim_{\gamma \to 0} \dot{q}_1^+ = 0 \text{ m/s}, \ \lim_{\gamma \to 0} \dot{q}_2^+ = 0 \text{ m/s}, \ \lim_{\gamma \to 0} \dot{q}_3^+ = 1 \text{ m/s} \tag{15}$$

This well coincides with the situation of sequential impacts given in [29]. So the two solutions given by Han and Gilmore are just two limit cases for stiffness ratio.

3 The multi-impact dynamics in multibody systems

Motivated by the theoretical results obtained by inserting a compliant contact model into the simple 3-ball system, some facts arising in multiple impacts should be paid attention: the duration of impacts is very small as ω is very high for a body that can be approximated as a rigid body. During such a short time the displacement of the system is almost zero, while the velocities vary abruptly. These facts allow us to make the assumption of a constant configuration during multiple impacts.

3.1 The Darboux-Keller impulsive differential equations

Pfeiffer and Glocker [9, 10] provide a general method to describe the kinematic constraints and impulsive equations during impacts. Here we will use their framework to establish the Darboux-Keller's model of frictionless multi-impact problems.

Let us consider a multibody body system with s frictionless contacts. The maximum number of degrees of freedom n is obtained when none of the contacts

is closed. In this state the system may be described by a set of generalized coordinates $\mathbf{q} \in R^n$, and the equations of motion take the form

$$\mathbf{M}(\mathbf{q})\ddot{\mathbf{q}} - \mathbf{h}(\mathbf{q}, \dot{\mathbf{q}}, t) - \sum_{i=1}^{s} \mathbf{w}_i(q)\lambda_i = 0 \tag{16}$$

where $\mathbf{M}(\mathbf{q})$ is a symmetric and positive-definite mass matrix, $\mathbf{h}(\cdot,\cdot,\cdot)$ contains the inertial and applied forces, and the sum relates to the contact forces. For each contact point i, λ_i is the scalar value of the normal contact forces along the common normal to the surfaces of the contacting bodies. The connection between normal contact forces and the generalized forces is defined by $\mathbf{w}_i(q)$, which is related to the Jacobian matrices of the contact points.

The kinematic state of a contact is determined by the distance $\delta_i(\mathbf{q}, t)$ between the contacting bodies. Clearly δ_i represents the normal elastic deformation when contact is established. The relative velocity of the contact points is expressed as

$$\dot{\delta}_i(\mathbf{q}, t) = \mathbf{w}_i^T(q, t)\dot{\mathbf{q}} + \hat{\mathbf{w}}_i(q, t) \tag{17}$$

where $\hat{\mathbf{w}}_i(q, t)$ is the nonlinear terms related to time, and often is zero if all constraints excluding contact are ideal and time invariant. The directions of the relative normal velocities depend on the contact kinematics as illustrated in [55], and we always define that $\dot{\delta}_i > 0$ for the colliding bodies approaching (compression phase), while $\dot{\delta}_i < 0$ for separation (expansion phase). In matrix notation, equations (16) and (17) become (we drop the arguments)

$$\mathbf{M}\ddot{\mathbf{q}} - \mathbf{h} - \mathbf{W}\lambda = 0 \tag{18}$$

$$\dot{\delta} = \mathbf{W}^T\dot{\mathbf{q}} + \hat{\mathbf{W}} \tag{19}$$

Let $[t_0, t_f]$ denote the time interval of the impact, which can be further divided into much smaller intervals $[t_i, t_{i+1}]$. According to the Darboux-Keller's model, an integration over $[t_i, t_{i+1}]$ has to be done in order to achieve a representation of the equations of motion at the impulse level. Thus a set of differential equations with respect to the normal impulses can be obtained:

$$\begin{aligned} \int_{t_i}^{t_{i+1}} [\mathbf{M}\ddot{\mathbf{q}} - \mathbf{h} - \mathbf{W}\lambda]dt &= \mathbf{M}[\dot{\mathbf{q}}(t_{i+1}) - \dot{\mathbf{q}}(t_i)] - \mathbf{W}[\mathbf{P}(t_{i+1}) - \mathbf{P}(t_{i+1})] \\ &= \mathbf{M} \cdot d\dot{\mathbf{q}} - \mathbf{W} \cdot d\mathbf{P} = 0 \end{aligned} \tag{20}$$

The terms $\mathbf{M}$, $\mathbf{W}$ remain unchanged during the integration thanks to the assumption of constant configuration q on $[t_0, t_f]$. The vector $\mathbf{h}$ consists of finite, nonimpulsive terms and therefore vanishes by the integration. The quantities $d\dot{\mathbf{q}}$ and $d\mathbf{P}$ are the changes of generalized velocities and normal impulses during $[t_i, t_{i+1}]$, respectively.

For the impacts with only one contact point, equation (20) can be thought of as a set of differential equations with respect to the normal impulse dP, that is an independent variable for the differential equation. Supposing that the collision is made of a compression phase followed by an expansion phase allows one to assert that the normal impulse $P(\cdot)$ is a strictly increasing function of time, and may be used as a new time scale. However, the length of the collision

process depends on the differential equations and must be determined using an energetical coefficient of restitution (or Poisson's one for a frictionless single impact) to consider the dissipation of energy. Firstly the quantity of the normal impulse during the compressional phase, P_c should be calculated by summing the increments of dP that correspond to the values from the beginning of the impact to the instant of normal velocity vanishing. Then the total normal impulse P_f is obtained by using the coefficient of restitution. This value can be used to define the length of the integration for the impulsive differential equations.

Unlike the single impact situation, the impact differential equations for multi-impact problems will have multiple normal impulses. It is obvious that these normal impulses are not independent quantities since $d\mathbf{P}$ represents the changes of normal impulses during the same interval of time. In other words, in order to make the impact differential equations of multiple impacts solvable, the distribution among the normal impulses that contains the wave effects should be discovered. However, no information for the distribution can be found in using fully rigid body models. Adding one way or the other some compliance effects at the contact points is necessary when dealing with multiple impacts.

3.2 Distributing rule for the normal impulses in a mono-stiffness model

We suppose that the force/indentation mapping at the contact point i is:

$$\lambda_i = K_i(\delta_i)^\eta \tag{21}$$

where K_i is the contact stiffness, the exponent η determine the kind of contacts between bodies ($\eta = \frac{3}{2}$ is for Hertz contact, $\eta = 1$ is linear elasticity). The variable δ_i is the normal elastic deformation, which is assumed to be only a function related to the generalized coordinates $\mathbf{q}$. Therefore, the term of $\hat{\mathbf{w}}_i$ in $\dot{\delta}_i$ equals zero in (17).

This force/indentation mapping is denoted as a *mono-stiffness model* since the ones for the compressional and expansional phases take an identical formulation. The energy loss at the contact point i will be constrained, as shown in the subsection §3.4, by a global index of the energetical coefficient of restitution.

Let $P_i(t)$ denote the total normal impulse accumulated during the time interval $[0, t]$: $P_i(t) = P_i(0) + \int_0^t \lambda_i(s)ds$. So $\frac{dP_i}{dt}(t) = \lambda_i(t)$ and:

$$\frac{d\lambda_i}{dt} = \frac{d\lambda_i}{dP_i} \cdot \frac{dP_i}{dt} = \lambda_i \frac{d\lambda_i}{dP_i} \tag{22}$$

In terms of the compliant model expressed by (21), we have

$$\frac{d\lambda_i}{dt} = \eta K_i(\delta_i)^{\eta-1}\dot{\delta}_i = \eta K_i(\delta_i)^{\eta-1}\mathbf{w}_i^T\dot{\mathbf{q}} \tag{23}$$

Notice that δ_i can always be expressed as

$$\delta_i = \left(\frac{\lambda_i}{K_i}\right)^{\frac{1}{\eta}} \tag{24}$$

Substituting (24) and (23) into (22) leads to

$$\lambda_i{}^{\frac{1}{\eta}} d\lambda_i = \eta K_i{}^{\frac{1}{\eta}} \mathbf{w}_i^T \dot{\mathbf{q}} dP_i \tag{25}$$

The initial value of the normal impulse can be set to $P_i(0) = 0$, and the static contact force before impact is $\lambda_i(0) = 0$ for the case without initial precompression energy. The integration of equation (25) leads to

$$\lambda_i(P_i(t)) = \left[(\eta+1)\int_0^{P_i(t)} K_i{}^{\frac{1}{\eta}}\mathbf{w}_i^T\dot{\mathbf{q}}dP_i\right]^{\frac{\eta}{\eta+1}} \tag{26}$$

Noticing that $\lambda_i = dP_i/dt$ and only considering the variation in space, the ratio of the changes of normal impulses at the contact points i and j can therefore be expressed as

$$\frac{dP_i}{dP_j} = \left(\frac{K_i}{K_j}\right)^{\frac{1}{\eta+1}}\left(\frac{\int_0^{P_i(t)}\mathbf{w}_i^T\dot{\mathbf{q}}dP_i}{\int_0^{P_j(t)}\mathbf{w}_j^T\dot{\mathbf{q}}dP_j}\right)^{\frac{\eta}{\eta+1}} \tag{27}$$

We should note that dP_i and dP_j are the variations of the normal impulses of the two contact points during the same time interval. Meanwhile, $P_i(t)$ and $P_j(t)$ are the accumulated normal impulses during the same time interval $[0, t]$. The work functions are defined as:

$$E_i = \int_0^{P_i(t)}\mathbf{w}_i^T\dot{\mathbf{q}}dP_i, \quad E_j = \int_0^{P_j(t)}\mathbf{w}_j^T\dot{\mathbf{q}}dP_j \tag{28}$$

It is easy to find that E_i and E_j are just the works done by the normal contact forces at contact points i and j from the beginning of impacts to the instant P_i (resp. P_j), in which the energy is mapped into the velocity-impulse level.

These terms can also be thought of as the potential energy stored in the springs at contact points i and j. During the compressional phase, the spring will transfer the kinetic energy of the contact point into potential energy, such that $E_{(\cdot)}$ increases with $P_{(\cdot)}$. Once the potential energy at contact point $(\cdot)$ is saturated due to $\dot{\delta}_{(\cdot)} = 0$, the expansion phase of the spring will begin to release the potential energy that have been stored, such that $E_{(\cdot)}$ will decrease with $P_{(\cdot)}$ and the kinetic energy is transferred. Clearly the exchange process between kinetic and potential energy will finish at the instant when $E_{(\cdot)} = 0$.

Remark *The integrands have to be understood as functions of the new time scale P_i. Let $P_i : t \mapsto P_i(t) \triangleq \tau$. For a given function of time $f : t \mapsto f(t)$, one gets $f(\tau) = f \circ P_i^{-1}(\tau)$, where the inverse function $P_i^{-1}(\cdot)$ exists by assumption. Therefore $\dot{\mathbf{q}}$ in (28) denotes a function of τ.*

Let us introduce the ratios of contact stiffness $\gamma_{ji} = K_j/K_i$, and define

$$E_{ji} \triangleq \frac{E_j}{E_i} = \frac{\int_0^{P_j(t)}\mathbf{w}_j^T\dot{\mathbf{q}}dP_j}{\int_0^{P_i(t)}\mathbf{w}_i^T\dot{\mathbf{q}}dP_i} \geq 0, \quad (j = 1, 2, \ldots, s, j \neq i) \tag{29}$$

to represent a ratio of the energies stored at the contact points i and j. During the same time, the relationship between dP_i and the changes of normal impulses at other contact points can be expressed using (27) and (29) as

$$dP_j = \gamma_{ji}{}^{\frac{1}{\eta+1}}(E_{ji}(P_i, P_j))^{\frac{\eta+1}{\eta}}dP_i, \quad j = 1, 2, \ldots, s, j \neq i \tag{30}$$

It is noteworthy that the above expressions are deduced from the force/identation mapping at the contact points and represent the dynamical conditions for the increments of normal impulses in space. In other words, if the normal impulse at contact point i increases with a value of dP_i at a certain time, the normal impulses at other contact points during the same time interval must change to the new values satisfying the relationships (30). Obviously these expressions reflect the wave behaviors generated in multiple impacts and depend only on the properties of the contact constraints: *the relative stiffness and the relative potential energies accumulated in the contact points*. Since the potential energy at contact points will change during impacts, the assumption that the distribution of normal impulses are constant (as stated in [12] by defining a constant ICR) is invalid in most cases. As indicated in [42, 61], the wave effects are due to the elastic properties of the bodies, though, as we shall see later, the local dissipations at the contacts may influence them.

3.3 The selection for the independent variable

Combining the distributing relationships (30) with the Darboux-Keller's model (20), it is obvious that the impulsive equations (20) can be expressed as a set of first order differential equations with respect to a single integral variable related to the normal impulse P_i.

A problem arising when solving the first order differential equations is which normal impulse among all the contact points can be selected as a "time-like" independent variable. Since all normal impulses are monotonously increasing for the points keeping contact, in principle any one among all the normal impulses can be taken as the independent variable. However, inappropriate selection for the independent variable will result in certain numerical difficulties. For instance, if the normal impulse at the contact point with little potential energy is selected as the independent variable, it is clear from (30) that the little change of the independent variable will make the normal impulses at other contact points vary abruptly. In order to avoid the numerical difficulties and respect the physical meaning that the multiple impacts should be dominated by the contact point that takes the maximum value of energy, we present a guideline for the selection of the independent variable. If the energy at contact point i satisfies

$$E_i \geq E_j, \quad j = 1, 2, \ldots, s, j \neq i$$

then the normal impulse corresponding to this contact point can be selected as the independent variable. We denote it as the *primary colliding point*. Since the energy among contact points is transferred and exchanged during impacts, the primary colliding point may change from one contact point to another during the integration process. It is also noteworthy that in some cases there may be several possible candidates for the primary colliding point (when equality holds). There is no strict limitation for the selection of the primary impulse when E_i and E_j are near the same value for some i and j. The Bernoulli's system treated in section 7 exhibits such a situation, as the two contact points may have the same energy. In a linear chain of balls in which a solitary wave is produced by the impact, the primary colliding point corresponds to a peak in the acceleration wave (and to a minimum of the velocity wave since a peak in the velocity wave

corresponds to a maximum of kinetic energy, and consequently to a minimum of potential energy).

Once the primary colliding point is determined, the impulse related to this point can be considered to increase monotonously like the time variable. The normal impulses at other contact points will increase according to the relationship (30).

At the beginning of impacts, a problem will arise for the selection of the independent variable since no energy is stored at any contact point. This corresponds to a singular point in the simulation. Let us denote $\triangle P_i(1)$ and $\triangle P_j(1)$ the possible increments of the normal impulses. $\dot{\delta}_i^0$ and $\dot{\delta}_j^0$ are the initial relative velocities at the contact points i and j. In terms of (27) and (17), we have

$$\frac{\triangle P_i(1)}{\triangle P_j(1)} = \left(\frac{K_i}{K_j}\right)^{\frac{1}{\eta+1}} \left(\frac{\dot{\delta}_i^0 \triangle P_i(1)}{\dot{\delta}_j^0 \triangle P_j(1)}\right)^{\frac{\eta}{\eta+1}} \tag{31}$$

This form can be further simplified to

$$\frac{\triangle P_i(1)}{\triangle P_j(1)} = \frac{K_i}{K_j} \left(\frac{\dot{\delta}_i^0}{\dot{\delta}_j^0}\right)^{\eta} \tag{32}$$

Obviously, the impact behaviors will be firstly dominated by the contact point at which the relative velocity takes the maximum value. Therefore, the normal impulse at this point can be selected as the initial independent variable. The normal impulses at other contact points will vary with the independent variable in terms of the expression (32).

Substituting expressions (32) or (30) into (20) leads to a set of differential equations with respect to the independent variable dP_i. This is a strongly nonlinear differential equation since E_{ij} varies during the impact process, and the selection procedure is $E_{ij} \geq 1$. Usually an analytical result is hard to obtain, and numerical methods by discretizing the equations about the normal impulse P_i should be applied in order to obtain the solutions.

3.4 Energetical constraint for the local energy loss

The strong interactions between contacting points usually dissipate a part of the energy that cannot be recovered by the expansion phase. During a contact process with a single compression/expansion circle, the compression phase will transfer the external kinetic energy into the potential energy of spring (the elastic deformable potential of the colliding bodies), while the expansion phase will make the deformable energy be released into the kinetic energy of the colliding bodies. For the colliding bodies that can be well approximated by rigid body models, the input/output relationship between kinetic and potential energies will mainly depend on the contact properties. The energetical coefficient e_s establishes a relationship between the input and output energies. Based on the FEM results and theoretical analysis [13, 49, 6], this relationship is usually nonlinear, and can be approximately linear when e_s is taken a constant value. For the colliding bodies made of materials without viscosity, the dissipation is mainly due to the plastic deformation at the local contact region [53]. So the energetical coefficient can always be expressed as a function with respect

to the work done by the contact force during compression phase (the potential energy stored in elastic deflection) [49, 6]. Then, we can use e_s as an energetical constraint to define the local energy loss.

According to the definition given by Stronge [6] and his predecessors like Routh and Boulanger (see [5, p.147]), the energetic constraint $e_{s,j}$ is given by:

$$e_{s,j}^2 = -\frac{W_{r,j}}{W_{c,j}} = -\frac{\int_0^{P_j(t_c)} \dot{\delta}_j dP_j}{\int_{P_j(t_c)}^{P_j(t_f)} \dot{\delta}_j dP_{Nj}} = -\frac{\int_0^{P_j(t_c)} \mathbf{w}_j^T \dot{\mathbf{q}} dP_j}{\int_{P_j(t_c)}^{P_j(t_f)} \mathbf{w}_j^T \dot{\mathbf{q}} dP_j} \tag{33}$$

where $W_{c,j} \geq 0$ and $W_{r,j} \leq 0$ are the works done by the normal contact force at point j during the compression phase $[0, t_c]$ and the expansion phase $[t_c, t_f]$, respectively. Obviously $W_{c,j}$ also corresponds to the potential energy accumulated during the compression phase, and can be obtained by summing the scalar product of dP_j and $\dot{\delta}_j(dP_j)$ from the beginning of the impact to the instant of $P_j(t_c)$ that corresponds to $\dot{\delta}_j(t_c) = 0$. Thus

$$P_j(t_c) = \int_0^{t_c} dP_j, \qquad \dot{\delta}_j(P_j(t_c)) = 0 \tag{34}$$

and

$$W_{c,j} = \int_0^{P_j(t_c)} dP_j \dot{\delta}_j(P_j), \qquad \dot{\delta}_j(P_j(t_c)) = 0 \tag{35}$$

If the contact point j is the primary colliding point, dP_j defines the size of the numerical step. Otherwise, dP_j is calculated by the distributing rule in (30).

The time t_c can be thought of as an instant of the potential energy saturated. After that, the potential energy will be transferred into the kinetic energy through the expansion phase. Since $e_{s,j}$ can always be identified off-line (as a function of $W_{c,j}$), the total recovered energy $W_{r,j}$ can be determined by $e_{s,j}$ and $W_{c,j}$. For instance, $W_{r,j}$ equals $W_{c,j}$ for fully elastic impact, and $W_{r,j} = 0$ for plastic impact. At any instant during the compression phase $P_j(t)$, the residual energy equals

$$E_j = \int_0^{P_j(t)} dP_j \dot{\delta}_j(P_j). \tag{36}$$

When $P_j(t)$ is located in the expansion phase, E_j is

$$E_j = \int_0^{P_j(t_c)} dP_j \dot{\delta}_j(P_j) + \int_{P_j(t_c)}^{P_j(t)} dP_j \dot{\delta}_j(P_j). \tag{37}$$

Since $\dot{\delta}_j$ is continuous and equal to $\mathbf{w}_j^T \dot{\mathbf{q}}$, the expressions (36) and (37) can always take the same form as in (28), and represent the potential energy stored at the contact point j. If the normal impulse reaches the instant of $P_j(t_f)$ satisfying

$$E_j(P_j(t_f)) = W_{c,j} - W_{r,j} = W_{c,j}(1 - e_{s,j}^2) \tag{38}$$

the process of energy transfer at contact point j will finish as the residual potential energy $E_j(P_j(t_f))$ will be dissipated based on the energetical constraint expressed by (33). At this time, the outcome of the post-impact velocities at this contact point can be obtained if it doesn't again participate into impacts, and all the ones related to the termination of multiple impacts can be determined when all the accumulated energy is completely released.

Remark *The contact model expressed in (21), denoted as mono-stiffness model, takes the same force/indentation relationships for the compression and expansion phases, in which the energetical constraint is not satisfied. So there is some residual energy $E_j(P_j(t_f))$ to be discarded at the end of the contact in order to respect the fact of dissipation in the energetical sense. Physically speaking, the energy loss should be consistent with the contact model. A bi-stiffness contact model that satisfies the energetical constraint will be illustrated in the next section.*

Due to the time-variable characteristic of the multi-impact problems, some complex situations may appear in the process. For example, the contact point may experience multiple compression/expansion phases due to the interactions between contact points [1]. I.e., the relative velocity $\dot{\delta}_j$ may change from $\dot{\delta}_j < 0$, related to an expansion phase, to $\dot{\delta}_j > 0$ that corresponds to a new compressional phase. We denote this as the *multiple compressional phenomenon*. In this case, before all the potential energy $W_{c,j}$ is transferred into the kinetic energy (the kinetic energy that can be transformed is equal to $W_{r,j}$), the contact point may experience a new compression phase to absorb the external kinetic energy. Let us denote the beginning of the new expansion phase appearing at the instant P_j^*, in which

$$E_j(P_j^*) = E_j^* > E_j(P_j(t_f)) = (1 - e_j^2)W_{c,j}, \;\; \dot{\delta}_j(P_j^*) = 0 \tag{39}$$

During the new compressional phase E_j will increase again and obtain a new value of $E_j(P_j^{**})$ at the instant of $P_j^{**} = P_j(t_{**})$, in which $\dot{\delta}_j(P_j^{**}) = 0$. We can put the energetical constraint $e_{s,j}$ on the potential energy $E_j(P_j^{**})$ to define the kinetic energy $W_{c,j}^{**}(P_j^{**})$, that will be recovered during a new expansion phase. In other words, if

$$E_j(P_j(t_f^*)) = (1 - e_j^2)W_{c,j}^{**} \tag{40}$$

the impact at contact point j finishes at the instant $P_j(t_f^*)$.

Remark *When the force/indentation relationship in (21) is used, it is obvious that $e_{s,j}$ cannot constrain the energy loss appearing in the first compression phase. This flaw can be overcome by using the bi-stiffness compliant model in the next section.*

[1] Interestingly enough such phenomena have also been noticed for single-impacts with Coulomb friction [41].

Another interesting phenomenon can also be found in the process of multiple impacts. At the same contact point, bodies will participate again into impacts after separation. We denote this case as a *repeating impact*. Obviously, a new process of energy accumulation and transfer will appear at that point, and the energetical constraints can be applied on each isolated impact based on the potential energy obtained from the compression phases.

3.5 Summary and comments

Let us provide a compact formulation for the analysis procedure of multi-impact problems. The multi-impact dynamics is summarized as follows:

- Contact parameters: γ_{ij}, $e_{s,j}$, $1 \le i \le m$, $1 \le j \le m$, η ($= 1$ or $= \frac{3}{2}$, or other values).
- Dynamical equation:

$$M\frac{d\dot{\mathbf{q}}}{dP_i} = W\frac{dP}{dP_i} \text{ if } E_{ji}(P_j, P_i) \le 1 \text{ for all } j \ne i \tag{41}$$

with

$$\frac{dP_j}{dP_i} = \gamma_{ji}^{\frac{1}{\eta+1}} \left(E_{ji}(P_j, P_i)\right)^{\frac{\eta+1}{\eta}} \tag{42}$$

$$E_{ji} = \frac{E_j(P_j)}{E_i(P_i)}, \ 1 \le i \le m, \ 1 \le j \le m \tag{43}$$

$$E_j(P_j) = \int_0^{P_j(t)} \mathbf{w}_j^T \dot{\mathbf{q}} dP_j, \ W_{r,j} = \int_0^{P_j(t_c)} \mathbf{w}_j^T \dot{\mathbf{q}} dP_j, \ W_{c,j} = \int_{P_j(t_c)}^{P_j(t_f)} \mathbf{w}_j^T \dot{\mathbf{q}} dP_j \tag{44}$$

and the time t_c at the contact j is calculated from $\dot{\delta}_j(t_c) = 0$, while t_f is calculated from the energy constraint $W_{r,j} = -e_{s,j}^2 W_{c,j}$.

Remark *The solution of the above set of ODEs is the function* $\dot{\mathbf{q}}(\tau) = \dot{\mathbf{q}} \circ P_i(t)$ *on the intervals where* P_i *is the dominant impulse. It is denoted as the derivative of the position for obvious reasons, however it is to be considered as the solution of this particular set of differential equations since the energy is mapped into the velocity-impulse level. The assumption of the position being constant is conducted for equation (41), and the infinitesimal time interval for the impact duration is adopted for the calculation of the outcomes of the post-velocities.*

Comments: Multiple impacts will make the energy of systems transfer and propagate among the contact points excluding the dissipation. So two significant scenarios should be well reflected in dealing with the multi-impact problems: *one that is the wave effects due to the coupling between various contacts, the other that is the description for dissipating energy.* If colliding bodies can be well approximated by rigid bodies models, the multi-impact process will only depend on the constitutive relationship of the compliance inserted at the contacts. The wave effects are reflected by the distributing law and the local energy loss is constrained by the energetical coefficient. The inconsistence between energy and

the force/indentation relationship can be overcome by modifying the compliant contact model. One advantage of this method is that the wave effects can be analyzed in the energetical sense and some small scales such as the elastic deformation can be avoided. In summary the approach which is presented in this paper brings a positive answer to the above items (4)-(10) and (12)-(14).

4 The distributing rule for the compliant contact model satisfying an energetical constraint

The distributing rule presented in section 3 is based on the assumption that the compressional and expansion phases satisfy the same relationship between the contact forces and the indentation. The energetical coefficient is applied as a global constraint in the energetic consideration to take into account the local dissipation of energy. Usually we should use two different modes of the contact forces to represent the compressional and expansion phases, respectively, such that the dissipated energy can be involved in the compliant contact model. In this section, we will adopt a compliant contact model that satisfies the definition in (33) to discuss the distributing rule.

4.1 The compliant contact model

Based on experimental results, Lankarani and Shivaswamy [22, 21] constructed a compliant contact model to represent the relationship between the contact force and indentation for the compression and expansion phases, respectively. Their model lacks of fundamental mechanical meaning as no material seems to satisfy such laws, however it has been proved to be quite useful in various contexts of impact dynamics [6, 66]. This bilinear model is the simplest means of representing plastic deformation. It has certain drawbacks such as not limiting maximal force. Nevertheless, it gives correct form of dissipation for rate-independent materials. It is not supposed to accurately represent any real material, and may be seen as a crude representation of the plastic indentation effect in elastic solids [53, §6.4]. Figure 2 shows the bi-stiffness compliant contact model by setting different force/indentation relationships for the expansion and compression phases. The relationship for the compression phase at the contact point j is expressed as

$$\lambda_{c,j} = K_j(\delta_{c,j})^\eta \tag{45}$$

and the one for expansion phase is

$$\lambda_{e,j} = \lambda_{m,j}\left(\frac{\delta_{e,j} - \delta_{r,j}}{\delta_{m,j} - \delta_{r,j}}\right)^\eta \tag{46}$$

where $\delta_{r,j}$ is the plastic deformation, and $\lambda_{m,j}$ and $\delta_{m,j}$ correspond to the maxima of the normal contact force and normal deformation at the end of the compression phase, which corresponds to the values when $\dot{\delta}_j = 0$. Clearly the dissipated energy is just the area enclosed by the compression and expansion curves. In addition, we use different symbols to represent the variables of contact force and deformation during compression and expansion phases in order to

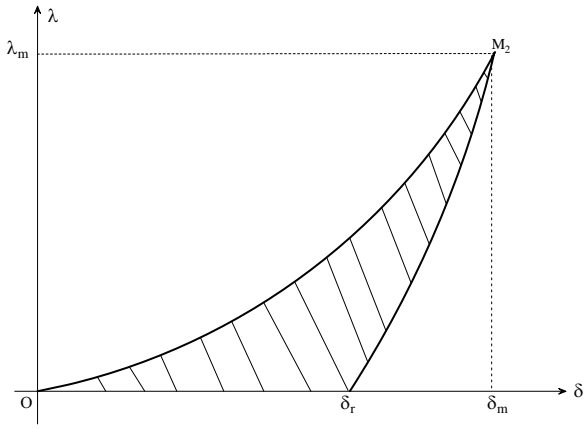

Figure 2: The bi-stiffness compliant contact model

clearly indicate the states of the compliant model. For simplicity we omit the subscript j in the following expressions (and also in Figure 2).

The scalar δ_r represents the permanent plastic deformation generated when the compressional phase finishes. Its value should depend on the dissipated energy at the contact point, such that the energetical constraint should be applied (in [22], the Newton's coefficient is adopted as the constraint condition). Let us first make an assumption for the contact processes:

- (a) the local dissipated energy is due to the plastic deformation at the contact points,
- (b) there is no other initial energy than the external kinetic energy.

The external kinetic energy will be completely absorbed by the work W_c done by the contact force during the compression phase, and the recovered kinetic energy after impact is related to the work done by the contact force during the expansion phase, W_r. Integration of expressions (45) and (46) leads to

$$\begin{aligned} W_c &= \int_0^{\delta_m} \lambda_c(\delta_c) d\delta_c = \frac{1}{\eta+1} K_j (\delta_m)^{\eta+1} \\ W_r &= \int_{\delta_m}^{\delta_r} \lambda_e(\delta_e) d\delta_e = -\frac{1}{\eta+1} K_j (\delta_m)^{\eta} (\delta_m - \delta_r) \end{aligned} \tag{47}$$

Based on the assumption in (33), W_c and W_r can be connected by a function $e_s = f(W_c)$. In the case of a constant e_s, we have from (47) and (33)

$$\delta_r = \delta_m (1 - e_s^2) \tag{48}$$

The indentation δ_m corresponds to the first instant t_c such that $\dot{\delta}(t_c) = 0$, so it is not a parameter of the impact dynamics. From (48) neither is δ_r. When the energetic coefficient takes a constant value, the energetical definition presents a linear relationship between the local plastic deformation δ_r and the maximum indentation δ_m, such that the dissipation of energy is reflected in an average level.

4.2 The potential energy at a contact point

The potential energy at a contact point will be accumulated during the compression phase and released in the expansion phase. Let us pick a point p in the curve of the compression phase. The potential energy E_p at p is equal to the work done by the contact force along the path $\widehat{Op}$.

$$E_p(\delta^p) = \int_0^{\delta^p} \lambda_c(\delta) d\delta \tag{49}$$

Let us assign a time factor on the compression process. δ^p denotes the deformation when the contact point moves along the routine $\widehat{Op}$ to the point p within a time interval $[0, t]$. This means that at any instant τ during the interval $[0, t]$, $\lambda_c(\tau)$ can always be expressed as $\lambda_c(\tau) = \frac{dP(\tau)}{d\tau}$, in which $P(\tau)$ is the normal impulse accumulated in the time interval $[0, \tau] \subset [0, t]$ corresponding to a deformation $\delta(\tau)$. Thus, we have

$$E_p(\delta^p) = \int_0^{\delta^p} dP(\tau) \frac{d\delta(\tau)}{d\tau} \tag{50}$$

Since $P(\tau)$ and $\delta(\tau)$ can be connected by a one-to-one mapping during the compression phases, we can use the variable $P(\tau)$ to replace $\delta(\tau)$ as the integral variable. Thus,

$$E_p = \int_0^{P(t)} \dot{\delta}_j(P(\tau)) dP(\tau) \tag{51}$$

where $P(t)$ is the normal impulse that is needed to make the indentation change from zero to δ^p by obeying the relationship (45).

The accumulation of energy at the contact point j will be ended when the compression process finishes. After that the potential energy will be released through an expansion phase. Let us select a point R in the curve of expansion phase $\widehat{M\delta_{r2}}$ as shown in Figure 3. The work done by the contact force along the compression routine $O \mapsto M$ can be expressed as

$$W_c(\delta_M) = \int_0^{\delta_M} \lambda_c(\delta) d\delta \tag{52}$$

This term is related to the potential energy accumulated in the compression phase, and corresponds to the area enclosed by the curve $O\widehat{M\delta}_M$. The total energy that can be recovered through the expansion phase is $e_s^2 W_c$ based on the energetic constraint and is associated with the area enclosed by the curve $\delta_{r2}\widehat{M\delta}_M$.

When the contact point j moves from M to R along the expansion curve, the recovered energy is $\int_{\delta_M}^{\delta_R} \lambda_r(\delta) d\delta$, where δ_R is the deformation related to the contact force λ_R.

$$\int_{\delta_M}^{\delta_R} \lambda_r(\delta) d\delta = \int_{\delta_M}^{\delta_{r2}} \lambda_r(\delta) d\delta - \int_{\delta_R}^{\delta_{r2}} \lambda_r(\delta) d\delta = -e_s^2 \int_0^{\delta_M} \lambda_c(\delta) d\delta - \int_{\delta_R}^{\delta_{r2}} \lambda_r(\delta) d\delta \tag{53}$$

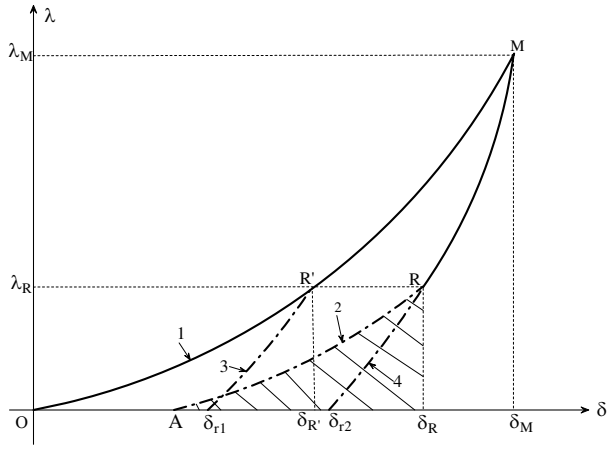

Figure 3: The potential energy when contact point is located at expansion phase.

The second term in expression (53) just equals the area enclosed by the curve $\delta_{r2}\widehat{R\delta}_R$. Let us determine the value of the potential energy E_R when the contact point is located at R, which should make the expansion force to generate the work with the value equal to the area enclosed by the curve $\delta_{r2}\widehat{R\delta}_R$, such that the contact point can move from R to δ_{r2} along the expansion curve. The following result is based on the properties of the contact force and the energetic constraint and deals with the residual energy.

Theorem: *When the contact point is expanded from M to reach the position R, the residual potential energy E_R at this point is equal to the work done by the contact force along the compression routine moving from O to the position R', in which the contact force takes the same value λ_R as the one in position R.*

Proof: Let us select a point R' in the compression curve to make the contact force with the same value λ_R as the one at position R. The elastic deformation at R' is δ'_R. If the compression phase stops at R', the contact point will be expanded along the routine $\widehat{R'\delta_{r1}}$. From (46) and (48), the contact force λ_3 along the expansion curve 3 can be expressed as

$$\lambda_3 = \lambda_R \left(\frac{\delta_3 - \delta_{r1}}{\delta_{R'} - \delta_{r1}} \right)^{\eta} = \lambda_R \left(\frac{\delta_3 - \delta_{r1}}{e_s^2 \delta_{R'}} \right)^{\eta} \tag{54}$$

Because $\widehat{R\delta_{r2}}$ is a piece of the expansion phase related to the compression phase $\widehat{OM}$, the expansion force λ_4 of any point in $\widehat{R\delta_{r2}}$ can be expressed as

$$\lambda_4 = \lambda_M \left(\frac{\delta_4 - \delta_{r2}}{\delta_M - \delta_{r2}} \right)^{\eta} = \lambda_M \left(\frac{\delta_4 - \delta_{r2}}{e_s^2 \delta_M} \right)^{\eta} \tag{55}$$

The expression (45) for the compression mode yields the following relationship

$$\frac{\lambda_R}{\lambda_M} = \left(\frac{\delta_R}{\delta_M} \right)^{\eta} \tag{56}$$

For the identical expansion forces, i.e. $\lambda_3 = \lambda_4$, we can therefore obtain

$$\frac{\lambda_R}{\lambda_M} = \left(\frac{\delta_R}{\delta_M}\right)^{\eta} \left(\frac{\delta_1 - \delta_{r1}}{\delta_2 - \delta_{r2}}\right)^{\eta} \tag{57}$$

i.e.

$$\delta_3 - \delta_{r1} = \delta_4 - \delta_r \tag{58}$$

This means that the curve $\widehat{R'\delta_{r1}}$ is parallel to the curve $\widehat{R\delta_{r2}}$. This property is provided by the compliant contact model to guarantee the permanent plastic deformation with a constant value during the expansion phase. Thus we have that the area $S_{\delta_{r1}\widehat{R'\delta_{R'}}}$ is equal to the area $S_{\delta_{r2}\widehat{R\delta_R}}$. So using (33)

$$S_{\delta_{r1}\widehat{R'\delta_{R'}}} = S_{\delta_{r2}\widehat{R\delta_R}} = \frac{1}{e_s^2} S_{O\widehat{R'\delta_{R'}}} \tag{59}$$

The expression in (59) illustrates that the energy provided by a compression phase through a routine $\widehat{OR'}$ can output the work done by the expansion force along the routine $\widehat{R\delta_{r2}}$. In other words, the residual energy E_R equals the work done by the compression force along $\widehat{OR'}$.

The theorem indicates that the work done by the expansion force from R to δ_{r2} can be expressed as

$$\int_{\delta_R}^{\delta_{r2}} \lambda_r(\delta) d\delta = -e_s^2 E_R \tag{60}$$

Substituting (60) into (53) leads to

$$E_R = \int_0^{\delta_M} \lambda_c(\delta) d\delta + \frac{1}{e_s^2} \int_{\delta_M}^{\delta_R} \lambda_r(\delta) d\delta \tag{61}$$

Similar to the compression phase, the residual potential energy for a dynamical process reaching the position R within a time interval $[0, t]$ can be expressed as

$$E_R = \int_0^{P_c} \dot{\delta}(P(\tau)) dP(\tau) + \frac{1}{e_s^2} \int_{P_c}^{P_t} \dot{\delta}(P(\tau)) dP(\tau) \tag{62}$$

where P_c is the normal impulse when the compression phase finishes (so $\delta = \delta_M$), $P(\tau)$ is an integral variable that is related to the normal impulse of the contact force experiencing a time interval $[0, \tau]$ by obeying the energetic relationship defined by the compliant contact model.

Remark: *Unlike the mono-stiffness compliant contact model in which the coefficient e_s is applied at the end of the impact to constrain the local energy loss, the expansion phase in the bi-stiffness compliant model will be constrained by the local loss of energy generated in the compression phase. So the form of (62) for the calculation of the residual potential energy is different from the one of (37) in section 3.*

4.3 The energetic constraint for the complex impact

In some cases, the contact point may take some initial energy due to the pre-compression or the experience of a complex process with multiple compression phases because of the coupling between the contact points. In a physical sense it is obvious that the dissipated energy should depend on the energy stored at the contact points. Here, we will extend the energetical coefficient e_s into the situations where the contact point has some initial energy, or is experiencing multiple compression phases.

Let us assume that the contact point j has an initial pressure λ_0 that makes the contact point with an initial energy E_0 and an initial deformation δ_0. Furthermore, we suppose that λ_0 and δ_0 satisfy the compression relationship expressed in (45). Then integration yields:

$$E_0 = \int_0^{\delta_0} \lambda_c(\delta) d\delta = \frac{(\lambda_0)^{\frac{\eta+1}{\eta}}}{(\eta+1)K_j^{\frac{1}{\eta+1}}} \geq 0 \tag{63}$$

Under the initial pressure, the energetical constraint is defined as follows:

$$W_r = -e_s^2(W_c + E_0) \tag{64}$$

where $W_r = \int_{\delta_m}^{\delta_r} \lambda_e(\delta) d\delta$ is the work done by the expansion force, and $W_c = \int_{\delta_0}^{\delta_m} \lambda_c(\delta) d\delta$ is the work done by the compression force.

Involving the initial potential into the energetic constraint permits to use the coefficient e_s as the index to describe the local dissipated energy for the contact point with multi-compression phases.

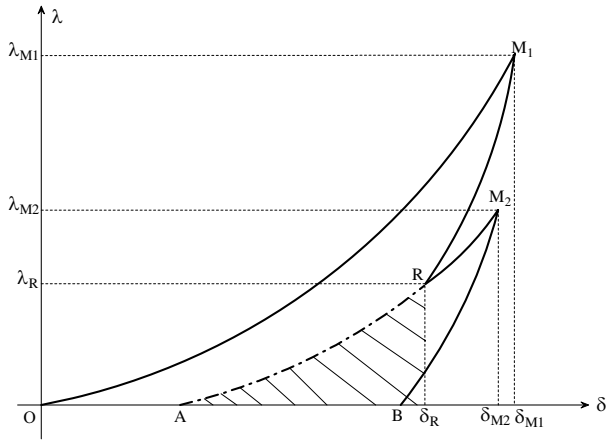

Figure 4: The contact point with two compression phases.

Let us present a clear scenario by conducting an example of the contact point j with two compression phases. Figure 4 shows that the contact point j will first experience a compressional phase along the curve $\widehat{OM_1}$, then begin an expansion process from M_1 to R. Before the total potential energy is released, a new compression phase starts at R, and the contact point will begin a second compressional phase along the curve $\widehat{RM_2}$. This second compression phase stops

at M_2, and then the accumulated potential will be completely released through an expansion phase along the curve $\widehat{M_2B}$.

Let us assume that the relationship between the contact force and the indentation is not changed for the second compression/expansion cycle. Therefore, the residual potential E_R at R can be thought of as an initial energy for a new compression/expansion cycle. So from (64) we get:

$$W_r = -e_s^2(W_c + E_R) \tag{65}$$

The energy E_R can be obtained by using (61) or (62), and

$$W_r = \int_{\delta_{M_2}}^{\delta_B} \lambda_e(\delta)d\delta, \;\; W_c = \int_{\delta_R}^{\delta_{M_2}} \lambda_c(\delta)d\delta \tag{66}$$

Let us set a time interval $[0, t]$ on the micro-movement of the contact point, and replace t by $P(t) = \int_0^t \lambda(\tau)d\tau \geq 0$. The potential energy at Q in different phases can be expressed as

$$E(P(t)) = \begin{cases} E_0 + \displaystyle\int_0^{P(t)} \dot{\delta}(P(\tau))dP(\tau), \;\; Q \in \widehat{OM_1} \\ E_{M_1} + \dfrac{1}{e_s^2}\displaystyle\int_{P_{M_1}}^{P(t)} \dot{\delta}(P(\tau))dP(\tau), \;\; Q \in \widehat{M_1R} \\ E_R + \displaystyle\int_{P_R}^{P(t)} \dot{\delta}(P(\tau))dP(\tau), \;\; Q \in \widehat{RM_2} \\ E_{M_2} + \dfrac{1}{e_s^2}\displaystyle\int_{P_{M_2}}^{P(t)} \dot{\delta}(P(\tau))dP(\tau), \;\; Q \in \widehat{M_2B} \end{cases} \tag{67}$$

where $E_{(\cdot)}$ and $P_{(\cdot)}$ are the residual potential energy and the normal impulse at the location $(.) = M_1, R, M_2$, respectively.

4.4 The distributing rule for the bi-stiffness compliant contact model

Since the compression and expansion forces adopt different relationships, we should separately analyze the evolution of energy during the compression and the expansion phases. Let us suppose that the initial pressure at the contact point j is $\lambda_{0,j}$, such that at the beginning of the impact process the point will take the initial energy $E_{0,j}$, given by (63). Based on (26) and setting $\lambda_j(0) = \lambda_{0,j}$, we can obtain:

$$\begin{aligned} \lambda_j(P_j(t)) \;\; &= (1+\eta)^{\frac{\eta}{\eta+1}} K_j^{\frac{1}{\eta+1}} \left(\frac{(\lambda_{0,j})^{\frac{\eta+1}{\eta}}}{(\eta+1)K_j^{\frac{1}{\eta+1}}} + \int_0^{P_j(t)} \dot{\delta}_j(P_j(\tau))dP_j(\tau) \right)^{\frac{\eta}{\eta+1}} \\ &= (1+\eta)^{\frac{\eta}{\eta+1}} K_j^{\frac{1}{\eta+1}} \left(E(P_j(t))\right)^{\frac{\eta}{\eta+1}} \end{aligned} \tag{68}$$

where $E(P_j(t))$ takes the form of the first term in (67).

In terms of the compliant model expressed in (46) for the expansion force, we can deduce

$$\lambda_{e,j}d\lambda_{e,j} = \eta\lambda_{m,j}\left(\frac{\delta_j - \delta_{r,j}}{\delta_{m,j} - \delta_{r,j}}\right)^{\eta-1} \frac{\dot{\delta}_j}{\delta_{m,j} - \delta_{r,j}}dP_j \tag{69}$$

Since $\delta_{m,j} - \delta_{r,j} = e_{s,j}^2 \delta_{m,j}$, and

$$\frac{\delta_j - \delta_{r,j}}{\delta_{m,j} - \delta_{r,j}} = \left(\frac{\lambda_{e,j}}{\lambda_{m,j}}\right)^{\frac{1}{\eta}} \tag{70}$$

Expression (69) can be further simplified as

$$(\lambda_{e,j})^{\frac{1}{\eta}} d\lambda_{e,j} = \eta (\lambda_{m,j})^{\frac{1}{\eta}} \frac{\dot{\delta}_j}{e_{s,j}^2 \delta_{m,j}} dP_j \tag{71}$$

At the end of the compression phase, the maximum compression force $\lambda_{m,j}$ can always be expressed as

$$\lambda_{m,j} = K_j (\delta_{m,j})^{\eta} \tag{72}$$

So,

$$(\lambda_{e,j})^{\frac{1}{\eta}} d\lambda_{e,j} = \frac{1}{e_{s,j}^2} \eta \, (K_j)^{\frac{1}{\eta}} \, \dot{\delta}_j dP_j \tag{73}$$

The initial value of the normal impulse at the beginning of the expansion phase is set as $P_{c,j}$ that is related to $\dot{\delta}_j = 0$. The contact force at this instant $\lambda(P_{c,j})$ can be obtained by (68)

$$\lambda(P_{c,j}) = (1+\eta)^{\frac{\eta}{\eta+1}} \, K_j^{\frac{1}{\eta+1}} \, (E(P_{c,j}))^{\frac{\eta}{\eta+1}} \tag{74}$$

Integration of (73) and using (74) leads to

$$\begin{aligned} (\lambda_{e,j})^{\frac{\eta+1}{\eta}} &= (\lambda(P_{c,j}))^{\frac{\eta+1}{\eta}} + (\eta+1) \, (K_j)^{\frac{1}{\eta+1}} \, \tfrac{1}{e_{s,j}^2} \textstyle\int_{P_{c,j}}^{P_j(t)} \dot{\delta}_j dP_j \\ &= (\eta+1) \, (K_j)^{\frac{1}{\eta+1}} \left(E_j(P_{c,j}) + \tfrac{1}{e_{s,j}^2} \textstyle\int_{P_{c,j}}^{P_j(t)} \dot{\delta}_j dP_j) \right) \\ &= (\eta+1) \, (K_j)^{\frac{1}{\eta+1}} \, E_j(P_j(t)) \end{aligned} \tag{75}$$

Thus, the contact force at the impulse instant $P_j(t)$ is

$$\lambda_{e,j} = (1+\eta)^{\frac{\eta}{\eta+1}} \, K_j^{\frac{1}{\eta+1}} \, (E_j(P_j(t)))^{\frac{\eta}{\eta+1}} \tag{76}$$

Remark: *The expressions (68) and (76) indicate that all the contact forces in compression or expansion phases can take the form of a function with respect to the potential energy.*

Since the contact forces can always be expressed as the differential of the normal impulse with respect to time, from (76) the ratios between the increments of normal impulses among various contact points j can be expressed as in (42), i.e.:

$$\frac{dP_i}{dP_j} = \gamma_{ij}^{\frac{1}{\eta+1}} (E_{ij}(P_i, P_j))^{\frac{\eta+1}{\eta}}, \quad i = 1, 2, \ldots, s, i \neq j \tag{77}$$

The distribution of the increments of normal impulses depends on *the relative stiffness and the relative potential energy among various contact points.*

Remark: *The distributing law in (77) takes the same form as the one expressed in (30) even though we adopt two different kinds of constitutive relationships for the compliances at contacts. This may gives us an expectation that an impulsive process with any kind of compliance could be dominated by the underlying law with the form expressed in (77). In other words, the evolution of motion in an impulsive process just depends on the relativity of the contact stiffness and the potential energy resided in the system. This may extremely facilitate the understanding of the energy transmit during a network of contacts.*

5 The numerical algorithm

In this section, we will present a numerical algorithm to calculate the post-impact velocities for multi-impact problems without friction. Obviously the structure of the impact differential equations will change due to the separations of the contact points and the integral dumb variable will vary with the evolution of the potential energy. Moreover, since the ratios of potential energy are used to define the ones of increments of normal impulses, at the beginning of impacts the numerical simulation may be obscured by some singularities. Therefore, some special attention should be paid to the realization of the numerical algorithm.

Let us denote n the number of steps, and adopt a step size ΔP. Obviously the accuracy and efficiency of the numerical results depend on the selection of n and ΔP. The normal impulse scale is associated with a concrete dynamical process, and differs from the time scale. In order to choose reasonable values ΔP and n, we can define the following norm to estimate the possible value of the normal impulse at the momentum level:

$$P_{\text{est}} = \sum_{i=1}^{n} \sum_{j=1}^{n} m_{ij} |\dot{q}_j^0| \tag{78}$$

where m_{ij} is the $ij-$th element of the matrix M, and $\dot{\mathbf{q}}^{\mathbf{0}}$ is the initial velocity of the system. The step size can be set as

$$\Delta P = \frac{P_{\text{est}}}{n} \tag{79}$$

At the beginning of the impact, the primary contact point i can be selected as the point that takes the maximum value of relative velocity

$$\dot{\delta}_i^0 \geq \dot{\delta}_j^0, \quad j = 1, 2, ..., s, j \neq i \tag{80}$$

and $\dot{\delta}^0$ is the initial relative velocities that can be obtained by using equation (19). Then, the increment of normal impulse at contact point i can be set as $\Delta P_i^{(0)} = \Delta P$, and the increments at other contact points can be determined according to (32), in which

$$\Delta P_j^{(0)} = \gamma_{ji} \left(\frac{\dot{\delta}_j^0}{\dot{\delta}_i^0} \right)^{\eta} \Delta P, \quad j = 1, 2, ..., s, j \neq i \tag{81}$$

In most cases we can take a constant value ΔP as the step size. However, we may change the step size in order to find some critical points. Let us denote ΔP^l the step size at $l-th$ step and use the Euler's explicit difference scheme to discretize the impulsive differential equations (20). The quantities with the superscript l represent their initial values at l-th step, and the ones with the superscript $(l+1)$ represent the terminate values. The difference formulations for (20) can be expressed as

$$\dot{\mathbf{q}}^{(l+1)} = \dot{\mathbf{q}}^{(l)} + \mathbf{M}^{-1}\mathbf{W}\Gamma^{(l)}\Delta P^l \tag{82}$$

where $\Gamma^{(l)}$ is a matrix related to the ratios of contact stiffness and the ones of potential energy at the instant $P^{(l)}$, i.e.

$$P^{(l)} = \sum_{j=1}^{l-1} \Delta P^j \tag{83}$$

Let us assume that i is the primary contact point, then $\Gamma^{(l)}$ can be expressed as

$$\Gamma^{(l)} = \left[(\gamma_{1,i})^{\frac{1}{\eta+1}}(E_{1,i}^{(l)})^{\frac{\eta+1}{\eta}}, \cdots, (\gamma_{i-1,i})^{\frac{1}{\eta+1}}(E_{i-1,i}^{(l)})^{\frac{\eta+1}{\eta}}, 1, \cdots, (\gamma_{s,i})^{\frac{1}{\eta+1}}(E_{s,i}^{(l)})^{\frac{\eta+1}{\eta}}\right]^T \tag{84}$$

where, $\gamma_{(\cdot),i}$ is the relative stiffness at contact point $(\cdot)$ comparing with the primary contact point i, and $E_{(\cdot),i}^{(l)}$ is the relative potential energy of the contact point $(\cdot)$ at the impulse step l. Once $\dot{\mathbf{q}}^{(l+1)}$ is obtained, we can use the expression (19) to obtain the relative velocity ($\hat{\mathbf{W}}$ is set to zero and $\mathbf{W}^T$ is a constant matrix) at the instant $P^{(l+1)}$:

$$\dot{\delta}^{(l+1)} = \mathbf{W}^T\dot{\mathbf{q}}^{(l+1)} \tag{85}$$

If $\dot{\delta}_j^{(l+1)} > 0$, the contact point j is located at the compression phase. Thus, the potential energy of the contact j at the instant $P^{(l+1)}$ can be calculated by

$$E_j^{(l+1)} = E_j^{(l)} + \frac{\dot{\delta}_j^{(l+1)} + \dot{\delta}_j^{(l)}}{2}\Delta P^{(l)} \tag{86}$$

If $\dot{\delta}_j^{(l+1)} < 0$, the work done by the normal impulse during the interval ΔP^l should be converted to the quantity of the potential energy that has been released. Therefore, $E_j^{(l+1)}$ is

$$E_j^{(l+1)} = E_j^{(l)} + \frac{1}{e_{s,j}^2}\frac{\dot{\delta}_j^{(l+1)} + \dot{\delta}_j^{(l)}}{2}\Delta P^{(l)} \tag{87}$$

For the mono-stiffness model where the compression and expansion phases take the same relationship as expressed in (21), $e_{s,j}$ is equal to 1 as the energetical constraint is applied on the end of the impact. After that we can compare the values of the potential energy among all the contact points to re-select the primary contact point i in order that

$$E_i^{(l+1)} \geq E_j^{(l+1)}, \quad j = 1, 2, ..., s \tag{88}$$

It is noteworthy that the stiff ODE problem arising by directly using the compliant model [58, Section VII.7] can be avoided by this method since we can set $dP_j = 0$ if the ratio of the potential energies E_{ji} approaches zero. Moreover, the multiple compression phenomenon does not need any special treatment in the calculation of the potential energy since its evolution is continuous during impacts.

The termination of the impact can be identified according to the values of $E_j^{(l+1)}$. For the mono-stiffness model, the impact at contact point j will be terminated by the energetical constraint

$$E_j^{(l+1)} = (1 - e_{s,j}^2) W_{c,j}, \text{ and } \dot{\delta}_j^{(l+1)} < 0 \tag{89}$$

where, $W_{c,j}$ is the work done by the compression force, which is also related to the maximum value of E_j for an impact with a single compression/expansion cycle (if the impact has a multi-compression phase, the value of $W_{c,j}$ will correspond to the last compression phase). Since the energetical constraint has been applied on the bi-stiffness compliant contact model, the terminating condition can be expressed as

$$E_j^{(l+1)} = 0, \text{ and } \dot{\delta}_j^{(l+1)} < 0 \tag{90}$$

In order to improve the accuracy of the numerical results, a variable step size can be applied for searching for the critical points such as $\dot{\delta} = 0$ and $E_j = 0$. If the energetical constraint is satisfied at contact point j, the contact point j will remain open on some non-zero interval of time (i.e. $h_j(q) > 0$), and the accumulated normal impulse as well as the relative velocities, $P_j^{(l+1)}$ and $\dot{\delta}_j^{(l+1)}$ will not change if separation at contact point j is kept ($\dot{\delta}_j^{(l+1)}$ is always less than zero). These values can be thought of as the outcomes of the contact point j after multiple impacts.

However, the relative normal velocity $\dot{\delta}_j$ will be influenced by the motion of the adjacent colliding bodies that still participate into impacts at other contact points. Thus, the contact point j may participate into the impact again, and the value of the $\dot{\delta}_j$ may change from negative to positive values. Based on the assumption of impacts with infinitesimal time interval, the injected velocity $\dot{\delta}_j$ for the new impact can be assigned as the value of $\dot{\delta}_j^{(l+1)}$ when the separation occurs at the instant of $P^{(l+1)}$.

Let us denote the impulse instant at which the new impact appears as $P^{(m)}$, in which contact i is the primary contact point with potential energy $E_i^{(m)}$ and the step size at this instant is $\Delta P^{(m)}$. Similarly to the situation at the beginning of impacts, we have to determine the possible increments of normal impulse at contact point j when it participates to the impacts again. The work done by the compression force at the contact point j during the time interval $[0, t]$ (resp. $\Delta P^{(m)}$) can be approximated as

$$W_j^{(m+1)} = \int_0^{\int_0^t \lambda_j(\tau)d\tau} \dot{\delta}_j dP_j \triangleq \dot{\delta}_j^{(m)} \Delta P_j^{(m)} \tag{91}$$

where $\Delta P_j^{(m)}$ is the increment of the normal impulse at the contact point j when the normal impulse at point i increases by $\Delta P^{(m)}$ during a time interval $[0, t]$. Based on the distributing law (27), or (77), and using (91) we have

$$\frac{\Delta P_j^{(m)}}{\Delta P_i^{(m)}} = \gamma_{j,i}^{\frac{1}{\eta+1}} \left(\frac{\dot{\delta}_j^{(m)} \Delta P_j^{(m)}}{E_i^{(m)}} \right)^{\frac{\eta}{\eta+1}} \tag{92}$$

Thus, the possible increment of the normal impulse $\Delta P_j^{(m)}$ at the beginning of the new impact can be expressed as

$$\Delta P_j^{(m)} = \gamma_{j,i} \left(\frac{\dot{\delta}_j^{(m)}}{E_i^{(m)}} \right)^{\eta} (\Delta P^{(m)})^{\eta+1} \tag{93}$$

Once $\Delta P_j^{(m)}$ is obtained, we can modify the matrix $\Gamma^{(m)}$ and use the difference equation (82) to calculate the generalized velocities $\dot{\mathbf{q}}^{(m+1)}$, and thus, the quantities related to the next moment can be obtained.

In summary, the numerical procedure can be described as follows:

- **(1)** use the expressions (78) and (79) to estimate the step size,
- **(2)** determine the initial primary contact point i and the ratios of the increments of normal impulses based on (80) and (81),
- **(3)** begin the numerical simulation and use expressions (82), (85) and (86) or (87) to obtain the quantities of velocities and the potential energy,
- **(4)** base on (88) to determine which contact point is selected as the primary point and use (85) to determine other increments of normal impulses,
- **(5)** the impact at the contact point j will be terminated if the expressions (89) or (90) are satisfied, and the repeating impact can be solved by using expression (93),
- **(6)** the outcomes of multiple impacts correspond to the instant when all the contact points separate from each other.

The integration is done with the impulse time-scale and integration stepsize ΔP. The "real" time-step h is given by $h = \frac{\Delta P}{\lambda}$ where λ is the force. If λ is large then h becomes small. It is noteworthy that this has no influence on the calculation process because one does not need to come back to the h-integration to compute the post-impact velocities. Consequently the algorithm can be seen as a black-box representing the collision mapping when inserted in a code for the simulation of a multibody system.

6 The problem of Newton's cradle

The well-known problem of Newton's cradle is a typical system with multiple impacts (shown in Figure 5). This system has been studied by many authors as a benchmark for multiple impacts [5] and also plays an important role for many applications like granular material [43, 46, 47, 42, 60, 61]. In this section, this problem is investigated by comparing the numerical results obtained from compliant contact models (Hertz or linear springs) [28] and the experimental results presented in [12], with the results obtained from the integration of the impulsive dynamics studied in the foregoing section.

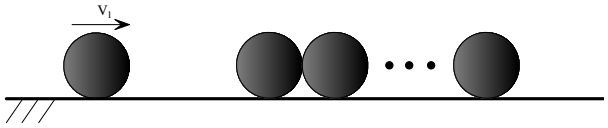

Figure 5: The problem of Newton's cradle

6.1 Problem description

Consider a chain of balls that consists of N aligned balls B_i. Initially all the balls but B_1 are at rest, in contact, and unstressed. The first ball B_1 with mass m_1 and radius r_1 collides this chain with the initial velocity v_0. Let us denote x_i the displacement of the mass center of the ball B_i, with mass m_i and radius r_i. When a compliant contact model is used, the contact force F_i between the balls B_i and B_{i+1} is:

$$F_i = K_i(\delta_i)^\eta \tag{94}$$

where K_i and δ_i are the contact stiffness and the elastic deformation at the contact point i. The exponent η determines the kind of contacts between the balls. The kinematic state of a contact i is expressed as:

$$\delta_i = (x_i + r_i) - (x_{i+1} - r_{i+1}) = q_i - q_{i+1} + (r_i + r_{i+1}) \tag{95}$$

If $\delta_i > 0$, the balls B_i and B_{i+1} are separated, while $\delta_i < 0$ corresponds to the closed contact situation between B_i and B_{i+1}. The dynamics can be expressed as

$$\begin{bmatrix} m_1 & 0 & \dots & 0 \\ 0 & m_2 & \dots & 0 \\ \vdots & & \ddots & \vdots \\ 0 & 0 & \dots & m_N \end{bmatrix} \begin{bmatrix} \ddot{q}_1 \\ \ddot{q}_2 \\ \vdots \\ \ddot{q}_N \end{bmatrix} = \begin{bmatrix} -1 & 0 & \dots & 0 & 0 \\ 1 & -1 & \dots & 0 & 0 \\ \vdots & & \ddots & & \vdots \\ 0 & 0 & \dots & 1 & -1 \\ 0 & 0 & \dots & 0 & 1 \end{bmatrix}_{N\times(N-1)} \begin{bmatrix} F_1 \\ F_2 \\ \vdots \\ F_{N-1} \end{bmatrix}_{N-1} \tag{96}$$

and the complementarity conditions

$$0 \leq -F_i \perp -F_i + K_i(\delta_i)^\eta \geq 0, \;\; 1 \leq i \leq N-1 \tag{97}$$

During the first multiple impact, all the contacts are closed and the integration of (96) over $[t_i, t_{i+1}]$ yields the impact differential equations with the following matrix notation:

$$\mathbf{M}d\dot{\mathbf{q}} = \begin{bmatrix} \mathbf{w}_0 \\ \mathbf{w}_1 \\ \vdots \\ \mathbf{w}_{N-2} \end{bmatrix} d\mathbf{P} \tag{98}$$

According to (95), the relative velocity at the contact i can be written as:

$$\dot{\delta}_i = \dot{q}_i - \dot{q}_{i+1} = \mathbf{w}_i \dot{\mathbf{q}} \tag{99}$$

Since the initial impact occurs between the balls B_1 and B_2, the impulse dP_1 can be firstly specified as the independent variable for the impact differential equations. Therefore, the distributing rule for the changes of normal impulses at the other contact points is

$$dP_i = \left(\frac{K_i}{K_1}\right)^{\frac{1}{\eta+1}} \left(\frac{\int_0^{P_i(t)} (\dot{q}_i - \dot{q}_{i+1}) dP_i}{\int_0^{P_1(t)} (\dot{q}_1 - \dot{q}_2) dP_1}\right)^{\frac{\eta}{\eta+1}} dP_1, \qquad i = 2, 3, \ldots \tag{100}$$

Initially, the distribution of the change of normal impulses with respect to $\triangle P_1$ is

$$\triangle P_i = \left(\frac{K_i}{K_1}\right) \left(\frac{\dot{q}_i^0 - \dot{q}_{i+1}^0}{\dot{q}_1^0 - \dot{q}_2^0}\right)^{\eta} \triangle P_1, \qquad i = 2, 3, \ldots \tag{101}$$

6.2 Numerical results

Case 1. Three-ball system

In [12], Ceanga and Hurmuzlu presented an impulsive correlation ratio for a triplet of identical balls. With the help of the Stronge's energetic coefficient, they showed that the post-impact velocities of the balls can be numerically approximated. In their experiments, four types of balls, designated as A, B, C, and D with masses $m_A = 45$, $m_B = 53$, $m_C = 53$, and $m_D = 166$ grams, are used. The experimental results of ICR and e_s for the system with identical balls are presented in Table 1 (see Tables 1 and 2 in [12]).

Table 1: experimental results in [12]

Ball Type	A	B	C	D
e_s	0.97	0.36	0.27	0.85
ICR	0.167	0.310	0.338	0.080

Let us assume that the initial velocity of B_1 is $\dot{q}_1^0 = 1$m/s. According to the values of ICR in Table 1 and using the expressions (31)-(33) in [12], we can compute the post impact velocities of the three balls, which are thought of as the experimental outcomes reported in Table 2. Let us set $\eta = 3/2$ for

Table 2: Outcomes for three ball system

Ball Type	Results from experiment				Theoretical prediction			
	$\dot{q}_1^+$	$\dot{q}_2^+$	$\dot{q}_3^+$	$\sum(\dot{q}_i^+)^2$	$\dot{q}_1^+$	$\dot{q}_2^+$	$\dot{q}_3^+$	$\sum(\dot{q}_i^+)^2$
AAA	-0.0747	0.0559	1.0188	1.046	-0.0466	0.0783	0.9683	0.946
BBB	0.1953	0.2733	0.5314	0.394	0.2513	0.2787	0.4700	0.362
CCC	0.2359	0.2905	0.4737	0.364	0.2798	0.3099	0.4103	0.344
DDD	0.0365	0.0863	0.8772	0.778	0.0306	0.1094	0.8600	0.752

the Hertzian contact and $\gamma_{12} = 1$ due to the identical balls. The comparison between the theoretical prediction according to the method described in sections 3-5 and these experimental outcomes is presented in Table 2.

The observation from Table 2 shows that theoretical results coincide fairly well with the experimental results presented in [12]. Clearly the qualitative properties are comparable since the wave effects are present in both sets of results in Table 2. The discrepancies between experiments and prediction for the values of $\sum(\dot{q}_i^+)^2$ are less than 10 percent, and may be due to the inaccuracies induced by the transfer of the experimental signals to the digital values for the velocities. For instance, the value of $\sum(\dot{q}_i^+)^2$ related to the normalized value of the post-kinetic energy of the system for type-A is greater than the initial value (it is equal to 1) based on the data converted from experimental results (this data is not credible since the kinetic energy of the system is created during the impact).

Remark: *Since the numerical results are not provided accurately in [12] (only graphical results in Figures 10–12 are available in [12]), it is not possible to make precise comparisons between the algorithm in [12] and the algorithm in this paper. At best one can compare some qualitative features of the schemes.*

Figure 6 shows the evolution of the velocities accompanying the normal impulses for the ball of type A, calculated with the algorithm of section 5. At the beginning of the impact, dP_1 is selected as the independent variable since contact point 1 contains more potential energy than contact point 2. After the end of the compression phase at contact point 1, its potential energy will decrease, while the potential at contact 2 will continue to increase. When the potential energy at contact point 2 is greater than the one resided in the contact point 1, the independent variable dP_1 for the impulsive differential equations will be changed into dP_2. In this situation, dP_1 will depend on dP_2. Clearly, the ratio between dP_1 and dP_2 is not linear, but depends on the potential energy stored at the two contact points. Before the compressional phase at contact point 2 finishes, the ball B_1 will lose contact from the chain. Finally, all balls will separate with different post-impact velocities.

Let us investigate the difference between the theoretical predictions obtained from the bi-stiffness and mono-stiffness models, in which both the models are set with the same exponent $\eta = 3/2$ for the force/indentation relationships, and $e_{s,1} = e_{s,2} = 1$. In the mono-stiffness model, the coefficients of restitution are used as a global index to confine the local energy loss, while in the bi-stiffness model the local energy loss is considered by using different force/indentation relationships for the compression and expansion phases. As shown in Table

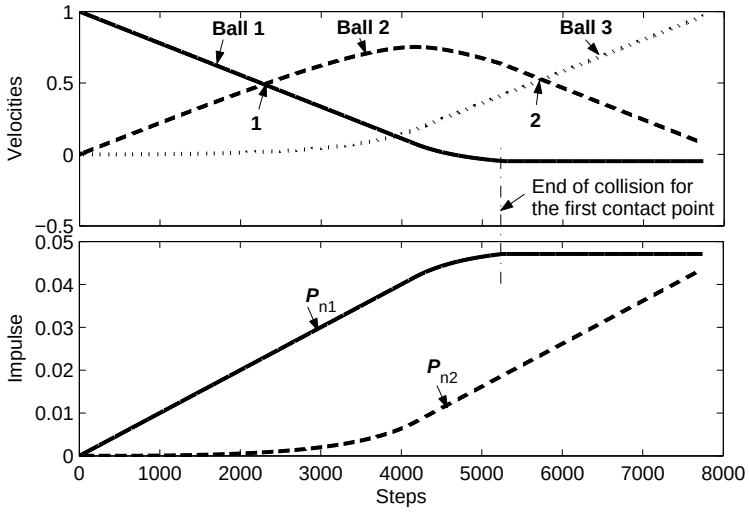

Figure 6: The evolutions of the normal impulses and the relative velocities at two contact points.

Table 3: The theoretical prediction by using bi-stiffness and mono-stiffness models

Ball Type	bi-stiffness model (section 4)				mono-stiffness model (section 3)			
	$\dot{q}_1^+$	$\dot{q}_2^+$	$\dot{q}_3^+$	$\sum(\dot{q}_i^+)^2$	$\dot{q}_1^+$	$\dot{q}_2^+$	$\dot{q}_3^+$	$\sum(\dot{q}_i^+)^2$
AAA	-0.0520	0.0843	0.9677	0.946	-0.0466	0.0783	0.9683	0.946
BBB	0.2515	0.2775	0.4710	0.3621	0.2513	0.2787	0.4700	0.362
CCC	0.2798	0.3093	0.4109	0.343	0.2798	0.3099	0.4103	0.344
DDD	0.0218	0.1178	0.8603	0.7544	0.0306	0.1094	0.8600	0.752

3, the theoretical predictions obtained from different compliant contact models with the same coefficients of restitution have only very small discrepancies for the outcomes of the post-velocities. In other words, the method developed in this paper can provide a relative precise information for an impulsive process even though the constitutive relationship associated with the contacts is ambiguous.

Case 2. The particle chain with five balls

Complex behavior will appear when multiple impacts occur between different types of balls. In particular, the mass ratios between the balls and the stiffness ratios between the contact points will significantly influence the process of multiple impacts. In the following a particle chain involving 5 balls will be investigated by using the impulsive differential equations and the compliant contact model.

Except for the imparting ball, the balls in the chain are assumed to be identical. The mass of the first ball is set as $m_1 = 1$kg. The mass ratio and stiffness ratio between the first ball and other balls is defined by

$$\alpha = \alpha_{1,i} = \frac{m_1}{m_i}, \quad \gamma = \gamma_{1i} = \frac{K_1}{K_i}, \quad i \neq 1$$

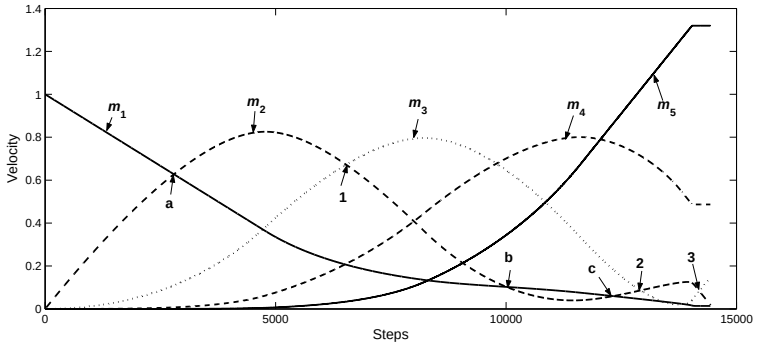

Figure 7: Evolution of the relative velocities for the 5-ball system ($\alpha = 2, \gamma = 1$)

The contact forces are assumed to be linear elastic. This permits $e_s = 1$ and the exponent $\eta = 1$. The initial velocity of the imparting ball is set as $v_0 = 1\text{m/s}$. For the case of $\alpha = 2$ and $\gamma = 1$, figure 7 shows the evolutions of the relative velocities during impacts, using the impulsive model of section 3 (or section 4 as the impact is fully elastic).

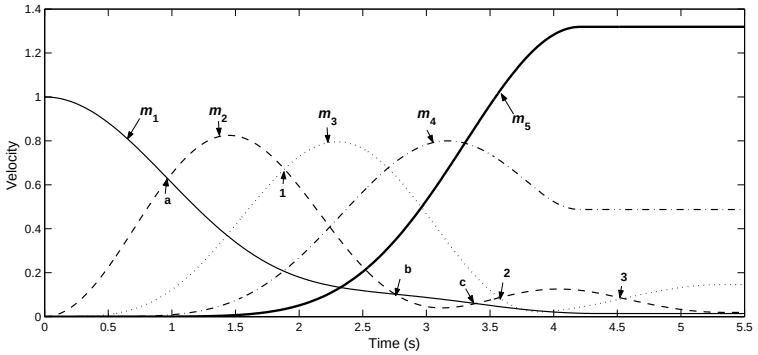

Figure 8: The relative velocities obtained from the linear compliant model ($\eta = 1$, $K_i = 1$ N/m).

Observation from Figure 7 clearly shows that the compressional process between B_1 and B_2 finishes at point a. Then, the potential energy will be released to make them separate. Before separation, however, ball B_1 and B_2 will again obtain the same velocities when normal impulse reaches the point b: a new compressional process occurs between B_1 and B_2. This process will change the velocities of B_1 and B_2 and make them obtain the same value at point c. After that, the potential energy will be completely released and the contact between $B1$ and B_2 will be finally open. Analogous process can also be found between B_2 and B_3, where the instants for $\dot{\delta}_2 = 0$ appear at point 1, 2 and 3, respectively. These multiple compression phenomena can also be observed by using the compliant contact model (shown in Figure 8). The results of Figure 8 were obtained with a stiffness of 1 N/m, which is not realistic, however the outcome is independent of the absolute values of the stiffnesses but depends only on their ratios in this example [25, 26]. This implicitly means that the small deformation

at contact points has little influence on the multi-impact process, confirming the validity of assumption (a) of section 1.3 in the impulsive dynamics of impact.

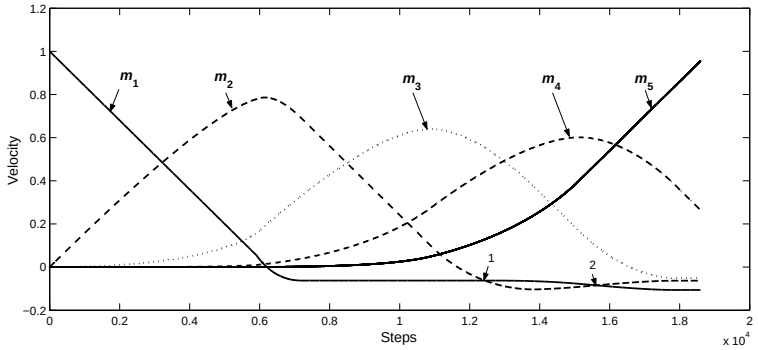

Figure 9: Evolution of the relative velocities for the 5-ball system ($\alpha = 1, \gamma = 2$).

The phenomenon that a repeating impact occurs at the same contact point can be observed by setting $\alpha = 1$ and $\gamma = 2$, as shown in Figure 9. Clearly ball B_1 and ball B_2 will collide again at the point 1 on the curves. The outcomes of post-impact velocities will change due to the second impact.

It may be helpful to compare the final outcomes of the post-impact velocities obtained from the impulsive method and the one obtained from the compliant model **(ii)**. By changing the values of the stiffness and mass ratios, Table 4 presents the final velocities of the system by using the impulsive method. The results obtained from the compliant contact model are presented in Table 5. Clearly the results obtained from the two different methods agree very well.

Table 4: Post-impact velocities obtained from the impulsive dynamics.

(α, γ)	$\dot{q}_1^+$	$\dot{q}_2^+$	$\dot{q}_3^+$	$\dot{q}_4^+$	$\dot{q}_5^+$
(1,1)	-0.1322	-0.0754	-0.0311	0.2958	0.9429
(2,1)	0.0140	0.0186	0.1469	0.4867	1.3198
(1,2)	-0.1062	-0.0628	-0.0508	0.2644	0.9554
(2,2)	-0.0341	0.0155	0.3516	0.3878	1.3132

Table 5: Post-impact velocities obtained from the compliant contact model.

(α, γ)	$\dot{q}_1^+$	$\dot{q}_2^+$	$\dot{q}_3^+$	$\dot{q}_4^+$	$\dot{q}_5^+$
(1,1)	-0.1323	-0.0753	-0.0310	0.2962	0.9424
(2,1)	0.0139	0.0192	0.1463	0.4875	1.3192
(1,2)	-0.1065	-0.0624	-0.0507	0.2646	0.9551
(2,2)	-0.0400	0.0159	0.3748	0.3816	1.3078

Case 3 The impulsive wave in a long chain

As proved theoretically and experimentally by many authors, an impulsive wave can be generated when a chain endures an impulse [45, 43, 46, 47, 48,

42, 59]. Let us set a chain with 15 identical balls that are stationary and keep contact with adjacent balls. The contact relationship between the balls is assumed to be nonlinear elastic and satisfies Hertz assumption (i.e. $\eta = 3/2$).

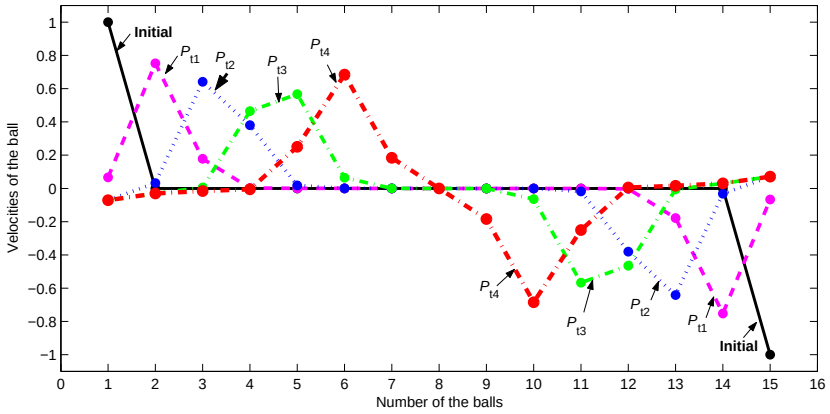

Figure 10: The impulsive wave in the 15-ball system.

Suppose that two balls with the same velocity, $|v_0| = 1$m/s collide against the ends of this chain from two inverse directions. Two impulsive waves will be generated at the ends of this symmetric structure, and are propagated through the chain (shown Figure 10). The five curves correspond to the velocities of the balls at 5 different instants (different P_j), where the solid line represents the initial condition of the chain, while the other four lines describe the impulsive wave behavior at different times.

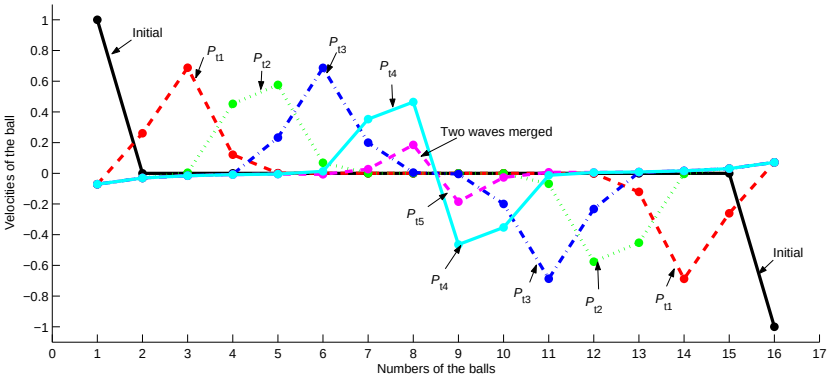

Figure 11: The impulsive wave in the 16-ball system.

Initially the imparting balls at the ends of this chain only influence the adjacent balls with limited length, and then two impulsive waves are formed due to the coupling between adjacent balls (self-organized behaviors among balls), then travel through the chain with an approximately fixed length and a constant amplitude (like a solitary wave). Meanwhile, the balls behind the wave will rebound backwards with a small velocities, confirming the scattering

phenomenon or bead detachment effect [42]. The length of the impulsive wave is confined in five balls, that well coincides with conclusions obtained from numerical results, theoretical analysis as well as the experiments reported in [43, 47, 48]. The two impulsive waves originated from the ends of this chain will meet at the chain center, in which the located particle always keeps motionless due to the symmetric structure of the chain. After that, the waves with unchanged shape will reflect from the center of the chain to make particles separate from each other.

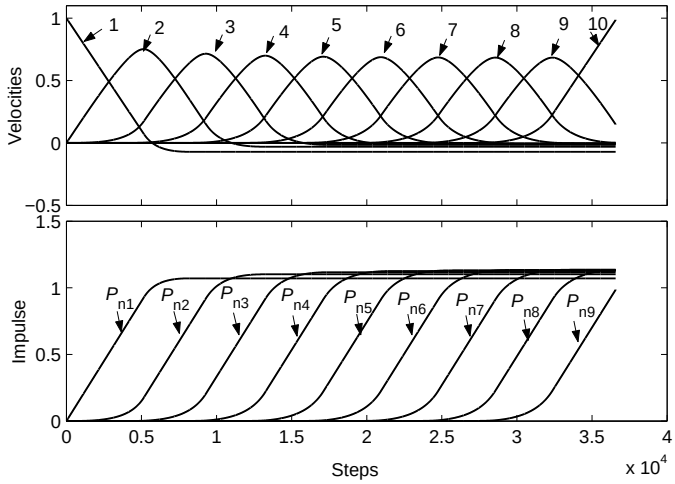

Figure 12: A regular wave in an 9-ball chain impacted by an identical ball.

If the number of balls in the chain is even, the two impulsive waves will interfere with each other when the waves reach the center of the chain. This phenomenon is well reflected in Figure 11 obtained by setting the chain with 16 identical balls. When the two waves met at the center of the chain, the velocities of the particles involved in the impulsive wave will abruptly decrease, and thus the momentums resided in particles will be redistributed to form a different shape of wave profiles. However, the variation of the wave profile has little influence on the final outcomes of the velocities after impacts.

Case 4 $n-$ball chains impacted by $m-$ball chains

As shown in case 3 and discovered by many physical scientists, a compressive wave with regular profile involving five particles can be formed when a uniform ball-chain system is impacted by an identical particle. However, this regularity of the wave behavior will be destroyed when the chain is collided by more than one impacting particles.

Let us denote a system with 10 balls that are identical and satisfy the Hertz's contact relationship. The parameter β is defined as the ratio between the numbers of the m impacting balls and the n impacted balls. For instance, $\beta = 1:9$ means that the chain with nine stationary balls is impacted by one particle (i.e. $n = 9$ and $m = 1$), $\beta = 2:8$ is related to situation that two particles collide against eight stationary balls (i.e. $n = 8$ and $m = 2$), etc. We will investigate the impulsive behaviors by changing β from $1:9$ to $4:6$. Similar to the above

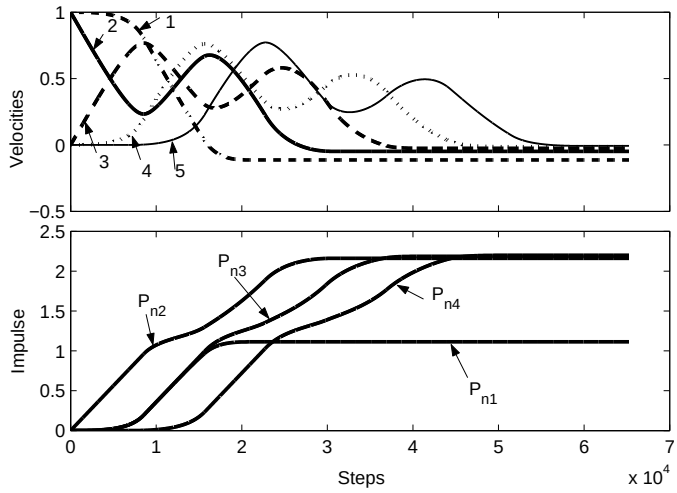

Figure 13: the impulsive behavior of the chain with $\beta = 2 : 8$ (ball 1 to 5)

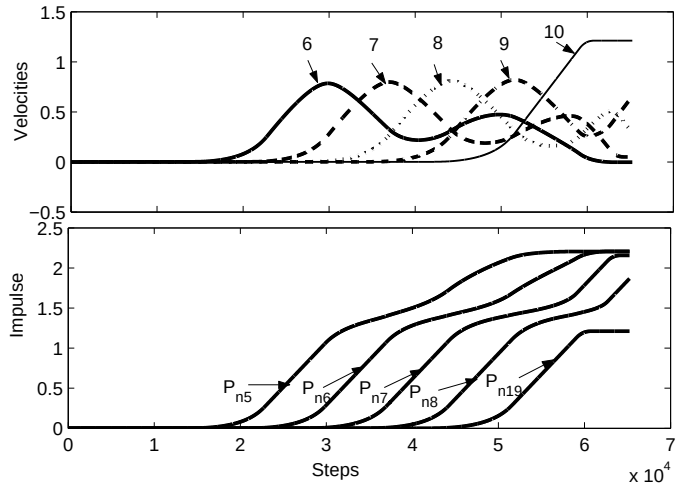

Figure 14: the impulsive behavior of the chain with $\beta = 2 : 8$ (ball 6 to 10)

cases, the initial velocities of the impacting balls are set as $v_0 = 1m/s$ and no energy is dissipated during impacts: $e_{s,i} = 1$ for all contacts i.

Figure 12 presents the evolutions of the velocities and the normal impulses for the case of the chain with parameter $\beta = 1 : 9$. Clearly a regular wave can be formed and only three balls move forward when the impact finishes. The values related to the final velocities for each ball are presented in Table 6, in which the last row shows the percentages of the forward kinetic energy (the sum of the kinetic energies of the balls with positive post-impact velocity) and of the energy of the final ball with respect to the total energy of the system, respectively. In this case, the percentage of the forward kinetic energy is about 99%, and the one of the final ball is near to 97.4%.

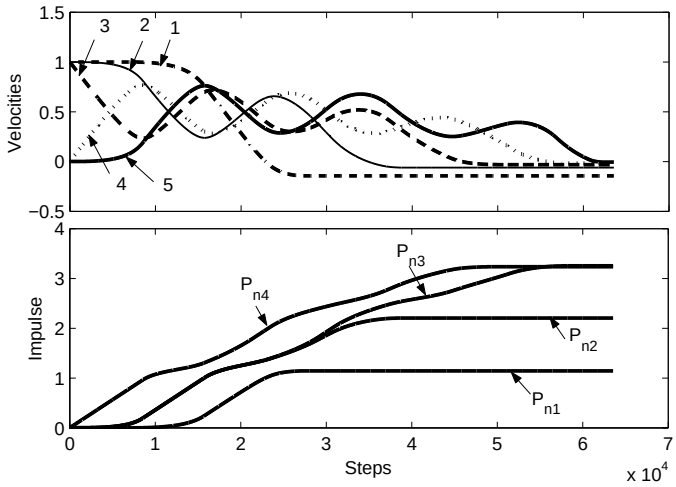

Figure 15: the impulsive behavior of the chain with $\beta = 3 : 7$ (ball 1 to 5)

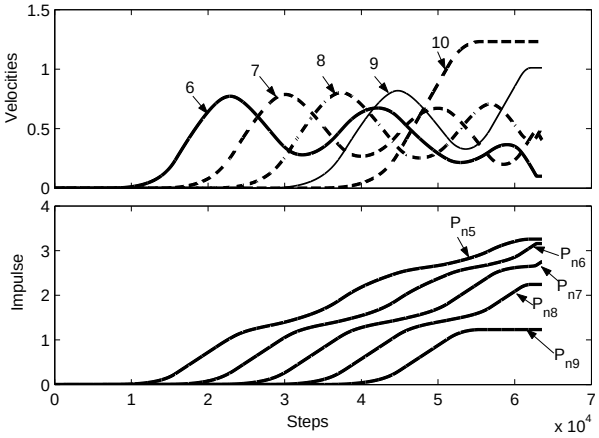

Figure 16: the impulsive behavior of the chain with $\beta = 3 : 7$ (ball 6 to 10)

When the chain is impacted by two identical balls, there are four balls finally moving forward, and the kinetic energy will be centralized in the last two balls. It is obvious that the wave behavior is not regular due to the complex coupling among various contacts. Figure 13 and 14 shows that the evolutions of the post velocities of balls and the normal impulses for balls 1 to 5 and for balls 5 to 10, respectively. Although most of kinetic energy of the system is still kept in the balls moving forward, the distribution of the post- velocities of the balls is much different from the one in the chain impacted by an identical ball. The forward kinetic energy is not concentrated in the last two balls, but will disperse in a length with about four balls.

As m increases, the interactions between the contacts becomes more complex, and the number of balls rebounding decreases. Figures 15 and 16 present the evolutions of the velocities and of the normal impulses for the balls from No.1 to 5 and from No.6 to 10 in chain with $\beta = 3 : 7$, respectively. Observing

Table 6: Outcomes of chains with different β.

β	(1:9)	(2:8)	(3:7)	(4:6)
$\dot{q}_1^+$	-0.0710	-0.1126	-0.1441	-0.1706
$\dot{q}_2^+$	-0.0303	-0.0481	-0.0612	-0.0729
$\dot{q}_3^+$	-0.0159	-0.0248	-0.0312	-0.0373
$\dot{q}_4^+$	-0.0089	-0.0133	-0.0169	-0.0146
$\dot{q}_5^+$	-0.0052	-0.0068	-0.0054	0.1274
$\dot{q}_6^+$	-0.0030	-0.0022	0.0996	0.4648
$\dot{q}_7^+$	-0.0018	0.0497	0.4043	0.4847
$\dot{q}_8^+$	0.0025	0.2893	0.5108	0.9111
$\dot{q}_9^+$	0.1467	0.6570	1.0118	1.0928
$\dot{q}_{10}^+$	0.9869	1.2118	1.2323	1.2145
Percentage	(99.5, 97.4)	(99.3, 73.4)	(99.2, 50.6)	(99.2, 36.9)

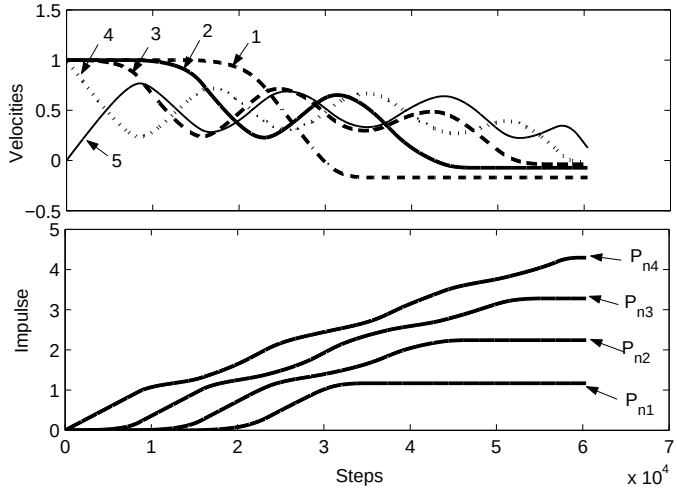

Figure 17: the impulsive behavior of the chain with $\beta = 4:6$ (ball 1 to 5)

the values presented in Table 6 we can find that the forward kinetic energy changes little, while the number of balls moving forward is five and the kinetic energy is dispersed in a more wide scope.

When m increases to four, the post velocity of the last ball changes very little in comparison with the cases of a chain impacted by 2 balls or 3 balls, while the forward kinetic energy will disperse in the chain with 6 balls as shown in Table 6. The evolutions of the velocities of each ball and the impulses among various contacts are shown in Figure 17 and 18.

Conclusions: *As m increases, the ratio* $\frac{\textit{forward post-impact kinetic energy}}{\textit{total kinetic energy}}$ *remains constant* $\approx 99\%$*. The number of balls with a positive post-impact velocity increases as $m+2$. These results confirm that the proposed scheme is able to reproduce the dispersive effects observed for such impacts [42, 61].*

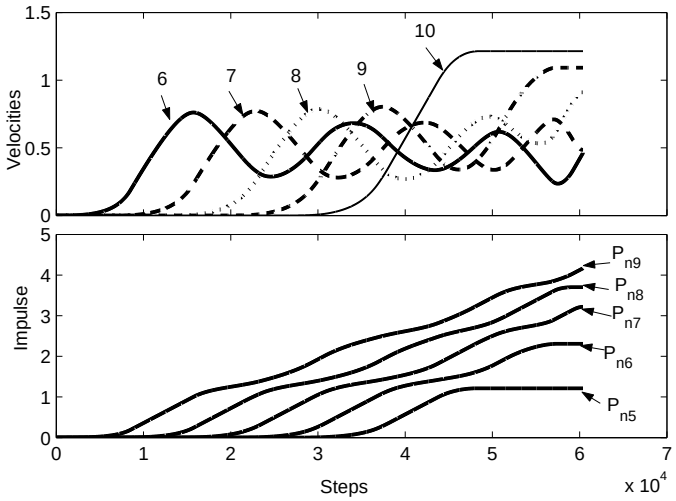

Figure 18: the impulsive behavior of the chain with $\beta = 4 : 6$ (ball 6 to 10)

7 The Bernoulli's problem

The more general situation that the impacts between the balls occur in the plane is also attractive and crucial for multi-impact problems in granular material. In this section, the well-known Bernoulli's example [2] will be analyzed.

7.1 Problem description

Two geometrically identical balls B_1 and B_3 are stationarily placed on a smooth plane. Let a ball B_2 with mass m_2 and initial velocity v_2^0 collide the two balls along their symmetrical line. The masses for B_1 and B_3 are m_1 and m_3, respectively. The contact between the balls is assumed to be satisfied with the Hertz model.

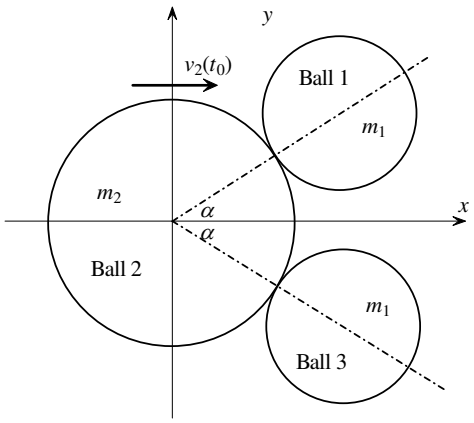

Figure 19: The Bernoulli's problem

Figure 19 depicts the system for the Bernoulli's problem. α is the angle formed by the mass centers of the balls at the instant of collision. Let us set the x axis along the symmetrical line. x_i and y_i represent the components of the position of the mass center for the ball B_i, $i = 1, 2, 3$. F_1 and F_2 are the normal contact forces between the balls B_1 and B_2, and the one between B_2 and B_3, respectively. The governing equations for the three balls can be written as:

$$\begin{cases} m_1\ddot{x}_1(t) = F_1\cos\alpha \\ m_1\ddot{y}_1(t) = F_1\sin\alpha \\ m_2\ddot{x}_2(t) = -F_1\cos\alpha - F_2\cos\alpha \\ m_2\ddot{y}_2(t) = -F_1\sin\alpha + F_2\sin\alpha \\ m_3\ddot{x}_3(t) = F_2\cos\alpha \\ m_3\ddot{y}_3(t) = -F_1\sin\alpha \end{cases} \tag{102}$$

where the contact forces satisfy a complementarity condition similar to (97). If the three balls are identical and the dissipated energy during impacts is assumed to be zero, Bernoulli [2] postulated that the impact outcome should be symmetric, and presented a theoretical solution by using momentum and energy conservations. This solution reads as:

$$\begin{cases} \dot{x}_1^+ = \dot{x}_3^+ = \dfrac{2}{3+\tan^2\alpha} \\ \dot{x}_2^+ = v_0 - \dfrac{4}{3+\tan^2\alpha} \\ \dot{y}_1^+ = -\dot{y}_3^+ = \dfrac{2\tan\alpha}{3+\tan^2\alpha} \\ \dot{y}_2^+ = 0 \end{cases} \tag{103}$$

Clearly this solution significantly depends on the symmetry conditions and on the assumption of elastic collisions at both contacts. Any condition that destroys the symmetry will make the real post-impact outcomes much different from the results in (103). In the following subsection, the impulsive method based on the method developed in sections 3 and 4 will be applied to the Bernoulli's problem.

7.2 Numerical results for the Bernoulli's problem

The impulsive differential equations for the Bernoulli's problem can be easily obtained from (102):

$$\begin{cases} m_1 d\dot{x}_1 = dP_1\cos\alpha \\ m_1 d\dot{y}_1 = dP_1\sin\alpha \\ m_2 d\dot{x}_2 = -dP_1\cos\alpha - dP_2\cos\alpha \\ m_2 d\dot{y}_2 = -dP_1\sin\alpha + dP_2\sin\alpha \\ m_3 d\dot{x}_3 = dP_2\cos\alpha \\ m_3 d\dot{y}_3 = -dP_1\sin\alpha \end{cases} \tag{104}$$

The relative velocity along the normal direction between the balls B_1 and B_2 and the one between the balls B_2 and B_3 can be easily expressed as:

$$\begin{cases} \dot{\delta}_{12} = (\dot{x}_2 - \dot{x}_1)\cos\alpha + (\dot{y}_2 - \dot{y}_1)\sin\alpha \\ \dot{\delta}_{23} = (\dot{x}_3 - \dot{x}_2)\cos\alpha + (\dot{y}_3 - \dot{y}_2)\sin\alpha \end{cases} \tag{105}$$

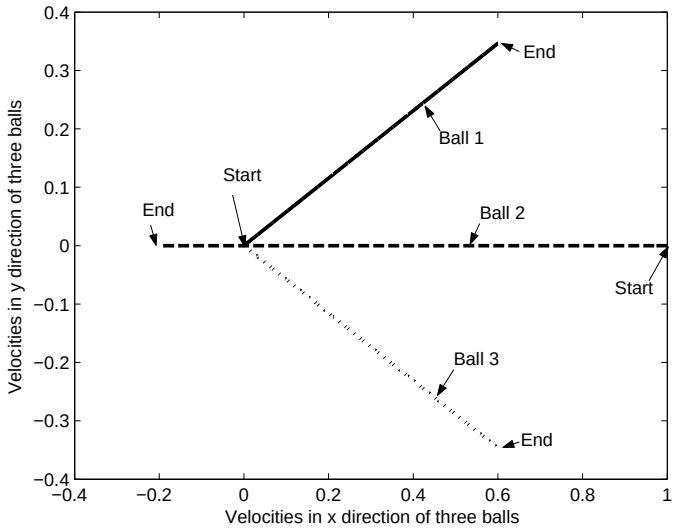

Figure 20: The fully elastic impacts at two contact points.

Hertz model at the contact points and the identical materials for the balls yield the following relationship between dP_1 and dP_2 (see (30)):

$$dP_1 = \left(\frac{\int_0^{P_1} \dot{\delta}_{12} dP_1}{\int_0^{P_2} \dot{\delta}_{23} dP_2} \right)^{\frac{5}{3}} dP_2 \tag{106}$$

During the numerical simulation, either dP_1 or dP_2 is selected as the independent variable for equation (104) based on the potential energy accumulated in the contact points.

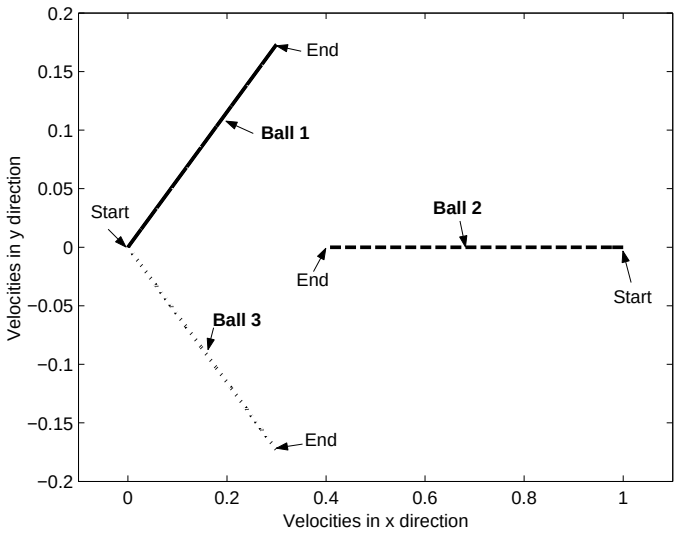

Figure 21: The fully plastic impacts at two contact points.

Let us set the three balls with identical mass $m = 1$kg and the coefficients of restitution in both contact points $e_{s1} = e_{s2} = 1$. The initial velocity of B_2 is set as $v_2^0 = 1$m/s. This is a symmetric situation where a theoretical solution could be obtained. Figure 20 presents the evolution of the velocities during impacts for the configuration with $\alpha = \pi/6$. Clearly the contact between B_1 and B_2 and the one between B_2 and B_3 will reach the compressional point and separate simultaneously, such that the outcomes for the post-impact velocities are symmetric.

Table 7 presents the numerical results obtained from equation (104) and the analytical results obtained from equation (103) of the post-impact velocities for the system in symmetric situations with various angles α. The results coincide very well.

Table 7: Post velocities $\left[\dot{x}_1^+, \dot{y}_1^+, \dot{x}_2^+, \dot{y}_2^+, \dot{x}_3^+, \dot{y}_3^+\right]$ in different α

(α)	Numerical results	Theoretical results
$(\frac{\pi}{8})$	$[0.63, 0.26, -0.26, 0.00, 0.63, -0.26]$	$[0.63, 0.26, -0.26, 0.00, 0.63, -0.26]$
$(\frac{\pi}{6})$	$[0.60, 0.35, -0.20, 0, 0.60, -0.35]$	$[0.60, 0.35, -0.20, 0.00, 0.60, -0.35]$
$(\frac{\pi}{4})$	$[0.50, 0.50, -0.00, 0.00, 0.50, -0.50]$	$[0.50, 0.50, 0.00, 0.00, 0.50, -0.50]$
$(\frac{\pi}{8})$	$[0.33, 0.58, 0.33, 0.00, 0.33, -0.58]$	$[0.33, 0.58, 0.33, 0.00, 0.33, -0.58]$

Obviously, the symmetry of the system can be preserved if both collisions between the balls are plastic impacts. The symmetric solution for the post-impact velocities should also be anticipated. This situation is illustrated in Figure 21 by setting $\alpha = \pi/6$ while the impacts at the two contact points are fully plastic ($e_{s,1} = e_{s,2} = 0$) [2]. After impacts, the solution of the system is still symmetric, while the kinetic energy preserved in the system becomes 0.185J due to local energy dissipation (its initial value is 0.5J).

The difference of the dissipated energy at the two contact points destroys the symmetry of the multiple impact. Let us consider a limit situation, in which the collision between B_1 and B_2 is assumed to be elastic (i.e. $e_{s,1} = 1$) while the collision between B_2 and B_3 is plastic (i.e. $e_{s2} = 0$: there is only a compression phase and the potential energy at the contact is dissipated completely). Figure 22 shows the evolution of the velocities during the impact for the system with $\alpha = \pi/3$. During the compression phase, the evolution of the velocities related to B_1 and B_3 is symmetric, and the velocity of ball B_2 is located in the symmetric line. However, after the compression phase finishes the motion of ball B_2 will diverge from the symmetric line and approaches the side of B_3. Before the impact between B_1 and B_2 finishes, B_3 will participate in the impact again to make B_2 move towards B_1 such that a little change for the velocity of B_2 is generated. Clearly, the outcomes for the Bernoulli's problem are sensitive to the configuration, the initial conditions, as well as the properties of the contact points [8].

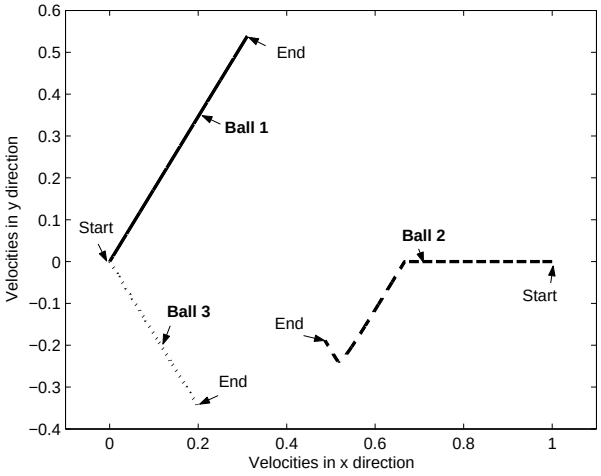

Figure 22: The influences of the coefficients of restitution on the outcomes of the post-impact velocities.

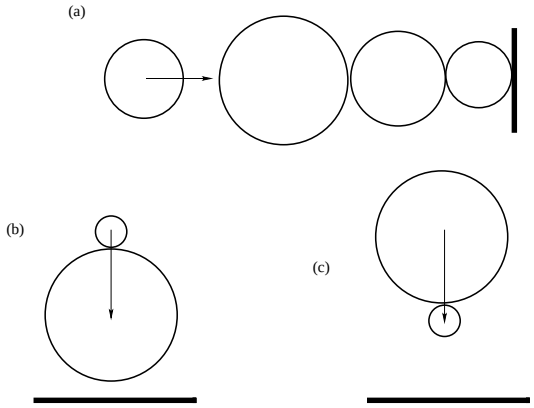

Figure 23: Chains of balls against a wall.

8 Chains of balls against a wall

Let us consider chains of balls that collide into a rigid wall as shown in Figure 23. A funny experiment consists of a 2-impact between a big ball, a small ball, and a ground. For instance one may take a tennis ball and a basket ball, and drop them while stuck together on the ground. When the tennis ball is on the top (case (b) in Figure 23), the post-impact outcome is that the tennis ball usually jumps very high (several meters), while the basket ball has a very small post-impact velocity. When the basket ball is on the top (case (c) in Figure 23), then the impact is no longer that spectacular as the basket ball rebounds just a little. In this section we show that our approach can well describe such phenomena and be used to determine the important parameters of such 2-impacts.

[2]The curves in Figures 20, 21 and 22 are parameterized with P_i, i.e. the start corresponds to $P_i(0) = 0$ and the end corresponds to $P_i(t_f)$.

8.1 Dynamics and simulation of the tennis-basket balls system

For a ball with internal pressure p contacting with a rigid contact surface, the centralized contact force F_s can be approximately expressed as

$$F_s = pS \tag{107}$$

where S is the contact area between the ball and the rigid contact surface. We suppose that the radius of the ball is R and the displacement of the center of the ball is represented by δ ($\delta \ll R$). Under the assumption that the internal pressure p is preserved to be constant and ignoring the term related to δ^2, the contact force F_s can be connected with the displacement δ by the following expression

$$F_s = p\pi(R^2 - (R-\delta)^2) \triangleq 2\pi pR\delta \tag{108}$$

So, the contact stiffness of the compliance between a rigid contact surface and a ball with internal pressure is

$$K_s = 2\pi pR \tag{109}$$

Let us set the tennis ball with radius R_t and mass m_t, and the basket ball with radius R_b and mass m_b, respectively. Considering a simple situation where the tennis ball and the basket ball take the same value of the internal pressure p leads to a simplified relationship for the contact force F and the displacement $\delta_{t,b}$ between the tennis ball and the basket ball

$$\delta_{t,b} = \delta_t + \delta_b = \frac{F}{2\pi pR_t} + \frac{F}{2\pi pR_b} \tag{110}$$

where $\delta_{t,b}$ is measured from the centers of the balls. Therefore, the contact stiffness of the compliance between the tennis ball and the basket ball is

$$K_b = 2\pi p\frac{R_tR_b}{R_t + R_b} \tag{111}$$

For the case (b) of the tennis ball set on the top as shown in Figure 23, the stiffness ratio $\gamma_{t,b,s}$ between two contacts is

$$\gamma_{t,b,s} = \frac{K_{b,s}}{K_b} = \frac{R_t + R_b}{R_t} = 1 + \frac{R_b}{R_t} \tag{112}$$

The stiffness ratio $\gamma_{b,t,s}$ for the case (c) shown in Figure 23 reads as

$$\gamma_{b,t,s} = \frac{K_{t,s}}{K_t} = \frac{R_t + R_b}{R_b} = 1 + \frac{R_t}{R_b} \tag{113}$$

The radius of a basket ball is much larger than the one of a tennis ball, such that $\gamma_{t,b,s}$ will much exceed the value of $\gamma_{b,t,s}$. The difference between $\gamma_{t,b,s}$ and $\gamma_{b,t,s}$ induced by the contact sequences setting on the balls will dramatically influence the dynamical behaviors when the balls stuck together collide against a wall.

According to the information obtained by surfing on internet, the tennis ball may rebound with a hight of $(134.62 \sim 147.32cm)$ when falling from a hight of 254cm, while the basket ball can detach away from the ground with a height of $(1.2 \sim 1.8m)$ if it is released from a height of 1.8m. So the coefficient of restitution between the tennis ball and the rigid ground, e_t changes approximately in a scope of $(0.52 \sim 0.58)$, and the one for basket ball, e_b is limited in $(0.67 \sim 1)$. Let us set $e_t = 0.55$ and $e_b = 0.8$, and assume the coefficient of restitution between the tennis and basket balls $e_{t,b}$ equals 0.326 (we estimate the value of $e_{t,b}$ by $1/e_{t,b} = 1/e_t + 1/e_b$). Other parameters related to the sizes and masses of the tennis and the basket balls are: $m_t = 58$gram, $R_b = 3.25$cm, $m_b = 580$gram, $R_b = 38$cm.

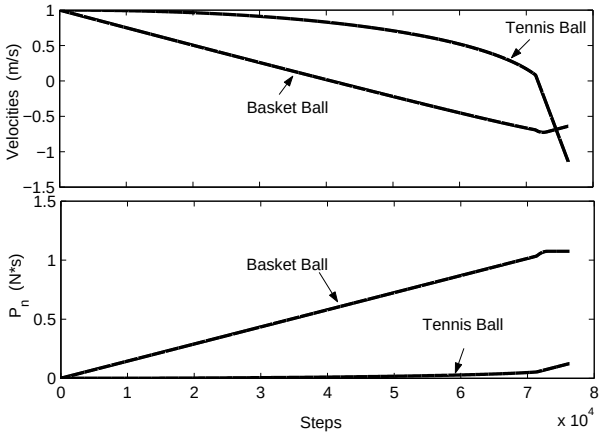

Figure 24: The case of the tennis ball on the top simulated by the bi-stiffness model.

The impulsive method with bi-stiffness mode (the force-indentation relationship in expansion phase is determined according to the restitution coefficient as shown in (46)) is adopted to simulate the 2-impact process. The initial velocities of both the tennis ball and the basket ball are set with the same value, $v_t^0 = 1$m/s and $v_b^0 = 1$m/s.

For the case of the tennis ball setting on the top and the basket ball colliding against the wall, Figure 24 presents the evolutions of the velocities and impulses during the 2-impacts. Numerical results indicate that in this case the tennis ball rebounds backward with a speed $v_t^+ = -1.1460$m/s, while the basketball detaches from the wall with a speed $v_b^+ = -0.6394$m/s. Although the total kinetic energy of the system decreases due to local energy dissipation with a variation from its initial value 0.319 J to 0.1567 J when impacts finishes, the tennis ball will gain energy through the impacts, and rebounds back with a speed larger in absolute value than its initial value.

If we alter the sequence of contacts by setting the basketball on the top and make the tennis ball impact into the wall, the dynamical behavior of the 2-impacts will dramatically change as shown in Figure 25 for the evolutions of the velocities and the impulses during impacts. The outcomes of the 2-impact are: $v_t^+ = -0.1034$m/s and $v_b^+ = -0.1178$m/s. Both the tennis ball and basketball leave from the wall with very small velocities, and more energy will be dissipated

during impacts (the kinetic energy of the system after impacts decrease to 0.0043 J, which is much less than its initial value, 0.319 J).

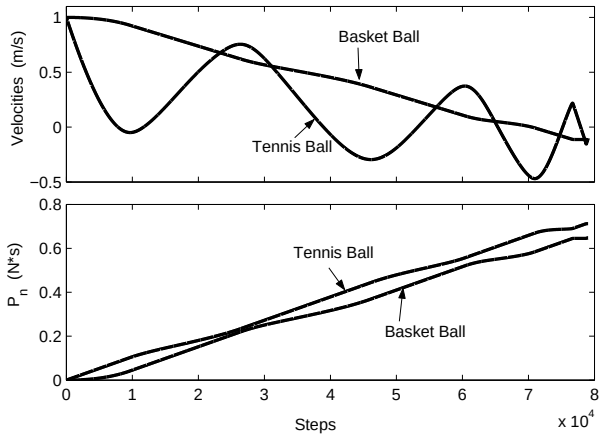

Figure 25: The case of the basketball on the top simulated by bi-stiffness model.

The reason for the discrepancy of the energy outcomes between two cases can be explained as follows: In case (b), Figure 24 shows that there is only one instant when the tennis ball and the basket ball reach the same velocities. This means that the contact between balls consists of a single compression/expansion cycle. In the situation of case (c), however, the phenomena of complex impacts with multiple compressional phases will appear (the tennis ball and the basket ball reach the same velocities at six instants as shown in Figure 25). According to the compliance model, each circle of compression and expansion will dissipate a certain energy in the system, such that less energy can be recovered in the case (c) for the system of two balls against a wall. Obviously, the multi-compression phenomenon is closely related to the stiffness ratios among the various contacts.

8.2 Robustness analysis

It is interesting to investigate the robustness of the method with respect to the uncertainties of modeling and physical parameters. The results of Table 3 in section 6 have already shown that the algorithm is robust with respect to the contact/impact model. The robustness (or the insensitiveness) can be further investigated by setting the compliance at contacts with a mono-stiffness model and taking the coefficients of restitution as a global index to constraint the local energy losses. We apply the same parameters as used in the above simulations with the bi-stiffness model, to the method with the mono-stiffness model. The numerical results for the two situations of the system with different contact sequences are presented in Figures 26 and 27.

In the case of the tennis ball on the top, the post-velocities of the tennis ball and the basket ball are $v_t^+ = -1.146$m/s and $v_b^+ = -0.6357$m/s, respectively. The discrepancies between the two models are very small and a good robustness of modeling is reflected. Let us set the basket ball on the top and make the tennis ball collide against the wall. The outcomes of the impact are: $v_t^+ = 8.6 \times 10^{-5}$m/s, $v_b^+ = -1.73 \times 10^{-4}$m/s. The kinetic energy of the system before

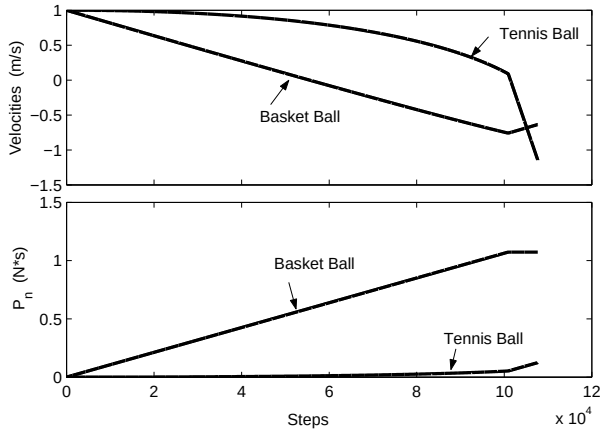

Figure 26: The case of the tennis ball on the top simulated by the mono-stiffness model.

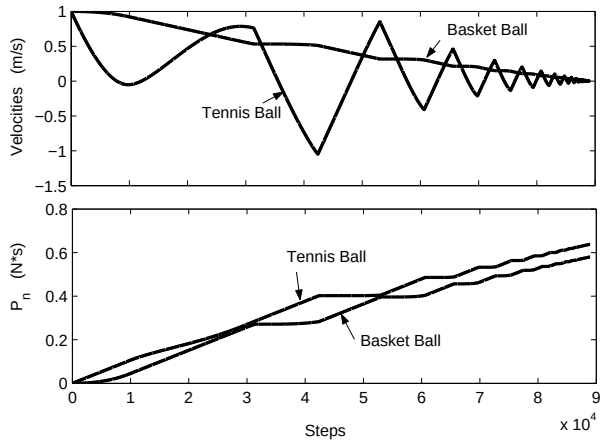

Figure 27: The case of the basketball on the top simulated by the mono-stiffness model.

and after 2-impacts varies from 0.319 J to near zero. Comparing with the first case of the tennis ball on the top, this time complex impact phenomena appears at contact points. The outcomes of the system will be slightly influenced by the mode of the compliant model due to the multiple compression phases among contacts. The discrepancy between the two models is due to the forced energetical constraint applied in the mono-stiffness model to make the system with more local energy losses. However, the global behavior of the system is still fairly well reproduced by the numerical simulations.

It is easy to understand that the real system with 2-impacts should not be sensitive to the little changes of the physical parameters (the masses and sizes of the balls as well as the coefficients of restitution of each contacts), since the impact dynamics is a first-order ODE. In the following, we will investigate whether the impulsive method can well keep the essential mechanical features

by setting the system with uncertainties of physical parameters. The numerical simulation is carried out by using the bi-stiffness mode.

Let us first consider the uncertainties of the radiuses of the basket ball and the tennis ball, which are changed from $R_b = 38 \sim 39$cm, and $R_b = 3.2 \sim 3.3$cm. Other parameters are kept in the same values as in above simulations. For the two cases of the system with different contact sequences, Table 8 clearly shows that the outcomes of the 2-impacts are robust with respect to the variations of radiuses of the balls.

Table 8: The theoretical prediction for the system with uncertainties in radius

case no.	$R_t(cm)$	$R_b(cm)$	tennis ball on top			basketball on top		
			$\gamma_{t,b,s}$	v_t^+	v_b^+	$\gamma_{b,t,s}$	v_t^+	v_b^+
1	3.2	38	12.875	-1.1485	-0.6350	1.084	-0.1019	-0.1169
2	3.2	39	13.187	-1.1489	-0.6339	1.082	-0.1026	-0.1176
3	3.3	38	12.515	-1.1479	-0.6364	1.087	-0.1008	-0.1161
4	3.3	39	12.818	-1.1486	-0.6352	1.085	-0.1014	-0.1168

The investigation of the robustness for the uncertainties of masses is carried out by setting the mass of the basket ball changing in the scope of $m_b = (570 \sim 660 gram)$. The numerical results presented in Table 9 illustrate that the system has a good robustness with respect to little variations of the masses.

Table 9: The theoretical prediction for the system with uncertainties in mass

case no.	m_t	m_b	tennis ball on top			basketball on top		
			$\gamma_{t,b,s}$	v_t^+	v_b^+	$\gamma_{b,t,s}$	v_t^+	v_b^+
1	57	590	12.875	-1.1522	-0.6424	1.084	-0.1170	-0.0902
2	57	600	12.875	-1.1536	-0.6456	1.084	-0.1171	-0.0840
3	57	620	12.875	-1.1570	-0.6517	1.084	-0.1172	-0.0711
4	57	640	12.875	-1.1602	-0.6573	1.084	-0.1170	-0.0572

8.3 The identification for the parameter $e_{t,b}$

The value of the parameter $e_{t,b}$ used in above simulations is estimated from the values of e_t and e_b, and may not well reflect the real dissipation of energy loss between the tennis ball and the basket ball. In the following let us investigate the robustness of the model with respect to the uncertainties of the coefficients of restitution by assigning $e_{t,b}$ with different values, and provide a way of identifying the parameter $e_{t,b}$ from the 2-impacts system. All the parameters except for $e_{t,b}$ are kept the same values as used in above simulations: $m_t = 58$gram, $m_b = 580$gram, $e_t = 0.55$, $e_b = 0.8$, $\gamma_{t,b,s} = 12.875$, $\gamma_{b,t,s} = 1.084$. The drop velocity of the balls stunk together is set as $v_0 = 1$m/s. Table 10 presents the variations of the post-velocities of the tennis ball and the basket ball for the two different contact sequences when $e_{t,b}$ varies from 0.3 to 0.6.

We can find from Table 10 that in the case of the tennis ball on the top the absolute value of the post-impact velocity of the basket ball will decrease, while the one of the tennis ball will increase when $e_{t,b}$ is larger. This can obtain an explanation from the viewpoint of the energy that less dissipation between the

Table 10: The theoretical prediction for the system with uncertainties in $e_{t,b}$

case no.	$e_{t,b}$	tennis ball on top			basketball on top		
		e_b	v_t^+	v_b^+	e_t	v_t^+	v_b^+
1	0.3	0.8	-1.1111	-0.6394	0.55	-0.0934	-0.0723
2	0.4	0.8	-1.2536	-0.6252	0.55	-0.1822	-0.1693
3	0.5	0.8	-1.3966	-0.6109	0.55	-0.2729	-0.1917
4	0.6	0.8	-1.5396	-0.5966	0.55	-0.3580	-0.2207

tennis ball and the basket ball will make more energy be transmitted into the tennis ball through a relative higher value of the stiffness ratio. In other words, the energy resided in the colliding system will flow into the contact bodies with softer stiffnesses. In the case of the basket ball on the top of this chain, both the absolute values of the post-impact velocities for the tennis ball and the basket ball increase very little even though the value of $e_{t,b}$ increases. The small value of the stiffness ratio will generate multiple compression phases that can dissipate most energy of the system during impacts.

Table 11: The outcomes of balls dropping from a height $h = 1.5m$

case no.	$e_{t,b}$	tennis ball on top				basketball on top			
		v_t^+	h_t^+	v_b^+	h_b^+	v_t^+	h_t^+	v_b^+	h_b^+
1	0.35	-6.21	1.97	-3.47	0.61	-0.56	0.016	-0.64	0.021
2	0.4	-6.78	2.35	-3.41	0.59	-0.92	0.043	-0.99	0.05
3	0.5	-7.55	2.91	-3.33	0.57	-1.04	0.055	-1.48	0.11
4	0.55	-7.93	3.21	-3.33	0.55	-1.11	0.06	-1.72	0.151

It may be interesting to investigate the phenomena of the 2-impacts system by dropping the balls stunk together from a usual height (the initial height can be set with a value near to 1.5m). In this case the spectacular scene observed in reality can be well reproduced if the value of the parameter $e_{t,b}$ is near to the real value. Contrarily, if the rebound heights of the tennis ball and basket ball after impacts could be measured accurately, the real value of $e_{t,b}$ can be extracted from the simple experiment. Let us set the dropping height $h = 1.5$m, that will make the initial velocity of impacts equal $v_0 = 5.4$m/s. The numerical results obtained from our method for the two cases of the system with different contact sequences are shown in Table 11, in which all the parameters except for $e_{t,b}$ are kept in the same values as in above simulations.

Although we don't carry out a experiment to certify the accurate values of the rebound heights of the balls, Table 11 clearly tell us that the results from simulations do qualitatively represent the reality very well, and the parameter of $e_{t,b}$ seems to be near 0.55. By setting $e_{t,b}$ with this value and the initial dropping height with the value of 1.5m, the evolutions of the impacts for the two cases of the system with different contact sequences are shown in Figure 28 and 29, respectively.

Comments: *The method developed in this paper keeps the essential mechanical features of the real system since the dynamical behavior is described at the*

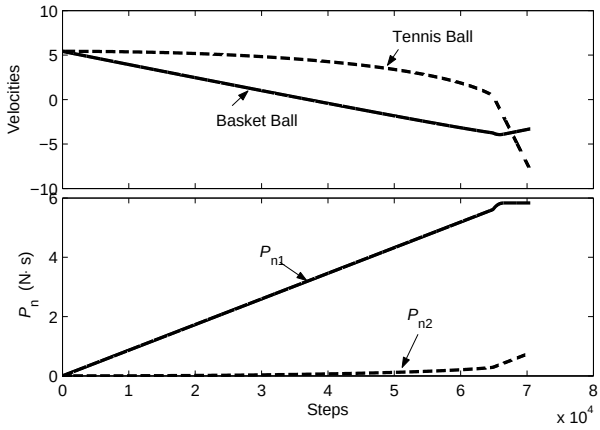

Figure 28: The case of the tennis ball on the top simulated by setting $e_{t,b} = 0.55$.

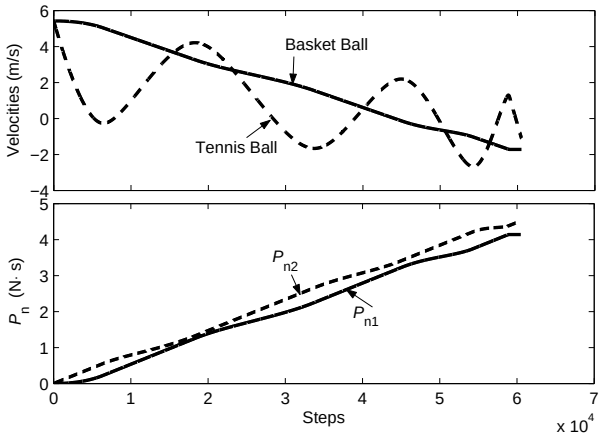

Figure 29: The case of the basketball on the top simulated by setting $e_{t,b} = 0.55$.

velocity-impulse level and respects the evolution of motion in the energy sense. Therefore, one may calculate the impact outcomes without going into a complicated and usually very delicate procedure to identify the physical parameters and the compliance model.

9 Calculation of the contact forces

As we have illustrated in sections 2, 3, and 4, and examined by numerical results for the examples mentioned above, the evolution of an impulsive process only depends on the mode of the potential energy accumulation (the exponent in the force/indentation relationship) and the relative quantities of the contact stiffness among various contacts. Thus, the post-impact velocities of the systems after impacts can be calculated by using the differential impulsive equations with respect to the primary normal impulse, a "time-like" independent variable used for ODEs.

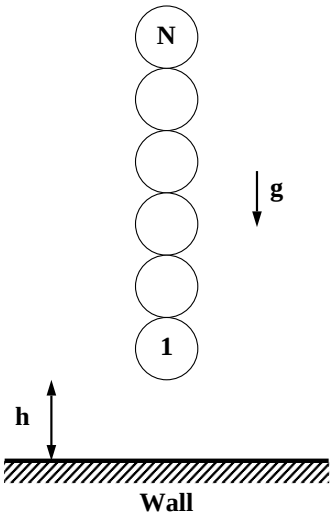

Figure 30: A column of beads colliding against a wall.

Let us recall equations (26), (68) and (76) in which the contact force λ_j is expressed as a function of the potential energy with respect to the normal impulse. If the value of the contact stiffness K_j can be estimated, the value of the contact force λ_j at the instant of $P_j(t)$ can be obtained according to the potential energy $E_j(P_j(t))$. Furthermore, the time t related to the normal impulse $P_j(t)$ can also be extracted by using $t = \frac{P_j(t)}{\lambda_j}$. This is a postprocessing associated with the impulsive differential equations. I.e. we store the information of the potential energy at each numerical step for the ODEs, then carry out an algebraic operation to obtain the values of the contact force and the corresponding time. In this section, we will apply our method to a one-dimensional column of beads colliding against a fixed wall, an example with experimental results presented in [42].

9.1 A column of beads

Figure 30 shows the granular system studied by [42], in which N identical stainless steel beads, each one 8mm in diameter, are put together to form a column colliding against a fixed wall. The column of beads leaves the wall with a height h and starts its free fall to collide against the wall. The number of beads may vary from $N = 1$ up to $N = 40$ for experiments, and the contact forces felt at the wall are recorded by a force sensor.

In order to reproduce the experimental results reported in [42], we use the bi-stiffness relationships expressed in equations (45) and (46) to model the interactions at contacts, in which the local energy loss is taken into account by the restitution coefficient $e_{s,s}$ for particle to particle and $e_{s,p}$ for particle to wall, respectively. Let us number the contact bodies in a sequence from the wall assigned with 0 to the last bead with N. The contact points are denoted in a sequence with number 1 for the contact between the wall (0-th contact

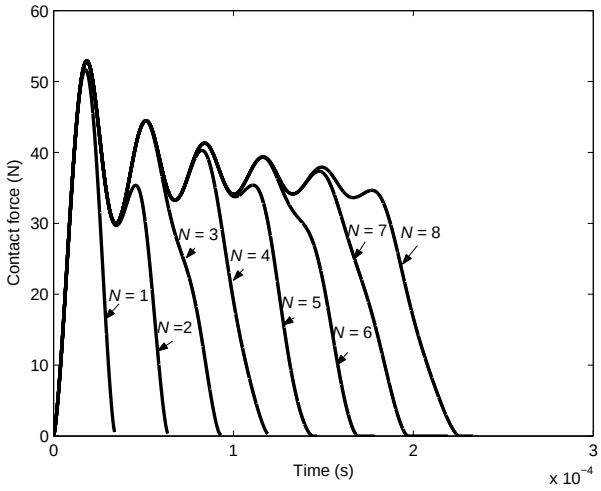

Figure 31: the contact force at the wall during the collision of a column of $N = 1, 2, \cdots, 8$ beads with fall height h=3.1mm, and $e_{s,s} = 0.96$, $e_{s,p} = 0.92$.

body) and the 1-th bead, and number N for the contact between $(N-1)$-th and N-th beads. According to the Hertz's theory, the exponent η equals 3/2 for the non-conforming contact mode between bodies, and the contact stiffness K_i at the contact point i, is expressed as

$$K_i = \frac{4}{3} R_i^{*\frac{1}{2}} E_i^*, \quad i = 1, ..., N \tag{114}$$

where R_i^* and E_i^* are the equivalent contact radius and the equivalent Young modulus between adjacent contact bodies, respectively.

$$R_i^* = \frac{R_i R_{i-1}}{R_i + R_{i-1}}, \quad i = 1, ..., N \tag{115}$$

$$\frac{1}{E_i^*} = \frac{1-\nu_{i-1}^2}{E_{i-1}} + \frac{1-\nu_i^2}{E_i}, \quad i = 1, ..., N \tag{116}$$

The mass of a stainless steel bead used in experiment is $m = 2.05 \times 10^{-3}$kg. The Young modulus and Poisson ratio for stainless steel are $E_s = 21.6 \times 10^{10} N/m^2$ and $\nu_s = 0.276$, respectively. Thus, the value of the contact stiffness, $K_i (i = 2, \cdots, N)$ for sphere-sphere contact is $6.9716 \times 10^9 N/m^{3/2}$. For the contact between the bead and the wall made of stainless steel, the value of the contact stiffness K_1 for the sphere-plane contact is $9.858 \times 10^9 N/m^{3/2}$.

9.2 The contact force felt at the wall during the collision

Based on the description in [42] for the experiments, two cases are investigated in the following numerical simulations: a column of N beads free fall to collide against the wall with two different height $h = 3.1$mm and $h = 5.1$mm, corresponding to the impacting velocities of the column ($v_{imp} = \sqrt{2gh}$) 0.246m/s and 0.316 m/s, respectively.

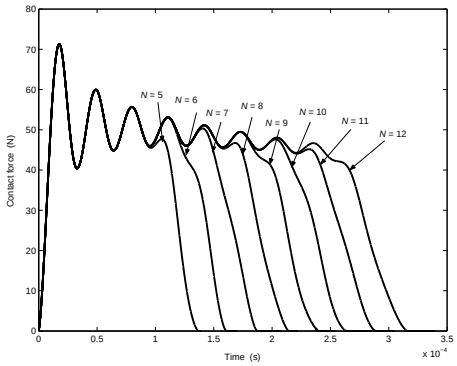

Figure 32: the contact force at the wall during the collision of a column of $N = 5, 6, \cdots, 12$ beads with fall height h=5.1mm, $e_{s,s} = 0.96$, $e_{s,p} = 0.92$.

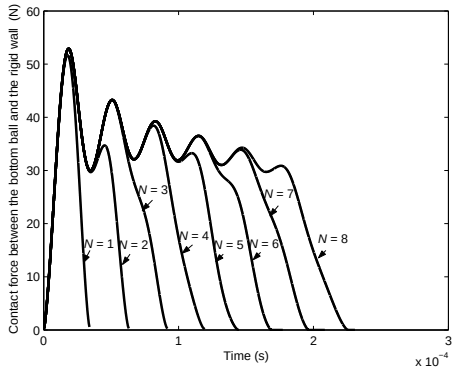

Figure 33: the contact force at the wall during the collision of a column of $N = 1, 2, \cdots, 8$ beads with fall height h=3.1mm, $e_{s,s} = 0.92$, $e_{s,p} = 0.92$.

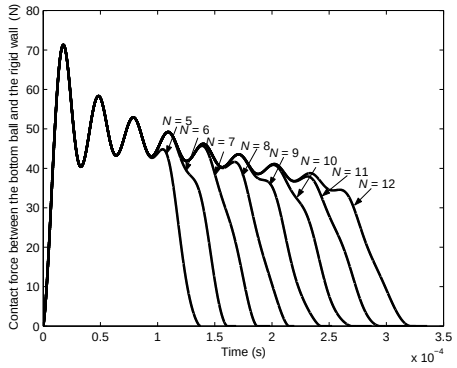

Figure 34: the contact force at the wall during the collision of a column of $N = 5, 6, \cdots, 12$ beads with fall height h=5.1mm, and $e_{s,s} = 0.92$, $e_{s,p} = 0.92$.

For the columns of beads with N changing from 1 to 8, colliding against the wall with $h = 3.1$mm, Figure 31 shows the outcomes of the contact forces

at the wall. It is clear that our numerical results can well reproduce the experimental phenomena discovered in [42], in which the maximum force F_{max} is approximately equal to 52N and very little influenced by N, while the duration of impact increases linearly with N. Moreover, the contact force oscillates with a period of $P \approx 32\mu s$ (the experimental value in [42] is $P = 32.4 \pm 1\mu s$), and is damped like the response of the motion describing the damped free vibrations of a system with viscous damping.

Let us set the fall height $h = 5.1$mm for the column of beads with various number of $N = 5, 6, \cdots, 12$, colliding against the wall. The numerical results obtained from our method is shown in Figure 32, in which the maximum force F_{max} is approximately equal to 71N and the period P for the oscillation of the contact force is around $31\mu s$. This well agrees with the experimental results in [42].

Since the value of the restitution coefficient is often estimated from an independent experiment, it may be interesting to investigate its influence on the contact force at the wall by setting e_s with a little perturbation. Let us set both the values for particle-particle coefficient of restitution and the particle-wall one as $e_s = 0.92$. Figures 33 and 34 present the numerical results for the contact forces felt at the wall that is collided by the column of beads with two different fall heights $h = 3.1, 5.1$mm, respectively. Comparing them with Figures 31 and 32, we can find that the little change of the coefficient of restitution has no identifiable influence on the value and the shape of the curves of the contact forces at the wall.

9.3 Distribution of the post-impact velocities

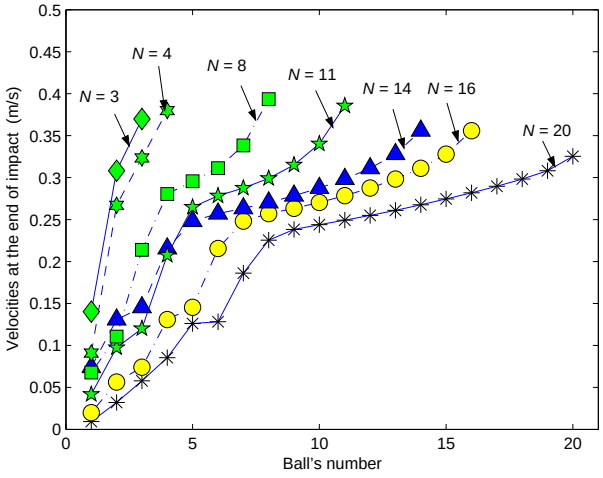

Figure 35: Result of numerical simulations: velocity of the ith bead, at the end of the collision with fall height h=5.1mm, as a function of the bead's number i, for different values of $N = 5, 6, \cdots, 12$ beads, and $e_{s,s} = 0.96$, $e_{s,p} = 0.92$

As illustrated in [42], at the end of the collision the beads in the column will detach from each other due to the energy redistribution within the system. This is easy to be understood from the viewpoint of our method: the kinetic

energy of the column will be first transferred into the potential energy among various contacts, then the evolution of the energy is dominated by the primary contact point to make it propagate through the chain (as pointed out earlier, the primary contact point evolves like the accceleration wave). Obviously the evolution of energy depends essentially on the distributing law discovered by our theory (i.e. the intrinsic nature of the interaction law between contact bodies, stated by Falcon [42]). In this subsection, we will apply our method to investigate the phenomena of the detachement effect found in [42, 61] by presenting the post-impact velocities of the beads after collisions.

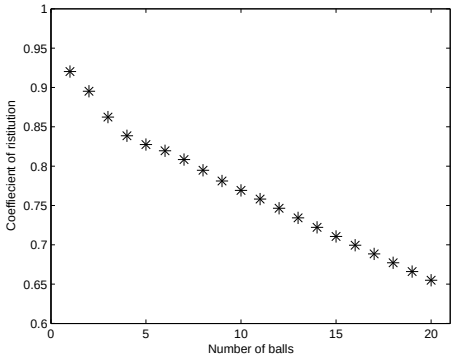

Figure 36: The coefficient e_{eff} for the column with different N dropped from a height $h = 5.1$mm, and setting $e_{s,s} = 0.96$ and $e_{s,p} = 0.92$.

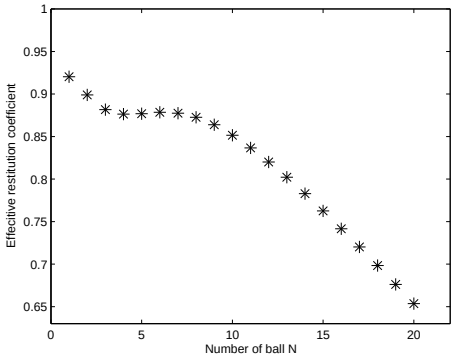

Figure 37: The coefficient e_{eff} for the column with different N dropped from a height $h = 5.1$mm, and setting $e_{s,s} = e_{s,p} = 0.92$.

The definition of the end of the column-wall collision given in [42], in which the collision is assumed to be finished at the time at which the bead at the bottom leaves the wall, is different from ours: we use the energy calibration to define the end of the column-wall collision, corresponding to the instant when all the potential energy among various contacts is completely released. Figure 35 shows the post-velocities of the beads obtained from the simulation for the column free falling from a height $h = 5.1$mm. It is clear from this figure that the upper beads of the column go away with velocities greater than $v_{imp} =$

0.316m/s, while the lower beads have velocities smaller than v_{imp}. Moreover, we can also find that the post-velocity of the last ball will increase with N, and reach the maximum value at $N = 8$, then decrease when N is further enlargered. Unlike a uniform chain impacting by an identical particle, where a regular wave could be formed and confined within five particles, the wave behavior in the column is complex and unregular like the phenomena discovered in section 6.2 for case 4, in which n-ball chains are impacted by m-ball chains. However, we can still observe the following interesting phenomena: If $N < 8$, the beads will separate one after the other from the top of the column. For $N > 8$, some beads separate, while others are leaving in a cluster since the discrepancies between the post-impact velocities of the beads are very small. If $N > 8$, the local energy loss will make the post-impact velocity of the top-bead decrease. Due to the local energy loss, it is imaginable that the top-bead will not bounce if the column is long enough.

The *effective coefficient of restitution* for the whole chain, proposed in [61] and then applied in [42], is defined as:

$$e_{eff} = \frac{\sum_{i=1}^{N} v_i^+}{\sum_{i=1}^{N} v_i^-} = -\frac{1}{N v_{imp}} \sum_{i=1}^{N} v_i^+, \tag{117}$$

where v_i^+ corresponds to the post-impact velocity of i-th beads after collision. It is noteworthy that the value of v_i^+ is different from the one of v_i^f in eq.(7) of [42], where all the values for each v_i^f correspond to the instant when the force felt at the wall equals zero. Figure 36 presents the value of e_{eff} varying with N for a column free fall with a height $h = 5.1$mm. The tendency of the variation of e_{eff} well agrees with [42, Figure 11]. However, when $N > 4$ there is an obvious discrepancy between the value of e_{eff} obtained from our numerical results and the one shown in [42, Figure 11]. This can be attributed to the different definitions for v_i^+ in the two figures for the calculation of e_{eff}.

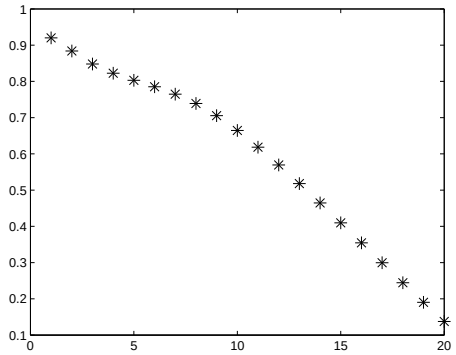

Figure 38: The coefficient e_{eff} for the column with different N dropped from a height $h = 5.1$mm, and setting $e_{s,s} = 0.7$ and $e_{s,p} = 0.92$.

In comparison with Figures 31 to 33, and Figures 32 to 34, we can find that the variation of the value of the restitution coefficient $e_{s,s}$ has little influence on the value of the contact force at the wall. However, it will change the distribution of the post-velocities of beads (the dispersion effect) that seems not

to be ignorable. Let us only change the value of $e_{s,s}$ from 0.96 to 0.92 while keeping other parameters with the same values as used for Figure 36. We can find from Figure 37 that the curve of e_{eff} has an identifiable variation due to the little change of $e_{s,s}$. This means that the local energy loss will influence the distribution of the post-impact velocities of the beads, and can be further confirmed by the following Figure 38, in which $e_{s,s}$ is assigned as 0.7, and the effective coefficient of the whole column, e_{eff} for $N = 20$ is near to 0.1, corresponding to the column with a small bounce.

Table 2. Experimental results during the collision between N stainless steel beads and a force sensor covered with various material sheets, for a fixed height of fall $h = 2.9$ mm.

Material	Thickness (mm)	N_d	$\tau_{max}(N = 1)$ (μs)	$\tau_{max}(N = N_d)$ (μs)
none	-	1	17	17
brass	1.2	2	47.5	46
adhesive tape	0.3	4	47.5	112
PVC	1	6 ± 1	67.5	171 ± 19
PMMA	1	8 ± 1	69	228 ± 11
cardboard II	0.5	11 ± 1	191	396 ± 21
beech	2	15 ± 1	127.5	468 ± 26
cardboard I	0.8	22 ± 2	227	743 ± 23
rubber	1	28 ± 4	221	950 ± 57

Figure 39: Table 2 in [42].

9.4 Influence of the mechanical properties of the wall

The mechanical property of the wall will significantly influence the collision processs as exhibited in [42]. Further investigations can also be found in recent studies in the physics community [48, 47, 63]. For instance, Job et al [48] performed a precise experiment to reflect the dependence of the impulsive wave on the wall mechanical properties. Similar phenomena are also found in the experiments by Daraio et al [64].

In [42], Falcon et al carried out different experiments by setting the column of beads colliding against the wall with different materials. According to the output signal from the force sensor they found that the rigidity of the wall will much influence the collision behavior. For example, experimental results show that the maximum contact force felt at the wall will depend on the number N when a soft material sheet is stuck on the sensor. Figure 39 presents the experimental results (Table 2 in [42]) obtained for the column of beads colliding against a plane covered with various material sheets.

Since the mechanical parameters for the materials covered in the wall are not provided in [42], we use the duration for one bead colliding a plane to

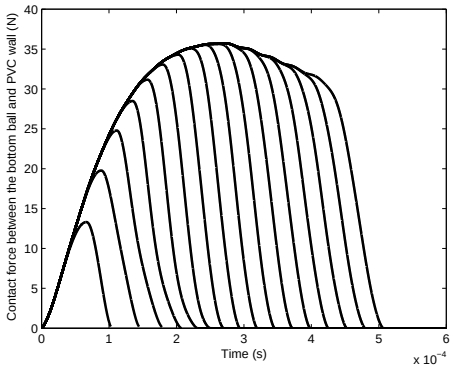

Figure 40: the contact force at the wall with PVC during the collision of a column with $N = 1, 2, \cdots, 16$, $h = 2.9$mm, $e_{s,s} = 0.92$, $e_{s,p} = 0.7$

estimate the contact stiffness between the bead and the plane covered with various material. According to Hertz theory, the contact time τ_1 between a bead dropped from a height h and a plane assumed of infinite mass, can be approximately expressed as

$$\tau_1 = 2.94 \left(\frac{5m}{4K_1} \right)^{\frac{2}{5}} v_{imp}^{-1/5} \tag{118}$$

For a bead with mass $m = 2.05 \times 10^{-3}$kg falling from a height $h = 2.9mm$ ($v_{imp} = \sqrt{2gh} = 0.2385$m/s), Table 12 presents the values of K_1 extracted from the $\tau_{max}(N = 1)$ in Figure 39 and expression (118).

Table 12: The value of the contact stiffness K_1 estimated from experiments.

Index no.	Material	$\tau_{max}(s)$	$K_1(N/m^{3/2})$
1	steel	17	1.15×10^{10}
2	PVC	67.5	3.67×10^{8}
3	beech	127.5	7.5×10^{7}
4	rubber	221	1.89×10^{7}

We can find from Table 12 that the value of K_1 extracted from the experiment of the stainless steel bead colliding with a stainless steel plane is larger than the theoretical value ($K_1 = 9.858 \times 10^9 N/m^{3/2}$), so it is not possible to provide a precise comparision for the contact force between our numerical results and the experimental ones in [42, Figure 13]. At best one can compare some qualitative features of the collision due to the variation of the material in the sheet.

Let us first investigate the contact force at the wall covered with PVC (related to the index 2 in Table 11) by setting a column of beads with various N free falling from a height $h = 2.9$mm. From Figure 40, the experimental phenomena discovered in [42] are well reproduced in our numerical results, in which the maximum force increases with N at low values of N, until it becomes

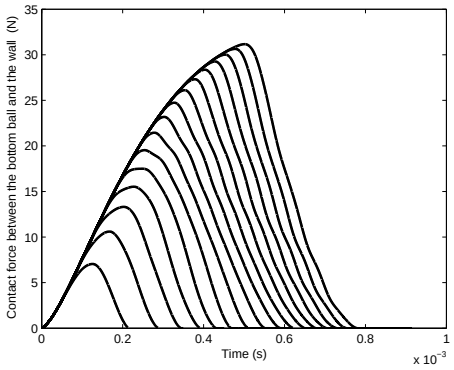

Figure 41: the contact force at the wall with beech during the collision of a column of $N = 1, 2, \cdots, 16$, $h = 2.9$mm, $e_{s,s} = 0.92$, $e_{s,p} = 0.92$

independent of N, finally the contact force will slightly decrease with N like a damping response.

If the wall is covered with softer material, it is imaginable that the number N related to the maximum independent force will increase, and the amplitude among all the maximum forces will decrease due to the small value of the contact stiffness between the bead and the wall. Figures 41 and 42 show the results obtained from our numerical method for the column of beads with various N-chains colliding against a wall covered respectively with beech and rubber materials. The qualitative charateristics discovered in [42] are well reproduced even though the values of the contact stiffness K_1 are roughly estimated with possible large errors compared with practical situations.

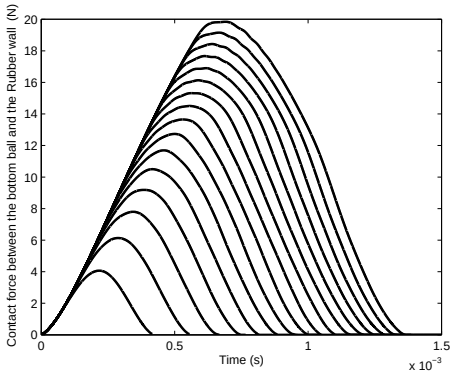

Figure 42: the contact force at the wall with rubber during the collision of a column of $N = 1, 2, \cdots, 16$, $h = 2.9$mm, $e_{s,s} = 0.92$, $e_{s,p} = 0.92$

Comments: *The impulsive behavior of an alignment of grains held within boundaries is not only closely related to the classical problem of multiple impacts in the field of non-smooth dynamics, but also has attracted significant attention in the physics community due to the rich phenomena that seems to be dominated by a underlying physical law. The method proposed in this paper clearly*

states that the mechanical energy transport in granular medium just depends on the relative stiffness and the mode of the potential energy accumulation among various contact points. This may highlight a way of better understanding the complex phenomena exhibited in granular systems and pave the way to determine the micro-parameters of the particles that can excite a special behavior of the global motion that is anticipated to appear in the system.

Based on this algorithm, the local energy loss can be easily taken into account by using energetical constraints and the information related to the contact force and the duration of impact could also be extracted from the solutions of the differential impulsive equations through simple algebraic operations. The comparisons between our numerical results and the experimental ones in [42] show good agreement and confirm some conclusions proposed therein.

10 Conclusions

This paper presents a method based on energy constraints to solve multi-impact problems. Based on the constitutive relationship of contact force/indentation at contact points and mapping the time variable into a impulse variable to stretch the integral scale, the evolution of the energy can be mapped into a velocity-impulse level. Then the properties of the distribution related to the increments of normal impulses in space are discovered, which are associated with the relative potential energy and the relative stiffness between various contact points. Combining the distributing law with the impulsive dynamics, one can deduce a set of first order nonlinear differential equations with respect to an independent "time-like" normal impulse. A guideline for the selection of the independent normal impulse is presented, in which it is selected as the one in the contact point taking the maximum value of the potential energy. The local dissipated energy is described by using an energetical constraint that can be defined by Stronge's energetic coefficient. The advantages of this method are:

- (a) the distribution of the normal impulses can be inserted in the rigid body model so that wave effects are modelled.
- (b) the kinetic energy that is dissipated locally at the contact points can be confined by energetic coefficients such that a consistent solution for the outcomes is calculable.
- (c) integrating stiff compliant problems is avoided as the small displacement and large contact force are not needed.
- (d) the calculated outcomes are robust w.r.t. uncertainties in the parameters (stiffnesses ratios, energetic restitution coeffcients).
- (e) the algorithm is easy to be implemented since the integral process respects the physical meaning of the multiple impacts dominated by the primary colliding point.

Experimental and numerical results published elsewhere confirm that the distribution of kinetic energy in chains of balls and the detachment effect, are due to the elastic properties of the materials which are responsible for the wave

effects. Dissipation however influences the dispersion in the chain. The model in this paper clearly separates dissipation effects (b) and wave effects (a). A numerical scheme is developed and comparisons with the experimental results published elsewhere and the numerical results obtained with compliant models, validate the proposed algorithm. The examples of the Newton's cradle and the Bernoulli's problem illustrate the developments. The investigation related to the uncertainties of the physical parameters and the compliant model in a system of a chain colliding against a wall is carried out. The phenomena discovered experimentally in exsisting literatur [42] are well reproduced by the numerical algorithom. This may highlight the way of better understanding the mechanism for the generation of the solitary wave in granular systems with local energy dissipation. It is expected that a generalization of the method to the situation with friction may be implemented and would then significantly enlarge the scope of applications in multibody systems.

Acknowledgements

The supports of the National Science Foundation of China (10772002,60334030,10642001) are gratefully acknowledged.

References

[1] J. d'Alembert, *Traité de Dynamique*, Paris, 1743.

[2] J. Bernoulli, *Die werk von Jakob Bernoulli*, Birkhäuser, Basel, 1969-1993.

[3] E. Delassus, "Considérations sur le frottement de glissement". Nouv. Ann. de Math., vol.20, pp.485-496, 1920.

[4] J.J. Moreau, "Some numerical methods in multibody dynamics : application to granular materials", European J. of Mechanics A/Solids, vol 13, no 4, pp. 93-114, 1994.

[5] B. Brogliato. *Nonsmooth Mechanics*, 2nd edition. Springer, London., 1999.

[6] W.J. Stronge, *Impact Mechanics*, Cambridge University Press, 2000.

[7] M. Frémond, *Non-Smooth Thermo-Mechanics*. Springer Verlag, 2002.

[8] A.P. Ivanov, "On multiple impacts", J. Applied Mathematics and Mechanics, vol.59, no 6, 887-902, 1995.

[9] Ch. Glocker, F. Pfeiffer, "Multiple impacts with friction in rigid multibody systems", Nonlinear Dynamics, vol.7, pp.471-497, 1995.

[10] F. Pfeiffer, Ch. Glocker, *Multibody Dynamics with Unilateral Contacts*. Wiley Series in Nonlinear Science, 1996.

[11] D. Stewart, "Rigid-body dynamics with friction and impact", SIAM Review, vol.42, no 1 pp.3-39, 2000.

[12] V. Ceanga and Y. Hurmuzlu, "A new look at an old problem: Newton's cradle", ASME Journal of Applied Mechanics, vol.68, no 4, pp.575-583, 2001.

[13] X. Zhang, L. Vu-Quoc "Modeling the dependence of the coefficient of restitution on the impact velocity in elasto-plastic collisions". International Journal of Impact Engineering, vol.27, 2003, pp.317-341.

[14] C. T. Lim, W. J. Stronge, "Oblique elastic-plastic impact between rough cylinders in plane strain", International Journal of Engineering Science, vol.37, 1999, pp.97-122.

[15] C.S. Liu, K. Zhang, R. Yang, "The FEM analysis and approximate model for cylindrical joints with clearances", Mechanism and Machine Theory, vol.42, no 2, pp.183-197, 2007.

[16] R. Seifried, B. Hu B. and P. Eberhard, "Numerical and experimental investigation of radial impacts on a half-circular plate", Multibody Systems Dynamics, 9: 265-281, 2003.

[17] Z. Zhao, B. Chen, C. Liu, H.Jin, "Impact model resolution on Painlevé's paradox", Acta Mechanica Sinica, vol.20, no 6, pp.649-660, 2004.

[18] D. Stoianovici, Y. Hurmuzlu, "A critical study of the applicability of rigid-body collision theory", ASME J. Appl. Mech.vol.63, pp.307-316, 1996.

[19] A.S. Yigit, A.G. Ulsoy, R.A. Scott, "Spring-dashpot models for the dynamics of a radially rotating beam with impact", Journal of Sound and Vibrations, vol.142, 1990, pp.515-525.

[20] Y. Khulief, A. Shabana, "A continuous force model for the impact analysis of flexible multi-body systems", Mechanism and Machine Theory, vol.22, 1987, pp.213-224.

[21] H. Lankarani and P. Nikravesh, "Continuous contact force models for impact analysis in multibody systems", Nonlinear Dynamics, vol.5, 1994, pp.193-207.

[22] S. Shivaswamy, *Modeling Contact Forces and Energy Dissipation During Impact in Multibody Mechanical Systems*, Ph.D. Dissertation,. Wichita State University, Wichita, USA, 1997

[23] O.A. Bauchau, J. Rodriguez, "Modeling of joints with clearance in flexible multibody systems", International Journal of Solids and Structure, vol.39, 2002, pp.41-63.

[24] S. Peng, P. Kraus, V. Kumar and P. Dupont, "Analysis of rigid-body dynamic models for simulation of systems with frictional contacts", Journal of Applied Mechanics, vol.68, pp.118-128, 2001.

[25] V. Acary, B. Brogliato, "Concurrent multiple impacts modelling: Case study of a 3-ball chain", Proc. of the MIT Conference on Computational Fluid and Solid Mechanics, 2003 (K.J. Bathe, Ed.), Elsevier Science, pp.1836-1841.

[26] V. Acary, B. Brogliato, "Toward a mutiple impact law: the 3-ball chain example". Actes du sixième colloque National de Calculs des Structures. Volume 2. Giens 2003., Var, France, pp.337–344. Published by Imprimerie de l'Ecole Polytechnique.

[27] V. Acary, D.E. Taha. "Concurrent Multiple impacts in rigid bodies. Formulation and simulation". In: D. H. van Campen (ed.), ENOC 2005, Fifth Euromech Nonlinear Dynamics Conference. Eindhoven University of Technology, 7-12 August 2005.

[28] M. Wei, C. Liu, "The theoretical analysis of three balls systems with multiple impacts", Chinese Journal of Theoretical and Applied Mechanics, (Chinese) vol.38, no 5, pp.674-681, 2006.

[29] I. Han and B. J., Gilmore, "Multi-body impact motion with friction-Analysis, simulation and experimental validation", ASME J. of Mechanical Design, vol.115, pp.412-422, 1993.

[30] W.J. Stronge "Swerve during three-dimensional impact of rough rigid bodies". Transactions of ASME Journal of Applied Mechanics, vol.61, pp.605-611, 1994.

[31] Ch. Glocker, "Concepts for modeling impacts without friction", Acta Mechanica, vol.168, pp.1-19, 2004.

[32] A. Chatterjee, A. Ruina, "Two interpretations of rigidity in rigid body collisions". Transactions of ASME Journal of Applied Mechanics, vol.65, pp.894-900, 1997.

[33] C.E. Smith," Predicting rebounds using rigid-body dynamics". Transactions of ASME Journal of Applied Mechanics, 1991, vol.58, pp.754-758.

[34] R. Seifried, W. Schiehlen and P. Eberhard, "Numerical and experimental evaluation of coefficient of restitution for repeated impacts", International Journal of Impact Engineering, vol.32, pp.508-524, 2005.

[35] J.L. Escalona, J.R. Sany and A.A. Shabana, "On the use of the restitution condition in flexible body dynamics", Nonlinear Dynamics, vol.30, pp.71-86, 2002.

[36] A.P Ivanov, "The Problem of Constrained Impact", Journal of Applied Mathematics and Mechanics, vol.61, no.3, pp.341-353, 1997.

[37] G. Darboux, "Etude géométrique sur les percussions et le choc des corps", Bulletin des Sciences Mathématiques et Astronomiques, deuxième série, tome 4, pp.126-160, 1880.

[38] J.B. Keller, "Impact with friction". ASME Journal of Applied Mechanics, vol.53, pp.1-4, 1986.

[39] R.M. Brach, "Impact coefficients and tangential impacts". ASME. J. of App. Mech., vol.64, pp.1014-1016, 1997.

[40] J.A. Batlle, "The sliding velocity flow of rough collisions in multibody systems". ASME J. Applied Mechanics, vol.63, pp.804-809, September 1996.

[41] J.A. Batlle, S. Cardona, "The jamb (self-locking) process in three-dimensional rough collisions". ASME J. Applied Mechanics, vol.65, pp.417-423, June 1998.

[42] E. Falcon, A. Laroche, S. Fauve, C. Coste, "Collision of a 1-d column of beads with a wall". The European Physical Journal B, vol.5, pp.111-131, 1998.

[43] W. Ma, C. Liu, B. Chen, "Theoretical model for the pulse dynamics in a long granular chain", Physical Review E, 74-046602, 2006.

[44] C.Liu, Z.Zhao, B. Chen, "The bouncing motion appearing in a robotics system with unilateral constraints", Nonlinear Dynamics, vol.49, no 1-2, pp.217-232, 2007.

[45] E.J. Hinch, S. Saint-Jean, "The fragmentation of a line of balls by an impact", In Proceedings of the Royal Society, London, A 455, pp.3201-3220, 1999.

[46] V. F. Nesterenko, J. Appl. Mech. Tech. Phys. (USSR) vol.5, pp.733-743, 1984.

[47] C. Daraio, V. F. Nesterenko, E. B. Herbold, S. Jin, "Tunability of solitary wave property in one-dimensional strongly nonlinear phonic crystals", Phys. Rev. E 73, 026610, 2006.

[48] S. Job, F. Melo, S. Sen, and A. Sokolow, How Hertzian solitary waves interact with boundaries in a 1-D granular medium, Physical Review Letter, 94, 178002, 2005.

[49] W. Yao, B. Chen and C. Liu, "Energetic coefficient of restitution for planar impact in multi-rigid-body systems with friction", International Journal of Impact Engineering, vol.31, pp.255-265, 2005.

[50] T.R. Kane, D.A. Levinson *Dynamics: Theory and Applications*. New York: McGraw-Hill Ltd, 1985.

[51] J.F. Deck, S.Dubowsky, "On the limitations of predictions of the dynamic response of machines with clearance connections", ASME Journal of Mechanical Design, vol.116, 1994, pp.833-841.

[52] S. Hutzler, G. Delaney, D. Weaire, and Finn MacLeod, "Rocking Newton's cradle", Am. J. Phys. vol.72, no 12, pp.1508-1516, 2004.

[53] K.L. Johnson, *Contact Mechanics*. London: Cambridge University Press, 1992.

[54] M.Y. Louge, M.E. Adams, "Anomalous behavior of normal kinematic restitution in the oblique impacts of a hard sphere on an elastoplastic plate", Phy. Rev. E, vol.65, 021303.

[55] F. Pfeiffer, "Unilateral problems of dynamics", Archive of Applied Mechanics, vol.69, pp.503-527, 1999.

[56] M. Payr, C. Glocker, C. Bosch, "Experimental treatment of multiple-contact-collisions", In ENOC-2005 Proceedings, Eindhoven TU/e, pp.450-459, August 2005.

[57] R. Leine, N. van de Wouw, "Stability properties of equilibrium sets of non-linear mechanical systems with dry friction and impact", Nonlinear Dynamics, in press, 2008.

[58] Hairer, G. Wanner, *Solving Ordinary Differential Equations II. Stiff and Differential-Algebraic Problems*, Springer Series in Computational Mathematics 14, 1996.

[59] C. Coste, E. Falcon, S. Fauve, "Solitary waves in a chain of beads under Hertz contact", Physical Review E, vol.56, no 5, pp.6104-6117, November 1997.

[60] S. McNamara, E. Falcon, "Simulations of vibrated granular medium with impact-velocity-dependent restitution coefficient", Physical Review E, vol.71, 031302, 2005.

[61] S. Luding, E. Clément, A. Blumen, J. Rajchenbach, J. Duran, "Anomalous energy dissipation in molecular dynamics simulations of grains: The "detachment" effect", Physical Review E, vol.50, 4113, 1994.

[62] J.J. Moreau, "Numerical dynamics of granular materials", in *Contact Mechanics* J.A.C. Martins and M.D.P. Monteiro Marques (Eds.), pp. 1-16, Kluwer Academic Publishers, Solid Mechanics and its Applications, 2002.

[63] S.Job, F. Melo, A, Sokolow, S. Sen, "Solitary wave trains in granular chains: experiments, theory and simulations", Granular Matter, vol.10, pp.13-20, 2007.

[64] C.Daraio, V.F.Nesterenko, "Strongly nonlinear wave dynamics in a chain of polymer coated beads", Physical Review E, vol.73, 026612, 2006.

[65] L. Paoli, "Continuous dependence on data for vibro-impact problems", Mathematical Models and Methods in Appied Sciences, vol.15, no 1, pp.53-93, 2005.

[66] M.H. Sadd, Q. Tai, A. Shukla, "Contact law effects on wave propagation in particulate materials using distinct element modeling", Int. J. Non-Linear Mechanics, vol.28, no 2, pp.251-265, 1993.

Contents

Centre de recherche INRIA Grenoble – Rhône-Alpes
655, avenue de l'Europe - 38334 Montbonnot Saint-Ismier (France)

Centre de recherche INRIA Bordeaux – Sud Ouest : Domaine Universitaire - 351, cours de la Libération - 33405 Talence Cedex
Centre de recherche INRIA Lille – Nord Europe : Parc Scientifique de la Haute Borne - 40, avenue Halley - 59650 Villeneuve d'Ascq
Centre de recherche INRIA Nancy – Grand Est : LORIA, Technopôle de Nancy-Brabois - Campus scientifique
615, rue du Jardin Botanique - BP 101 - 54602 Villers-lès-Nancy Cedex
Centre de recherche INRIA Paris – Rocquencourt : Domaine de Voluceau - Rocquencourt - BP 105 - 78153 Le Chesnay Cedex
Centre de recherche INRIA Rennes – Bretagne Atlantique : IRISA, Campus universitaire de Beaulieu - 35042 Rennes Cedex
Centre de recherche INRIA Saclay – Île-de-France : Parc Orsay Université - ZAC des Vignes : 4, rue Jacques Monod - 91893 Orsay Cedex
Centre de recherche INRIA Sophia Antipolis – Méditerranée : 2004, route des Lucioles - BP 93 - 06902 Sophia Antipolis Cedex

Éditeur
INRIA - Domaine de Voluceau - Rocquencourt, BP 105 - 78153 Le Chesnay Cedex (France)
http://www.inria.fr
ISSN 0249-6399